# Validation of Kriging to Understand
# ‘Volcanic Eruption Event Temperature Profiles’
# To Improve
# Gradients in Numerical Weather Prediction Models

Thesis submitted in partial fulfilment

Of the requirements for the degree of

*Master of Science*

*in*

*Computer Science and Engineering*

*by Research*


By

MALINI KRISHNAN

201050026

malini.krishnan@research.iiit.ac.in

International Institute of Information Technology, Hyderabad

(Deemed to be University)

Hyderabad - 500032, INDIA


June 2023

International Institute of Information Technology

Hyderabad, India

# CERTIFICATE

It is certified that the work contained in this thesis, titled "**Validation of Kriging to Understand Volcanic Eruption Event Temperature Profiles to Improve Gradients in Numerical Weather Prediction Models**" by **Malini Krishnan**, has been carried out under my supervision and is not submitted elsewhere for a degree.

31-12-2022 Dr. K. S. Rajan

__________ ______________

Date Advisor

To My Cats Hari, Blacky &Whity

# Acknowledgements

I express my deep gratitude to Dr. K. S. Rajan, for being not just an advisor for my research but for being both a fatherly and motherly figure to me during these research years. If not for his motherly patience with which he listened to me and the fatherly support that he provided, I would not have been able to even imagine pursuing or completing the research.

I would like to thank the institute, IIIT-Hyderabad in innumerable ways. I wholeheartedly feel indebted to the support extended financially during tough times, the understanding of PG - Chair, the course faculties, and the teaching assistants of various labs during course work and research days helped me tide over different challenges arising at various points in time.

I would like to thank my best friend, Deepak Rajamohan. His physical and emotional support was the only pillar that I had at Hyderabad for years while wading through problems at work and at large in life. I would like to thank my landlord, Mr. S. Bharathy Mohan for blessing with me an affordable and peaceful environment for years that helped me focus on my research.

I want to thank my father, V. S. Krishnan for supporting my research passion in various ways. His financial support and his presence during emergencies were very helpful. Along with him, the prayers of my paternal aunt V. S. Poongothai and uncle A.C.A. Raja helped me sail through smoothly each day with hope.

I want to thank fellow lab students at the Lab for Spatial Informatics. Nishith Maheswari helped me immensely to get onboard with IIIT-H and LSI environment. I thank Salghuna Nair for introducing a plethora of GIS software, and valuable Spatial and Remote Sensing books and patiently answering my tons of questions from time to time. I also wish to thank my other lab mates Vani, Tarun, Srishti, Asiya, Akash for sharing their wonderful learnings from their domains during our discussions.

I would like to especially thank Dr. R. C. Prasad for giving me an opportunity to contribute during OS-GEO Conference on a variety of tasks. I want to thank Dr. Saroja and Mr. Devendra Dubey from Exact Humanities department for sharing their knowledge about music and sanskrit which indirectly helped me to understand how I can cross-apply my research ideas in the Arts domain. I would like to thank Dr. Kavita Vemuri for learning about Complex Systems through the course co-offered. I am also deeply indebted to Dr. Priyanka and Anuj Gupta for helping me on personal grounds.

On the work front, I want to thank my manager, mentor, and work-mom, Ms. Lori Huff for motivating my studies with so much enthusiasm. She defused stressful situations arising at work, promptly, from time to time along with my other mentors, Ms. Anjali Desai (HR Head), Aviation safety experts Ms. Mary Lombardi, and FAA DER Marc Nuessen. The emphasis they inculcated on safety rigor directly helped me aim for more accuracy in research results. I would like to thank Ms. Nan Mattai for discussing with me the challenges faced in designing avionics systems to warn pilots from an operational perspective in the event of volcanic eruptions.

Although it was towards the fag end of the research, that I had opportunity to intern at Airports Authority of India, it helped me understand the specifics of potential field application of my research work. In this regard, I would like to thank my manager Mr. R. S. Sridhar, air traffic controllers Mr. Kishore and airspace maps expert Mr. K. P. Sooraj. I also would like to thank my friend Suseendhar for helping me seek mentoring from aviation weather and accident related regulatory heads, Mr. Mohan Ranganathan and Mr. Venu.

I would like to thank my doctors Ms. Nimmibai and Ms. Malligeswari and counsel Mr. Velu for putting me back on track during low points in life.

I want to thank the institute for envisaging the concept of R&D showcase and providing a platform for students to know about how research is conducted in various domains. In addition to the robust infrastructure, I want to thank wholeheartedly the support staff at Yuktahar Mess for providing hygienic, affordable, nutritious and sattvik food that kept us healthy, the Security team members, Arogya doctors, meditation group members, campus canine group members, tree planting group members, basketball and music group friends from hostels with whom tea breaks during night studies provided valuable memories to cherish.

I want to dedicate this research to all my stray cats that include Blacky and late kittens, Hari and Whity. They were my only friends and roommates during the pandemic lockdowns, and their active presence during nights helped me stay passionate about everything I did related to the research and outside it too.

# Abstract

When volcanoes erupt explosively, the ash gets airborne and reaches till stratosphere vertically, and then spreads laterally to synoptic scales due to wind. Detecting the presence of ash in the atmosphere accurately is a challenge. Although several remote, in-situ, and near-sensing techniques exist, due to the variety and complexity of the physical and chemical properties of ash, that get ejected, even within between spells of the eruption of a given volcanic event, it is hard to distinguish it from other aerosols such as desert sand, ice clouds, etc. The false positives in the detection render these solutions unreliable and inconsistent. As a result, weather parameters are explored as an alternative strategy to predict the presence of ash. In specific, the temperature variable is identified as the proxy variable to study the spatial distribution of ash in the atmosphere. There are several beneficial reasons to study temperature because the values do not vary randomly, low-cost equipment suffice to gather the data, the diurnal variations can be accounted for easily, the ability to convert scales from negative to positive metrics for numerical calculations does not vary significantly with ash type, etc.

For this research, the eruption of the Icelandic volcano, Eyjafjallajokull is chosen, due to the severe negative impact it created on the economy across Europe in April and May 2010. World Meteorological Organisation (WMO) and International Civil Aviation Authority (ICAO) together have created Volcanic Ash Advisory Center (VAAC) to model the concentration and simulate the transportation of ash to inform the hazards of ash fall to various stakeholders across the world. The London VAAC used a VAFTDM known as Numerical Atmospheric-dispersion Modeling Environment (NAME) to model the ash spread. This theoretical model had several limitations, chief of them being related to the accuracy of the Numerical Weather Prediction (NWP) models that were supported for ash modeling. The UK Met Office dealing with the NWP associated with the NAME model supported and offered multiple models such as Unified Model (UM), ECMWF, and a few others to predict the weather variables. Since each VAAC uses its own NWP model that varies spatially and temporally, a benchmarking exercise was conducted to compare the Volcanic Ash Forecast Transport and Dispersion (VAFTD) models. The benchmarking allowed the use of either NCEP or ECMWF NWP. For this research, NCEP NWP was chosen for analysis since 6 out of 12 VAFTD models used this NWP.

On analysis, it was observed that NCEP NWP had large grid sizes and therefore small-scale spatial variations were not effectively captured, especially in the vertical extent, even across years. So, we chose to analyze the interpolation model used in the generation of gridded outputs for NCEP since there were limitations observed in using the Ensemble Kalman Filter (EnKF) technique. In this context, the suitability of regression-based interpolation methods was considered to model the NCEP values better. A sample of flight-based ash temperature data from the 2010 Eyjafjallajokull eruption was taken for case study. Initially, a linear regression technique was employed.

Since the outputs of the Multiple Linear Regression (MLR) method were not observed to be highly accurate in modeling the missing day’s temperature using 3 out of 4 day’s samples, a non-linear regression method, based on geostatistics, known as Kriging, was chosen.

Kriging, originally developed for ore mining problems was cross applied to an atmospheric problem in this research. The advantage of using Kriging is that it generates prediction surfaces. In addition, when compared against deterministic methods such as Inverse Distance Weighting (IDW), Kriging can produce error estimates too. Initially, Simple Kriging (SK) method was applied to generate profiles. Since the nature of the dataset was highly clustered and heteroskedastic, a better kriging method was required to model the variations better. A stochastic variant of kriging called Empirical Bayesian Kriging (implemented in ArcGIS version 10.3) was chosen to account for the non-stationary random field. Again, the effect of using an intrinsic random function (non-transitive) in generating and fitting the semivariograms over the use of a transitive function-based approach (by making transformations) was compared. The former is denoted as EBK while the latter is referred to as EBKT.

The non-linear kriging-based interpolation estimates were observed to be significantly better than the traditional MLR method when compared against the NCEP NWP estimates. In addition, a detailed error analysis was performed to compare the 3 kriging methods. EBK method outperformed SK and EBKT in both point estimates and block grade averages. The EBK prediction surfaces were then overlayed on NCEP NWP raster images, in the area of interest, to generate risk maps. The aviation domain was chosen as a case study to apply this methodology. Using the risk map generated, Go/No-Go Zones were identified to mark the presence of airborne ash to ensure safe routes for the operation of aircrafts.

# Contents

**List of Figures**

**List of Tables**

**List of Acronyms**

*AMDAR - Aircraft Meteorological Data Relay*

*ASHTAM - Ash (Notice) to Airmen*

*ATS - Air Traffic Services*

*BADC - British Atmospheric Data Center*

*CAA - Canadian Aviation Authority*

*DLR - Deutsches Zentrum für Luftund Raumfahrt (German)*

*EBK - Empirical Bayesian Kriging*

*EBKT - Empirical Bayesian Kriging - Transformed*

*ECMWF - European Centre for Medium-Range Weather Forecasts*

*EnKF - Ensemble Kalman Filter*

*ELR - Environment Lapse Rate*

*EPZ - Enhanced Procedure Zone*

*EPS - Ensemble Prediction System*

*ERA - ECMWF Re-Analysis*

*ESP - Eruption Source Parameters*

*FAAM - Facility for Airborne Atmospheric Measurements*

*FIR - Flight Information Region*

*FL - Flight Level*

*GEFS - Global Ensemble Forecast System*

*GFS - Global Forecasting System*

*HWRF - Hurricane Weather Research and Forecasting (Model)*

*HYSPLIT - Hybrid Single-Particle Lagrangian Integrated Trajectory (Model)*

*IAVW - International Aviation Volcanic Watch*

*IDW - Inverse Distance Weighting*

*IMD - Indian Meteorological Department*

*IFS - Integrated Forecasting System*

*IN/CCN - Ice Nuclei / Cloud Condensation Nuclei*

*INTF/NC/WKN (Intensifying/No Change/Weakening*

*IVATF - International Volcanic Ash Task Force*

*LAM - Local Area Models*

*LAMP - Localized Aviation MOS*

*MBR - Minimum Bounding Region*

*MER - Mass Eruption Rate*

*MLR - Multiple Linear Regression*

*MetUM - Meteorological Unified Model*

*MOGREPS-G - Met Office Global and Regional Ensemble Prediction System*

*MOS - Model Output Statistics*

*MWO - Meteorological Watch Office*

*NAME - Nuclear Accident Model*

*NAE - North Atlantic and European Region*

*NATS - National Air Traffic Services*

*NCEP - National Center for Environment Prediction*

*NCAR - National Center for Atmospheric Research*

*NFZ - No Fly Zone*

*NOTAM - Notice to Airmen*

*NWP - Numerical Weather Prediction*

*OPC - Optical Particle Counter*

*PIREP - Pilot Report*

*SK - Simple Kriging*

*SIGMET - Significant Meteorological (Information)*

*VAA - Volcanic Ash Advisory*

*VAAC - Volcanic Ash Advisory Center*

*VAFTAD - Volcanic Ash Forecast Transportation and Dispersion (Model)*

*VEI - Volcanic Explosivity Index*

*VONA - Volcano Observatory Notice for Aviation*

*WMO - World Meteorological Organization*

*WRF - Weather Research and Forecasting (Model)*

*TCAC - Tropical Cyclone Advisory Centre*

*VOL-CALPUFF - Volcano California Puff (Model)*

# I. Introduction

## 1. Volcanic Eruption and Impact to Airspace Due to Airborne Ash

Natural disasters are a class of phenomenon occurring over a short or long period of time. They cause widespread human, material, economic or environmental loss that exceeds the ability of the affected community to cope with available resources. Although disasters in earth are usually classified as geological or hydrological or meteorological, the impact of volcanic eruptions spans right from lithosphere to the atmosphere. Therefore, they are a potential global multi-hazard. The unpredictability of volcanic eruptions (both in timing and in location) has led to many disasters. Due to the variety of volcanic products and the large range of possible event sizes, volcanic risk presents a particular challenge for risk management. Two types of volcanic threats have to be considered: (1) city scenarios of local or regional extent and (2) rare extreme events with global consequences.

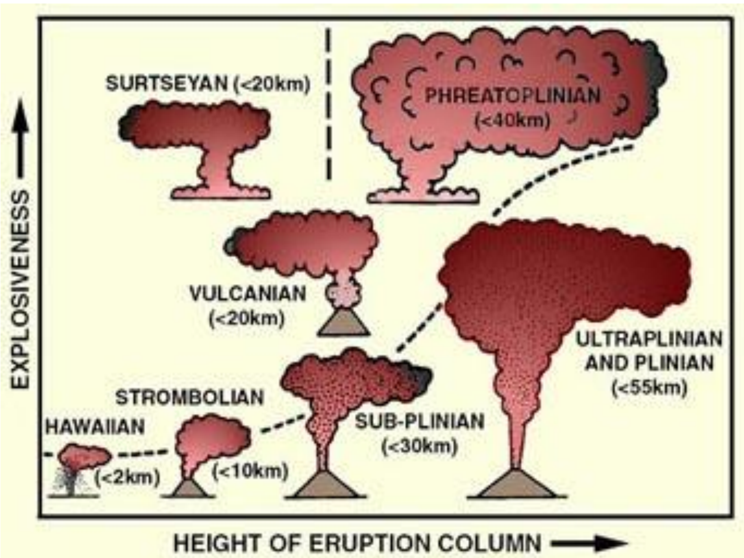


*Figure 1: Types of Volcanoes based on Ash Cloud Explosiveness*

*(Source: http://sci.sdsu.edu/how_volcanoes_work/Thumblinks/erupttypes_page.html)*

In an explosive phreatic event, gaseous magma abruptly gets depressurized as it nears the Earth's surface and jets out through a constrained vent. The ejected magma fragments into glassy shards and mineral particles as it cools. Any source of water gets converted as steam in phreatomagmatic eruptions. Else, the lava flows quietly from fissures in magmatic eruptions. Along with gases and air entrained from the surroundings, the convective plume rises upward. Such eruption columns rise at tens of meters per second and can quickly reach cruise altitudes of jet aircraft and beyond, to nearly 50 km. Plumes either entrain moisture to increase their buoyancy or bend due to local wind effects. In Plinian eruptions, as shown in *Figure 1*, the plume punches through the tropopause to form a mushroom-shaped pyro cumulus cloud. Volcanic fragments larger than several tens of microns fall out of a plume within hours and are generally deposited within a few hundred kilometres around the volcano, whereas finer ash remain suspended in the stratosphere for days. Once ejected into the atmosphere, the ash and gas are dispersed by prevailing winds as aerosols. If wind direction varies with height (wind shear), the eruption plume gets dispersed in multiple random directions.

Wilson et al., (2012) identify the 'critical infrastructure', essential for the smooth functioning of a society and economy that are most affected by volcanic eruptions at a local scale. This includes, electricity networks, gas and oil production, transport and distribution, telecommunications, water supply, sewage disposal drainage networks, food production and distribution, heating systems (e.g. natural gas, fuels); transportation systems (road and rail networks, airports, ports, inland shipping), farming and animal rearing.

Smolka and Käser, (2015) report the loss in millions of USD, as given in, *Table 1*, due to volcanic eruptions across different countries in the last few decades.

| **Location** | **Year** | **Economic Loss** | **Insured Loss** |
|---|---|---|---|
| Mount St. Helens (USA) | 1980 | 860 | 31 |
| Pinatubo (Philippines) | 1991 | 750 | 70 |
| Tavurvur, Papua New Guinea | 1994 | 300 | 66 |
| Montserrat | 1995-97 | 200 | 100 |
| Merapi (Indonesia) | 2010 | 380 | Minor |

*Table 1: Volcanic Eruptions since 1970 that caused Significant Insured Losses*

With global events, property damage is not necessarily the issue, as the volcanic centres tend to be at long distances away from large cities (Naples and few Indonesian volcanoes are exceptions to this rule). Thus, among multiple damage foci, one of the chief concern in recent years is to aviation. Particularly in the case of Icelandic region, which is the customary airspace over the North Atlantic that tends to be blocked for months due to threats from ash clouds. Rerouting of flights is not a sufficient work-around if a large number of aircrafts had to be grounded as in the case of spring 2010 eruption of Eyjafjallajokull eruption. It is estimated that 500+ airports worldwide are within 62 miles (100 km) of active volcanoes. Over the last sixty years, at least 100 airports have been impacted by eruptions on 171 separate occasions (some airports more than once). Gordeev and Girina, (2014), identify that United States and Indonesia, to have reported the most airport disruptions due to volcanic eruptions as shown in *Table 2*.

| Volcanoes | Eruptions | Eruption Date (UTC) |
|---|---|---|
| Shiveluch | 7 strong | 1993-2013; paroxysmal events: 22.04.1993, 19.05.2001, 28.02.2005; 22.09.2005, 29.03.2007, 27.10.2010 |
| Llyuchevskoi | 11 | 15.03.1993-02.10.1994; 02.04-1995; 01-09.1997;02-09.1998; 05-12.1999;22.03.2003-03.03.2004;10-01-03.04.2005;15-02-26.07.2007; 16-10.2008-29.01.2009; 18-09.2009-01.10.2010;01.09.2012-15.01.2013 |
| Bezymyannyi | 26 | 1993-2013; paroxysmal events; 20-23.10.1993; 05.10.1995;09.05.1997; 05.12.1997; 24.02.1999;13.03.2000;01.11.2000;06.08.2001;25.12.2002; 26.07.2003;13.01.2004;18-06.2004; 11.01.2005; 30.11.2005;09.05.2006;24.12.2006;11.05.2007;08.03.2012;01.09.2012 |
| Karymskii | 2 strong | 1996-2013; strong events;02.01.1996; 13-14.05.2006 |
| Chikurachki | 6 | 25.01-01.05.2002;17.04-16.06-2003;10.03-07.04.2005;04.03-07.04.2007;19.08-20.10.2007;29.07-15.08.2008 |
| Mutnovskii | 4 | 17.03.2000;29.06.200;17.04.2007;03.07.2013 |

*Table 2: Frequency of few of the eruptions at Kamchatka and Northern Kuril Islands from 1993-2003 Impacting Aviation Operations*

The most common effect is temporary operational disruption, ranging from flight cancellations to airport closures for periods of few hours to weeks. The main hazard to aviation is ash fall. The accumulation of only a few millimetres of ash on runways is sufficient to force temporary closure of an airport, although disruptions also have been caused by airborne ash in the vicinity of airports without the deposition of ash on the ground.

On the other hand, for aircrafts, there are several threats once it becomes airborne, such as, turbulent climatic conditions, bird strikes but volcanic ash is a special class of problem. It is spatially spread on a meso-scale region, and it can be encountered at various altitudes with no visible clues. The movement of the ash cloud dynamically changes in direction based on wind conditions. Ash clouds manifest themselves either as opaque or transparent or translucent forms requiring the need to differentiate it from various types of meteorological clouds. At any given time, as shown in the *Figure 2*, there are as many as 10,000+ flights that are airborne across the world.

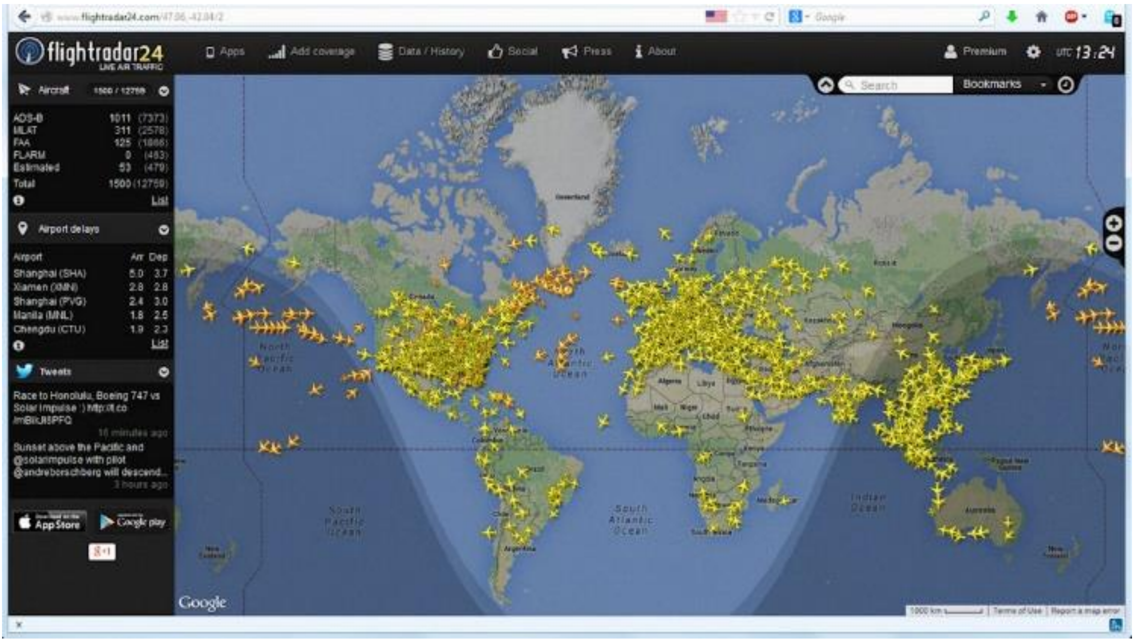


*Figure 2: World Map showing Live Air Traffic Density*

*(Source: Snapshot from FlightRadar24 website in January 2021)*

As shown in the map in *Figure 3*, there are about 1,500 active volcanoes on any given day with many in effusive eruption phase and a few erupting explosively. Given this scenario, there is always a high probability for a new volcanic eruption to begin anywhere on the land and/or sea with an aircraft potentially encountering the plumes mid-air.

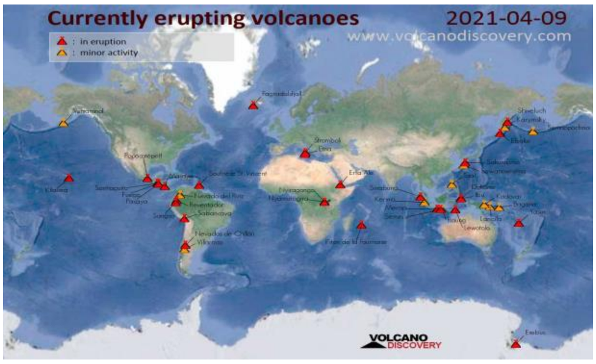


*Figure 3: World Map showing Volcanoes in Active State in 2021*

*(Source: https://www.volcanodiscovery.com/volcano-activity/news/126875/Volcanic-activity-worldwide-9-Apr-2021-Fuego-volcano-Popocatepetl-Dukono-Reventador-Sangay-Sa.html)*

Volcanic ash is a threat to the safety of aircrafts while at ground (taxi phase), during landing/takeoff phase and at cruising altitudes. But the safety threat to aircrafts rapidly transforms into threat for human lives especially when the aircraft is in take-off/landing & cruising modes since engines are operated near full throttle and are hence at high temperatures. While ash deposition on other parts of aircraft is also dangerous, it only impacts the ability to navigate and to communicate. Only when the ability to aviate is challenged, emergency is declared by pilots. *Figure 4* maps vulnerable regions across the world where even a minor eruption can cause major catastrophes due to airborne.


*Figure 4: World Map showing Encounters between Aircrafts & Volcanic Ash of Varying VEI*

*[Source: Encounters of Aircraft with Volcanic Ash Clouds: A Compilation of Known Incidents, 1953–2009, By Marianne Guffanti, Thomas J. Casadevall, and Karin Budding – Appendix 1.mdb]*

*Figure 5* depicts the number of encounters between ash clouds and aircrafts in 20th Century.

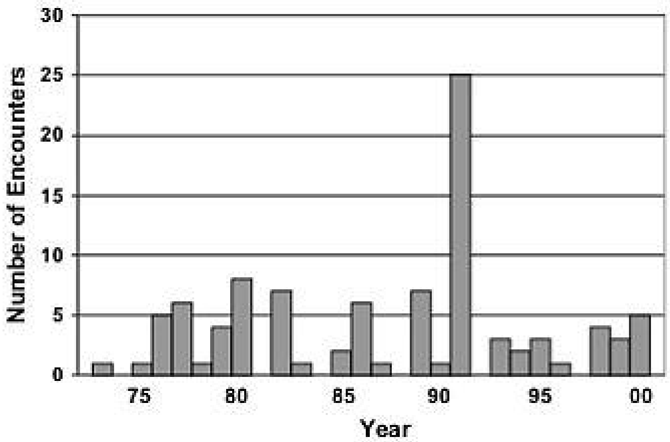


*Figure 5: Timeline of aircraft encounters with volcanic ash in 20th Century*

*[Source: Reducing the threat to aviation from airborne volcanic ash, Marianne Guffanti et al, U.S. Geological Survey; Air Line Pilots Association; 55th Annual International Air Safety Seminar, 2002, Dublin]*

i. Volcanic ash plume is an imminent threat to any country

Airborne volcanic ash is a non-localized hazard and its risks are exceptionally dynamic in short term since it injects significant amounts of ash into airspace traversed by thousands of aircrafts at any given time. Unlike the established societies that lie in the path of the volcano at ground, the aviation community experiences a continually changing risk with respect to location of dispersing clouds. Mitigation actions comprise specialized warning messages disseminated within tens of minutes of detection of ash clouds to aid in making decisions to diver the en route aircraft with ground dispatch and Air Traffic Control Centers, taking into account the forecast location of ash clouds. The mitigation framework is usually globally coordinated with responsibilities of reporting, forecasting. Every region on earth is equally at risk from volcanoes for the below described reasons.

ii. Volcanoes can form anywhere in land

Paricutin is a cinder cone volcano in Mexico. Usually volcanoes are classified as dead, dormant and active. Paricutin is unique in the fact that its evolution from creation to extinction was witnessed, observed and studied by human beings. The volcano began in 1943 as a fissure in a cornfield. The volcano grew quickly, reaching five stories tall in just a week, and could be seen from afar in a month. After roughly one year, the volcano had grown 336 metres (1,102 feet) tall. For the next eight years the volcano continued erupting. In 1952, the eruption ended and Parícutin attained a final height of 424 metres above the cornfield where it began. The volcano has been quiet since then. Like most cinder cones, Parícutin is believed to be a monogenetic volcano, which means that once it has finished erupting, it will never erupt again. Polygenetic volcanic fields generally occur where there is a high-level magma chamber and may last over 10 million years. There are tens of such volcanoes around the earth. Unlike monogenetic volcanoes, polygenetic volcanoes reach massive sizes. Polygenetic volcanoes include stratovolcanoes, complex volcanoes, somma volcanoes, calderas and many shield volcanoes.

iii. Volcanoes can form anywhere in sea (submarine/subaerial)

Submarine volcanoes are underwater fissures in the Earth's surface from which magma can erupt. They are estimated to account for 75% of annual magma output. The vast majority are located near areas of tectonic plate movement, known as ocean ridges. Although most are located in the depths of seas and oceans, some also exist in shallow water, which can spew material into the air during an eruption. The presence of water can greatly alter the characteristics of a volcanic eruption and the explosions made by these.

The Kolumbo underwater volcano in the Aegean Sea was discovered in 1650 when it burst from the sea and erupted, killing 70 people on the nearby island of Santorini. The Taman Peninsula in Sea of Azov, Ukraine has about 25 mud volcanoes, most of which are active. Their eruptions are usually quiet, spilling out mud, and such gases as methane, carbon dioxide and hydrogen sulfide, but are sometimes violent and resemble regular volcanic eruptions. A major eruption on 6 September 1799, near Golubitskaya, lasted about 2 hours and formed a mud island 100 metres in diameter and 2 metres in height; the island was then washed away by the sea. Similar eruptions occurred in 1862, 1906, 1924, 1950 and 1952. This shows that some regions are prone to repeated sudden eruptions from under water conditions too.

iv. Man-Made Eruptions

Accidental drilling has given rise to mud volcanoes in the past. But those were not considered to be violent eruptions. Sand volcanoes are also less explosive in nature. In 2003, a new type of submarine volcano known as Asphalt volcano was found. These are typically seamounts and generate water vapour but not generate silicate ash. Some occur after a long time of dormancy with little recognized warning, sometimes in remote parts of earth as in Siberia.

v. Subglacier volcanoes

These type of volcanoes are also explosive in nature. Whenever magma comes into contact with water bodies that are either on ground or near surface level, it gives rises to highly explosive eruptions. This includes snow-clad mountains also. The eruptions are called as phreatomagmatic in nature.

Also, each volcano can exhibit different types of eruption phases within its active period (or) vary between two different eruptions over a period of time. For example, Mt. Fuji (864 & 1707 eruptions) and Grimsvotneruptions in 2011. Of these, plinian type of eruptions are the ones that mostly cause hazards to aircrafts. One of the characteristic feature of plinian eruptions is the presence of rhyolite. It is a colourless acidic rock.Out of 1500 named sub-aerial & sub-glacial volcanoes in the world, around 30 volcanoes are active at any given point of time and explode with Volcanic Explosivity Index (VEI) greater than 2 on a scale of 1 (least explosive) to 10 (most explosive). Several dormant volcanoes in human uninhabited islands start erupting violently and rapidly from the very onset of eruptions signs.

To be able to detect them in all climatic conditions, time of the day is an open challenge till date. There are several key chemical elements in ash clouds/plumes that turn hazardous to aircrafts under flying conditions that makes the jet engines vulnerable to flameouts. Airborne volcanic ash is in principle visible under suitable daylight conditions. But “Visible ash” is not a reliable concept for decision making. Real-life detectability depends on many parameters and is therefore a complex, unsolved problem.

Although the danger due to even synoptic scale volcanic eruptions is largely analysed from the perspective of safety and livelihood of mostly humans, directly and indirectly, on air and at land, sometimes, even remote, human uninhabited islands undergo severe degradations with respect to flora and fauna. Even few intermittent, small eruptions lasting for 5 to 10 minute spells within a day but spanning across for few days can cause elevated temperature levels that could wipe out large volumes of fishes that keep moving across ocean currents for breeding purposes. Similarly migratory birds in air and exotic reptiles & endangered mammals that belong to species that are unique, local and native to those areas face rapid extinction in large numbers. Although the negative impacts of many such irreversible losses are not directly felt on majority of human beings, immediately, due to the remoteness of occurrence in oceanic regions, they still have their effects on airborne pollination process and waterborne seed dispersal patterns, even across continents. The April 1993 eruption of Barren Island volcano, in Andaman, India led to extinction of 10 out of 16 species of birds found only in that island. So, even eruptions as low as VEI 2 need to be quickly assessed for overall health of apparently disjoint biospheres.

The solution for the issue of tracking volcanic ash dispersal has been well attempted using Remote Sensing techniques from 1980s. A variety of platforms such as Satellites, Aircrafts, Ships, Drones, International Space Station and Balloons have been used to monitor various ash properties. A variety of sensors that tap different properties of EM spectrum have also been designed and developed for this purpose as part of in-situ sensing, near sensing and remote sensing studies.

Despite more than 3 decades of research efforts, no state-of-the-art technology has delivered promising results towards detection of volcanic ash. Despite the vast growth in the fields of meteorology, volcanology, oceanology, volcanoes, this problem continues to be a threat to human lives and livelihood due to the lack of accurate, cost-effective modelling/prediction systems.

Accuracy of state-of-the-art modeling/prediction models for presence of ash generally range only between 60%-70%. Issues of false positives due to spectral resemblance with desert sand, normal meteorological clouds, spatial resolution of sensor imageries, temporal frequency of data, sampling methodologies etc are some of the primary challenges encountered. Although a wide variety of traditional interpolation techniques are in use today for climatological modeling, each method has its own severe limitations.

In this context, the appropriateness of the application of spatial interpolation using geostatistics approach and its rigorous validation are investigated in this research.

In addition, since ash dispersion occurs in 3D space, ash concentrations are measured locally to cover across both the horizontal and vertical spaces. If there are multiple distal ash layers, as shown in *Figure 6*, then average ash concentration over vertical depth is computed. In addition, satellite instruments scan and measure column loadings over limited horizontal swaths. Given such partial clusters of data as inputs to any model forecasts, the estimates obtained are not usually effective. Knowledge about spatial and temporal distribution of ash and its properties is inevitable for better model outputs.

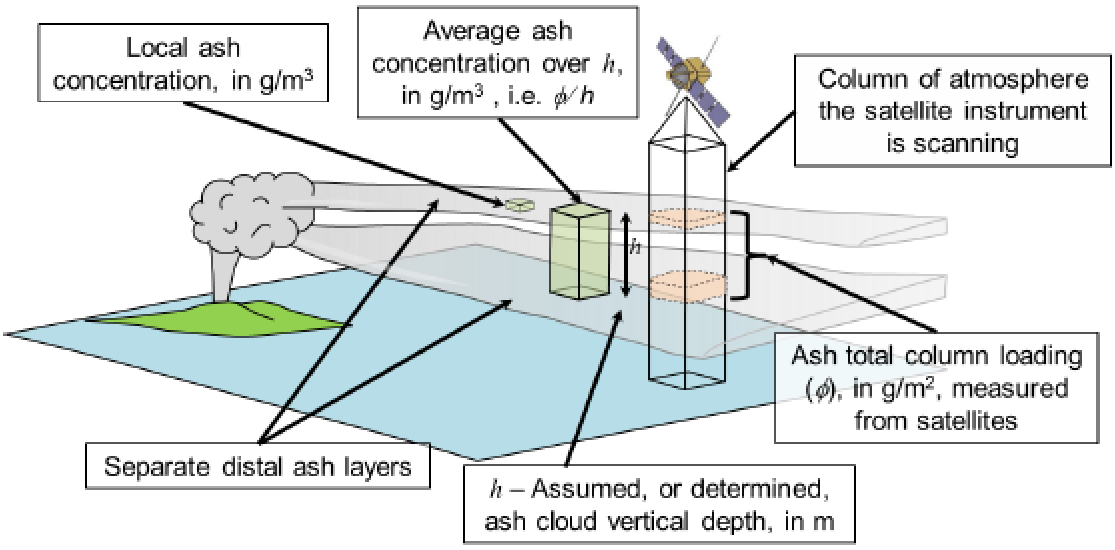


*Figure 6: Difference between an ash concentration within an ash layer and an integrated ash total column loading*

*(Source: Volcanic Ash and Aviation – Rolls-Royce Position, 2017)*

Given this background, the following sections explain the need for better modelling/forecasting algorithms that are able to simulate close to the physical processes in nature, especially from sparse experimental field data.

## 2. Airborne Volcanic Ash Dispersion Modeling

For this research, an Icelandic eruption in 2010 has been used as a case study. The key operational issue was to analyse by when, which extent of airspace is likely to be contaminated by various quantities of volcanic ash using air temperature as a proxy variable. Eyjafjallajokull is a smaller ice cap volcano on the southern tip of Iceland. It erupted once during 1821-1823 causing relatively minor damage. The 2010 eruption produced a massive cloud of ash that entered the jet stream above Iceland and floated over United Kingdom and continental Europe. Eyjafjallajokull's ash cloud, as shown in *Figure 7* rose as high as 30,000 feet into the sky, which is a critical height at which modern jet aircraft travel and it entered directly into an unexpectedly stable jet stream. A pilot's eye view of the ash cloud from the eruption is shown in *Figure 8.*

*Figure 7: Plume rises from under the Eyja glacier in Iceland*

*(Source: https://www.dailymail.co.uk/news/article-1268615/The-ash-cloud-How-volcanic-plume-UK-twentieth-safe-flying-limit-blunders-led-lock-down.html)*

*Figure 8: A Pilot's View of Ash Plume Pilot's view of the ash cloud above normal clouds at Netherlands. Altitude: 6000 feet*

*(Source: https://www.dailymail.co.uk/news/article-1268615/The-ash-cloud-How-volcanic-plume-UK-twentieth-safe-flying-limit-blunders-led-lock-down.html)*

i. Challenges in Measuring Ash

The first step in studying the impact of any volcanic eruption involves knowing how much ash is injected into the atmosphere. As the plume rises, it expands and cools. The plume height is proportional to the heat of the eruption and the quantity of magma ejected. Once the ash temperature reaches the same as the temperature of the surrounding air, it stops rising. Many of the fine ash particles then collide with each other and stick together, become heavier and drop out of the sky. This process, known as sedimentation, is modelled assuming each actual particle of ash is a sphere with a fixed density. These values are added to temperature and pressure components that are calculated from the Navier-Stokes equations, to give a fuller picture of ash movement over each time-step. About 95% of the volcanic ash is deposited to the ground. The key is then to find out where the remaining 5% is dispersing.

The unsettled ash particles are relatively larger in size. About 50% of the mass comes from dispersed particles greater than 3 microns diameter. Decelerating these ash aerosols to sample through a pipe in a research aircraft platform for studies is difficult. Therefore, ash needs to be measured in free flow outside the aircraft, as shown in *Figure 9*, using optical scattering instruments such as Optical Particle Counter (OPC), Nephelometer etc.

*Figure 9: Optical Particle Counter Remote Sensing Instrument*

*(Source: British Atmospheric Data Center, FAAM Aircraft Instrumentation)*

In addition, Turnbull et al., (2012) discuss the challenges related to observation of volcanic ash using in situ on airborne platforms such as The Facility for Airborne Atmospheric Measurements (FAAM) British Aerospace (BAE)-146 and German Deutsches Zentrum für Luft- und Raumfahrt (DLR) Falcon experimental research aircrafts. Lidar systems are not capable of measuring mass concentration of ash clouds neither directly nor using trace gases in both horizontal and vertical extents.

Also, aerosol mass loading experiments revealed extreme variations in mass concentration. Even small change in altitude (a few hundred metres) or geographic position (a few tens of km), equivalent to a few minutes of flight time) may result in an aircraft exposed to ash concentrations that change by a factor of more than 10, making it difficult to devise practical ash avoidance procedures for civil aircraft. Also in oceanic regions, ground-based sensor readings are not feasible.

Newman et al., (2012) discuss the high spatial variability at various scales while measuring using other sensors such as 3 wavelength nephelometer and satellite radiative sensors, as shown in *Figure 10*. As a result, numerical models such as Numerical Atmospheric-dispersion Modeling Environment (NAME), that use these platforms and sensors as input sources are unable to capture such variability explicitly, especially over small spatial scales.

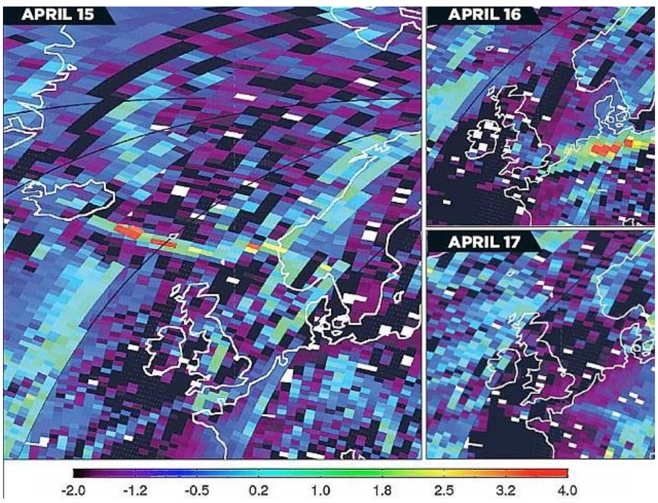


*Figure 10: Sequence of satellite images showing "aerosol index", the concentration of particles of ash or other pollution in the atmosphere. On April 15, the plume is clearly visible as a streak of orange, or 4.0 on scale. Values more than 2 in yellow could be ash.*

*(Source: https://www.dailymail.co.uk/news/article-1268615/The-ash-cloud-How-volcanic-plume-UK-twentieth-safe-flying-limit-blunders-led-lock-down.html)*

ii. Comments on UK National Air Traffic Services (NATS) Policy

The mandatory airspace closure policy enforced by UK NATS, during the 2010 eruption was based on theoretical models as shown in *Figure 11*. These were mainly derived, not from satellite observations of where ash was visible but only from theoretical models. This showed that entire region could be affected by minute concentrations of ash dispersed by weather systems. Across most of this, the ash was claimed to be so thin as to be invisible. Only as the situation evolved, a key decision was taken to discover how dense the ash clouds for recommending the closure of vast airspaces.

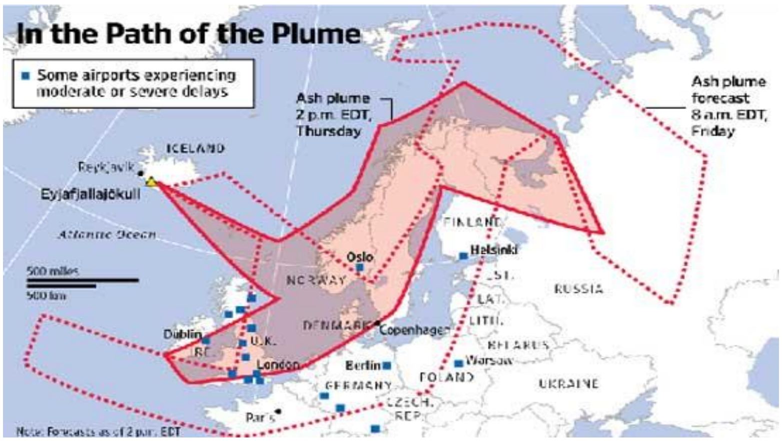


*Figure 11: A sample map produced by NAME model predicting the extent of ash spread*

*(Source: https://www.studentnewsdaily.com/daily-news-article/airlines-face-continued-disruptions-from-iceland-volcano/)*

In this context, it is worthy to assess the quality of recommendations that were provided by regulatory authorities to the aviation community during the 2010 Icelandic eruption using the NAME model, in specific. Although not a scientific publication, some of the news articles carry significant importance and reputation. One such *article* titled, "New ash density limits agreed for flights in the UK" (2010) shows the extensive usage of subjective phrases such as: ash is not *too* thick, *some* models of aeroplanes can fly, *changes* in ash density threshold after weeks of criticism, *too* strict cut off, safe *enough* to fly in *all* directions, gradual reduction based on OEM's *advice*, *something* like 350 cancellations over past 36 hours, threat moved *away*, *very* minor risk, doubling previous limit of ash *exposure*, allowed to fly *limited* time only, *medium* density, *much* denser, *nearly* 30,000 feet etc. In addition, instead of estimating the maximum density of ash in the atmosphere, based on jet engine tolerance limits of 0.004g per cubic metre of air was considered by NAME model to prepare the density chart that led to incomplete legends showing 4000+ micrograms of ash. Even for small errors in positions of narrow plumes, NAME produced large concentration errors.

The movement of the ash cloud depends on three main factors: the weather, sedimentation and small-scale turbulence - the NAME model accounts for all three. *Figure 12* shows the main steps described by Webster et al., (2012) in the operation of NAME dispersion model.

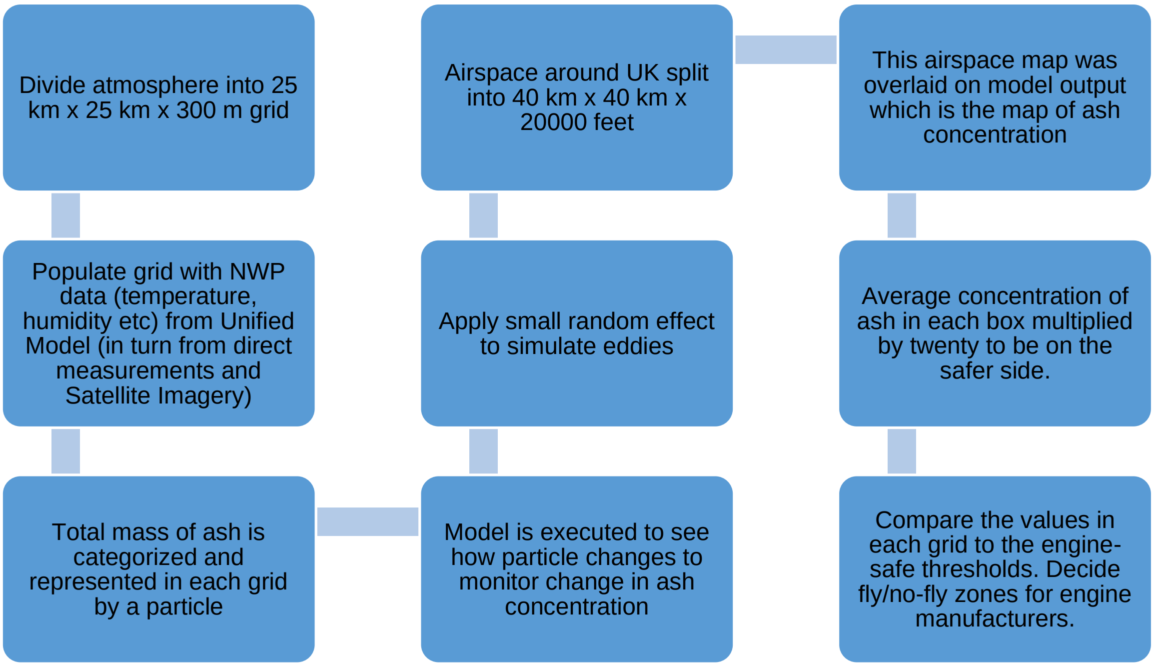


*Figure 12: Flowchart showing key steps in NAME Model Operation*

By using the Navier-Stokes equations, meteorologists can work out how the prevailing weather conditions will evolve over the next few days. However, despite carving up the atmosphere into relatively small grids, solving the Navier-Stokes equations and factoring in sedimentation, movement of ash on the smallest scales still needs to be taken into account. This small-scale diffusion is caused by eddies – small whirlpools of air that may or not follow the direction of the overall weather pattern. In order to mimic the effect of these eddies, a small random element of motion was applied to each particle. These small-scale turbulences are represented using Markov processes but always carry a near constant value.

The UK Meteorological (Met) Office encountered various other challenges too, critical to decision making (the adequacy of sampling), poor weather conditions to conduct experiments, operational issues with aircrafts (ceiling of turboprop aircrafts are less) and NWP models.

Some of the key issues w.r.t. NWP Models include:

- For while computer ash dispersion simulations have good short-term accuracy, modelling errors build up & they get less and less reliable.
- Models were not designed to readily give the all-important detail of particle density which determines if it is safe to fly.
- The stakeholders agreed on a more individualized nation-by-nation assessment of the risk under the NAME model, which allowed for a more differentiated assessment of risk from the ash cloud, while still respecting safety concerns.

Given these limitations, there was a clear need for a better modeling technique that accurately captures variations in weather variables in short spatial scales in the absence of a vast amount of experimental data in the context of severe weather scenarios that exist at synoptic scales. Bonadonna et al., (2012), identify five focus areas for various stakeholders to develop new and improved strategies for ash dispersal forecasting. They are:

a. Improve the definition of the source term,
b. Design models and forecasting strategies that can better characterize uncertainties,
c. Explore and identify the best ensemble strategies that can be adapted to ash dispersal forecasting,
d. Identify optimized strategies for the combination of models and observations and
e. Implement new critical operational strategies.

To resolve the issues arising due to the discrepancies observed in the Volcanic Ash Forecast Transport And Dispersion (VAFTAD) models due to underlying physics, parametrization of source terms and variations in inputs, a benchmarking exercise was conducted across nations. 13 recommendations were proposed as outcome and agreed to by participating states. Recommendations #3 to #7 discussed by Bonadonna et al., (2012) focus on the need for quantifying the sensitivity of numerical model accuracy on model discretization. This includes uncertainties related to both ash related inputs and meteorological inputs (from either mesoscale or global scale weather forecasts).

iii. Recommendation for identifying Probabilistic Estimation Methods

Ash dispersal modeling problem has a variety of uncertainties. While the randomness of the nature along with field measurement errors give rise to aleatoric uncertainties, errors arising due to sampling and numerical investigations cause epistemic uncertainties. While the former can be dealt with by identifying appropriate eruption activity and Probability Density Function of input parameters, the latter are reduced by improving the parametrization of physical processes, investigation techniques and numerical accuracies. Parameterization in a weather or climate model in the context of numerical weather prediction is a method of replacing processes that are too small-scale or complex to be physically represented in the model by a simplified process. Usually, weather and climate model grid boxes have sides of between 5 kilometres and 300 kilometres. On the other hand, a typical cumulus cloud has a scale of less than 1 kilometre and would require a grid even finer than this to be represented physically by the equations of fluid motion. So, sophisticated processes are required to ensure accuracy of forecasting. By routinely increasing model resolution, errors associated with the parameters increase. The estimates may be statistically valid for larger grid boxes but become questionable once the grid boxes shrink in scale towards the size of the ash cloud clusters itself. The resulting outputs therefore appear unrealistic in nature. This is why ash dispersal forecasting may be more accurate if it simply outputs a range of probability values as opposed to absolute values of ash properties or weather variables. It was therefore then anticipated that the stakeholders (e.g., aviation industry, decision makers) will eventually need to integrate probabilistic strategies into their processes of decision making.

So, to comprehensively analyse these significant, open issues to mitigate the risks and errors that could arise in policy proposals and challenge the overall reliability of prediction estimates, newer line of enquiries is required.

iv. As-Is Systems to Simulate Ash Dispersion

Atmospheric Dispersion Modeling is the mathematical simulation of how air pollutants disperse in the ambient atmosphere. The algorithms use mathematical equations governing pollutant dispersions in its algorithms. Close to erupting volcanic vents, the buoyancy causes pollutants to rapidly raise vertically. When the density of the ash plume is higher than the air, they get dispersed through winds and take even several months to settle down. Stefanescu et al., (2014) describes how Volcano Observatories (VONA) and Volcanic Ash Advisory Centers (VAACs) predict the likely position of ash clouds using deterministic mathematical models of advection and dispersion, known as Volcanic Ash Transport and Dispersal Forecasting (VATDF) models. These models require input data on volcanic source conditions as well as the wind field. As shown in *Figure 13,* the resulting maps are often understood to delineate ‘‘hard’’ exclusion zones. In contrast, most meteorological forecasts are issued as maps or reports giving the probability of an event or the occurrence of a phenomenon, like precipitation, in a certain region at a specific time. Partly because of this disparity between ash cloud and meteorological forecasting and the desire to produce ash forecast products comparable to the standard, a need has been explicitly stated on numerous occasions for reliable, probabilistic ash cloud forecasts.

*Figure 13* shows the three-zone system introduced by the UK Civil Aviation Authority (CAA) in May 2010. The Enhanced Procedures Zone (EPZ) permits aircraft to fly in ash concentrations either measured or forecast up to 2 mg per cubic metre, while a time-limited zone (grey-colored) was introduced as a “buffer” between the EPZ and a No-Fly Zone (NFZ), where aircraft were not permitted to fly in measured or forecast ash concentrations of 4 mg per cubic metre or higher. Outsider the three zones, normal operation procedures were applied.

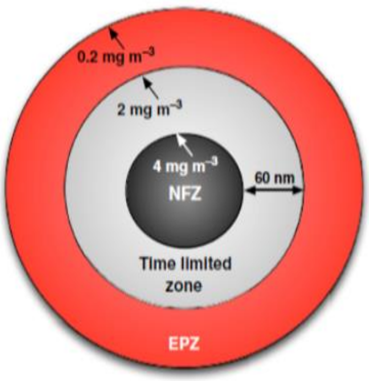


*Figure 13: Categorization of No-Fly Zones*

*(Source: https://www.sciencedirect.com/science/article/pii/B9780123859389000523)*

*Figure 14* shows an example of a fine ash mass loading retrieval based on MODIS Satellite data for 6th May 2010. The colours have been assigned to show levels at 0.2, 2 and 4 gram per square metre, which correspond to ash concentrations of 200, 2000 and 4000 microgram per cubic metre for an ash cloud 1 km deep.

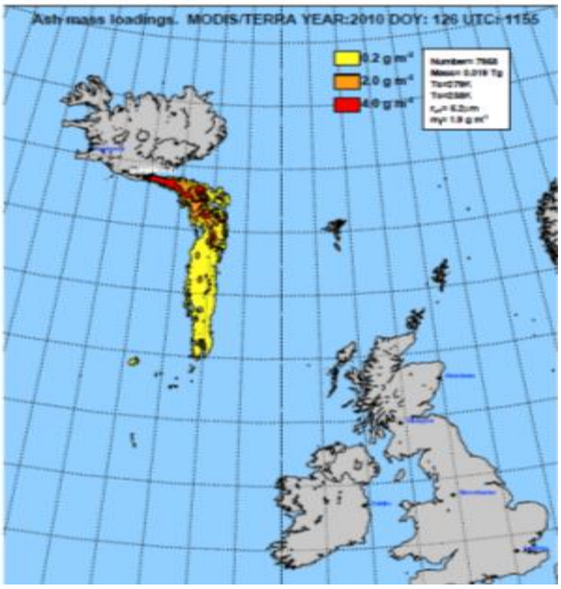


*Figure 14: Enhanced Procedure Zones*

*(Source: https://www.sciencedirect.com/science/article/pii/B9780123859389000523)*

*Figure 15* shows modelled ash concentration from Flight Level, FL000 to FL200 at 0000 UTC 20/04/2010.

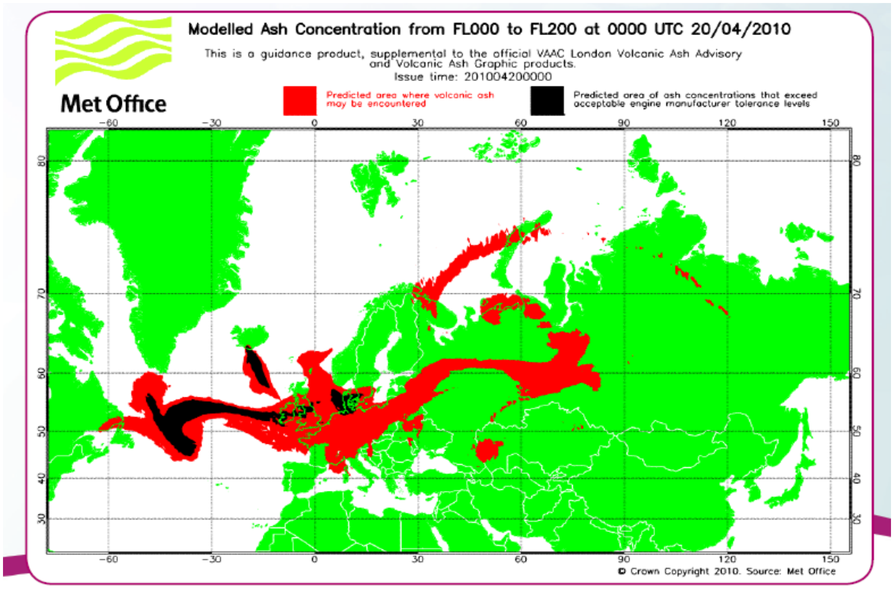


*Figure 15: Ash Concentration by NAME Model Simulations*

*(Source: https://www.sciencedirect.com/science/article/pii/B9780123859389000523)*

Volcanic ash dispersion models are used by an international network of scientific experts, as part of the initiative named, “Volcanic Ash Advisory Center (VAAC)”. This was created by International Civil Aviation Organization (ICAO), primarily for aviation industry. Currently they work in tandem with the Met-P Panel of yet another United Nations (UN) agency, namely, World Meteorological Organization’s (WMO), since the accuracy of the Numerical Weather Prediction (NWP) Model used by individual countries is critical to the effectiveness of the VATDFM recommendations, as discussed in Slide #21 of the *report* .

As of today, to detect the presence of ash in atmosphere, most VAAC dispersion models take imageries as input data for initial stages of forecasting from 1 to 3 different satellites that are marked as relevant and responsible for a given region in a continent. In addition, the forecasters rely on real time Pilot Reports (PIREP). In both the methods, the visibility by color of ash to human eyes without any other aid play a crucial role in determining the extent of the ash spread to determine the safety of airspaces.

If the ash is brown coloured, as shown in *Figure 16*, it appears similar to desert sand as shown in *Figure 17*.

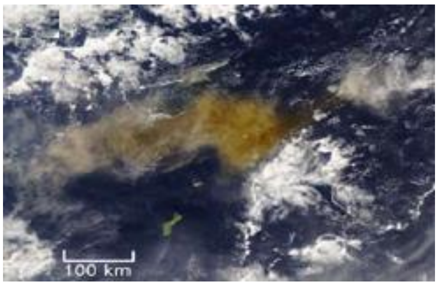


*Figure 16: Drifting ash and gas plumes from Karthala volcano*

*(Source: https://link.springer.com/article/10.1007/s11069-008-9273-z/figures/1)*

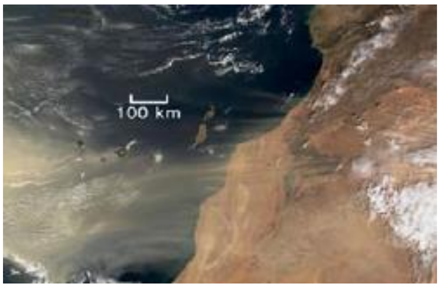


*Figure 17: Sand/Dust Outbreak at Canary Islands - MODIS Satellite Imagery*

If the ash is in grey color, as shown in *Figure 18*, then, it resembles towering cumulonimbus clouds, as shown in *Figure 19*.


*Figure 18: Greyish Ash in Gas Plume from Kluichevskoi Volcano in summer*

*(Source: https://link.springer.com/article/10.1007/s11069-008-9273-z/figures/1)*

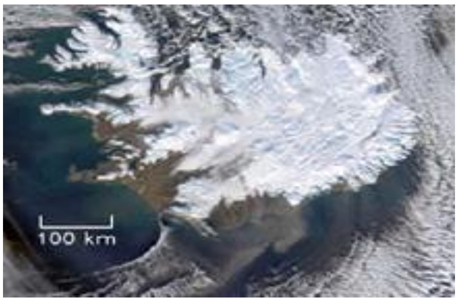


*Figure 19: Windblown resuspended Ash in Southern Coast of Iceland in the background of an hurricane clouds*

*(Source: https://link.springer.com/article/10.1007/s11069-008-9273-z/figures/1)*

If the ash is white in color, then, at times it resembles the snow at the terrain as shown in *Figure 20*.

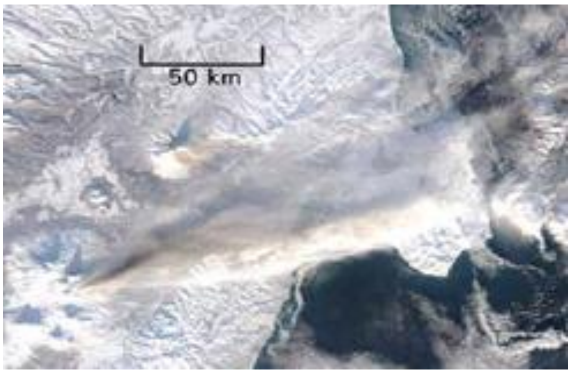


*Figure 20: Ash and gas plume indistinguishable over snow covered terrain, Kluichevskoi volcano*

*(Source: https://link.springer.com/article/10.1007/s11069-008-9273-z/figures/1)*

Also, if the ash in gas plume is white in color, it resembles the normal meteorological clouds too, as shown in *Figure 21*.

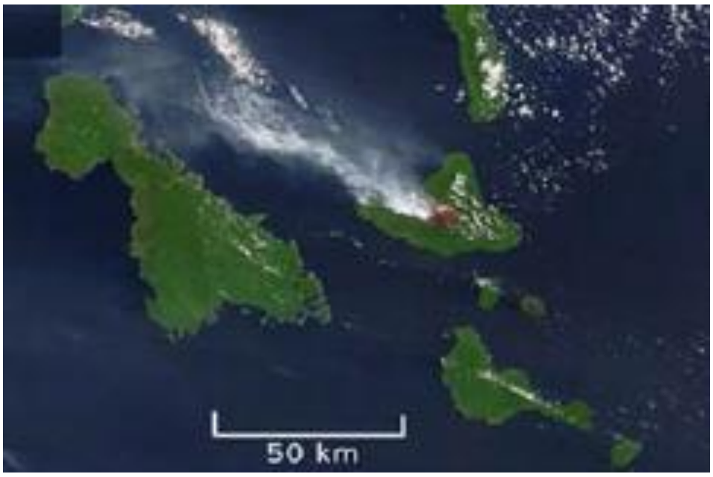


*Figure 21: Low level gas cloud plume from Kluichevskoi volcano*

*(Source: https://link.springer.com/article/10.1007/s11069-008-9273-z/figures/1)*

Weinzierl et al., (2012)  discuss the visibility of ash from aircraft platform without any visual aids to human eyes, as shown in *Figure 22*. This is another input source, used to subjectively identify the presence of volcanic ash in the atmosphere.


*Figure 22: Photographs of volcanic ash layers varying with low mass concentrations (12-32 mg per cubic metre) taken on 13th May 2010 over the North Sea close to Great Britain*

*(Source: https://www.sciencedirect.com/science/article/pii/S1474706512000496)*

Also, at an air temperature of around 255K, diluted concentrations of hydrophobic ash particles tend to aggregate under ideal humidity conditions and turn into potential Ice Nuclei (IN)/Cloud Condensation Nuclei (CCN) and resemble normal meteorological super cooled ice/water clouds, as shown in *Figure 23*.

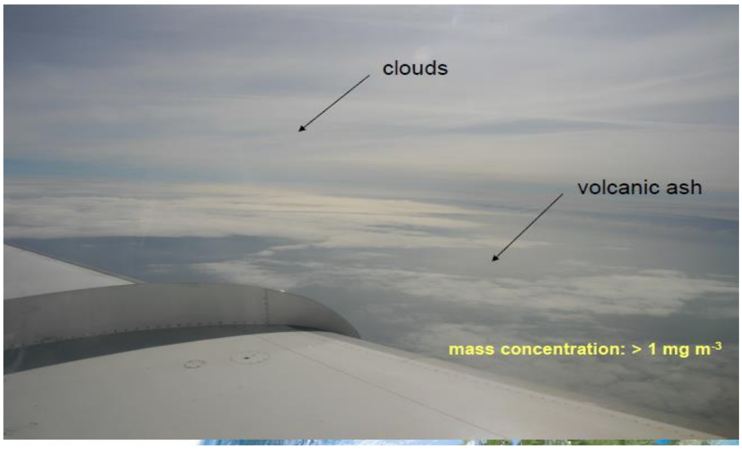


*Figure 23: Diluted ash concentrations alongside Normal Clouds*

*(Source: https://www.sciencedirect.com/science/article/pii/S1474706512000496)*

Further, the spatial resolution of some satellites such as Japan's Himawari-8 (used by Darwin VAAC at Australia) is as high as 1.25x1.25 degree and the temporal frequency is only once in 6 hours. In the event of an ongoing eruption, even the airborne sources of data such as PIREPs (Pilot Reports) are not available as inputs for VATDFMs. A sample list of VAAC details is given in *Figure 24*.

| VAAC | Region: Lon (°E) | Region: Lat (°N) | Geostationary Satellites | Dispersion model |
|---|---|---|---|---|
| Anchorage[1] | [150, −135] | [50, 90] | GOES | PUFF, HYSPLIT, CANERM |
| Buenos Aires[2] | [−90, −10] | [−90, −10] | MSG-3/GOES-E | |
| Darwin[3] | [75, 160] | [−90, 10] | MTSAT | HYSPLIT |
| London[4] | [−30, 60] | [45, 90] | MSG-3 | NAME |
| Montreal[5] | [−135, 0] | [45, 90] | GOES-E/GOES-W | CANERM |
| Tokyo[6] | [90, 165] | [15, 60] | MTSAT | |
| Toulouse[7] | [−30, 90] | [−90, 70] | MSG-3 | MEDIA/MOCAGE |
| Washington[8] | [−150, −40] | [−10, 45] | GOES/POES | HYSPLIT |
| Wellington[9] | [160, −140] | [−90, 0] | MTSAT | HYSPLIT |

*Figure 24: List of VAACs with locations across the world*

*(Source: Geostationary Satellites to Generate Ash Products and Dispersion Models)*

Further it is not always possible to precisely know from satellite imageries if an existing, named volcano has erupted or a new volcanic vent has emerged over oceanic region or multiple vents are spewing ash explosively from existing volcanoes atop glaciers. Many times, the vent itself is obscured by clouds or even by the ash plume itself.

Also, proxies such as $SO_2$ emission cannot be always relied as a marker for detecting presence of ash in the case of phreatomagmatic eruptions. Because, sometimes, ash could get airborne purely out of wind triggered resuspension process as in the case of Novarupta volcano. This Alaskan volcano last erupted in 1912 at Volcanic Explosivity Index (VEI) level 6. Yet large volumes of loose ash got aloft due to strong winds even as recent as September 2020.

Also, wind speeds increase significantly as altitude increases, enabling faster dispersion of ash over larger continental regions. As a result, there is a need for a sophisticated methodology that can rapidly estimate using near-static weather variables such as air temperature and yet produce upper air temperature prediction estimates that vary even in small spatial scales, to be, as accurate as $\pm 2^{o}$ C, 90% of the times for regions as large as 100 nm in extent to meet safety requirement standards.

The lack of data on ash is not just limited to direct quantities such as concentration but also extends to affect the collection of weather parameters such as temperature, humidity, wind speed/directions etc through the Aircraft Meteorological Data Relay (AMDAR) systems. AMDARs are typically used in commercial jet aeroplanes cruising at high altitudes. Given such a scenario, if only sparse samples can be collected using balloons and drones as platforms, in a random scheme, then, appropriate spatial interpolation techniques must be identified to understand the extent of ash field under investigation.

Also, two different VAFTD models are sometimes applied to a single country due to their partitioned geographies. For example, India's Bay of Bengal (east of the peninsular India) under Chennai Flight Information Region (FIR) is monitored by Darwin VAAC while the Arabian Sea (west of the peninsular India) monitored by the same Chennai FIR is monitored by France VAAC, as shown in *Figure 25*.

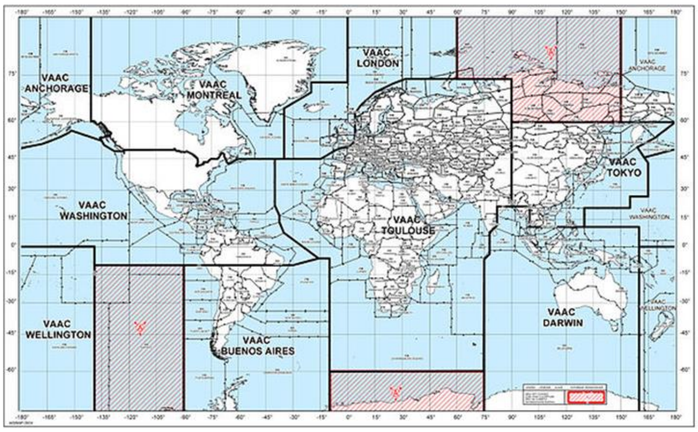


*Figure 25: World Map showing VAAC Partitions*

*(Source: https://www.ospo.noaa.gov/img/vaac/VAAC_Map_2017.jpg)*

Despite India's Meteorological Department (IMD) having its own set of NWP models, often authorities have to process recommendations arising from two different VAFTD models to arrive at their contingency routes (i.e. USA's Hybrid Single-Particle Lagrangian Integrated Trajectory (HYSPLIT) model from Darwin and France's MOCAGE model). The unified decision making is essential for countries like India with its vast continental airspace and transoceanic airspaces to reroute aircrafts at short notices without shutting airspaces due to shortfalls arising due to difficulties in planning. In addition, being a large country in terms of area, sometimes more than one severe weather scenario could arise too, in which case, there is a need of smooth interoperability between the various types of NWPs models currently in use by a given country. For example, to name a few, the Indian Meteorological Department (IMD) uses the following NWPs in parallel: Global GFS T1534, Regional WRF, Ensemble GEFS, Cyclone Hurricane Weather Research and Forecasting (HWRF) model etc.

Sometimes the horizontal spread of the volcanic ash plumes could be vast so as to span across FIRs of different countries or even across VAACs and yet the source of the cloud could be elusive since satellite imagery based forecasts provide updated imageries only once in 6 or 12 or 18 hour time gaps. In addition, quite often, the meteorological NWP grids and ash dispersion model of the same country grid cell sizes do not match each other and require regridding efforts.

Till date, Model Output Statistics (MOS) concept for aviation, such as USA's Localized Aviation MOS Program (LAMP) has been largely applied only in a highly localized point sources context. The Station Based LAMP issues persistent weather recommendations at airport levels (for example, Terminal Aerodrome Forecasts (TAFs)), for granular time periods, by augmenting the NWP estimates. So there is also a need for a MOS methodology that can be applied to even mesoscale (eg; Gridded LAMP) and synoptic scale extents, irrespective of the country of origin, that can be applied on data collected in irregular spatial scales and from across different altitudes. Dispersion models must also be able to produce prediction estimates and associated error estimates for airspaces affected in both vertical and horizontal extents so that they can customized to prepare safe air corridors, trajectories and routes. Some of the other common issues observed in visualizing and interpreting the outputs of a VAFTD model are discussed below:

a. The boundaries of Flight Information Region (FIR)/VAAC/Airline Routes are mostly well defined shapes as points or lines or polygons whereas Volcanic Vents/Ash plumes are irregular in spread. The spatial data types are also different for each type of input, especially for the NWP.

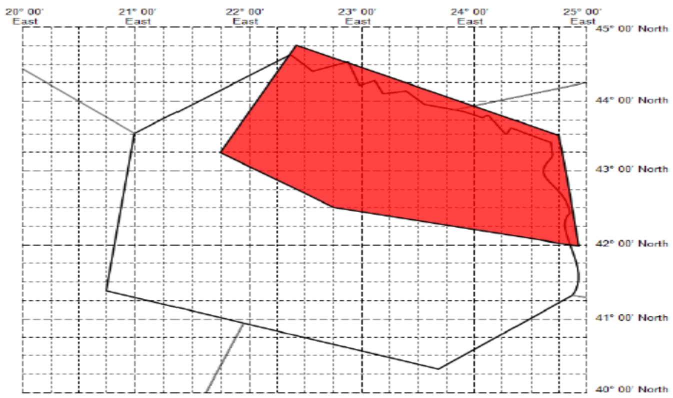


*Figure 26: Jagged Boundary Representation by ICAO*

*(Source: Asia/Pacific Regional SIGMET Guide, 6$^{th}$ Ed, 2017)*

b. The regional (Significant Meteorology) SIGMET guide also provides information regarding the necessary coordination between the Meteorological Watch Office (MWOs), Air Traffic Services (ATS), volcanic ash advisory centres (VAACs), Tropical Cyclone Advisory Centres (TCACs) and pilots, and their respective responsibilities. *Figure 26* shows the jagged boundary of FIR alongside adjacent FIRs with sample SIGMET guidance overlapped on the polygon.

As of today, the entire earth surface is categorized into 9 VAACs. The scope for increasing the number of VAACs is being explored. This proposal arises because, in the Potts, n.d. (2017), the need for a model that accurately predicts small scale variations in the ash concentration in the atmosphere is stated as: "*Following the Eyjafjallajökull eruption in 2010 there has been a need for more information on the spatial variation in ash concentration and the associated uncertainties to enable airlines to better manage operational risk. There are significant challenges with this objective."* This will enable National Civil Aviation Authorities to issue ASHTAM or ash NOTAM (Notice to Airmen) to alert pilots of any ash hazards enroute or at a specific location.

Aviation industry typically requires alerts for potential ash cloud threats upto 300 nm (555 km) even outside the FIR boundary. In the case of volcanic ash the hazard to jet transport is greatest within the first few hours following an eruption. Hence speed of notification between all links in the chain of communication is critical – viz civil aviation, meteorological and vulcanological authorities. Consistency across agencies regarding extent, trajectory and dispersion patterns of ash is mandatory. On the other hand, pilots at cruising altitude are at the top of the chain for whom rapid dissemination of information is crucial.

v. To-Be Systems

The "METP WG MOG 8 VA SN 02_IAVW_Roadmap (attachment).pdf " n.d. (2017) describes the need for development of next generation volcanic ash cloud forecasts that includes quantitative and probabilistic (uncertainty) information. The operation envisaged by the panel is summarized below:

Current volcanic ash forecasts, such as the Volcanic Ash Advisory (VAA), are qualitative, deterministic forecasts. They are a yes/no binary forecast with respect to the depiction of the airspace impacted by discernible volcanic ash and they give a single forecast with no uncertainty information. Volcanic ash transport and dispersion models can produce an array of solutions (e.g., forecasts) by varying the model input. Changes in meteorological parameters and eruption source parameters (ESP) can result in different forecast outputs that affect the 4-dimensional (4-D) shape (3-dimensional shape and change of shape with time) of the volcanic ash cloud and gases.

The next generation volcanic ash cloud forecasts, as well as forecasts of volcanic gases, is expected to provide both deterministic and probabilistic forecasts for contamination levels that will allow decision makers to use, taking into account their risk management practices and the quantitative exposures allowed by the engine manufacturers.

Specifically, the addition of probabilistic forecasts will have to provide decision makers with an assessment of the likelihood of the volcanic ash exceeding a defined magnitude (or threshold) at a particular time and place. The probabilistic element further helps decision makers apply their own operational constraints (i.e. business rules) to determine the risk to their operations.

From a high-level perspective, probability forecasts may be based on an ensemble approach. An ensemble is one way to account for some degree of uncertainty. For instance, a model or models can be run many times, each time with a realistic variant of one of the uncertain parameters (e.g. ash amount, ash column height, eruption start time and duration, input meteorology dataset, dispersion model used, with and without wet deposition, etc.). Taken as a whole, the variability of the ensemble member's output gives an indication of the uncertainty associated with that particular volcanic ash forecast.

The application of probabilistic forecasts is expected to suit both high- and low-density airspaces, where decision makers can benefit from more than just a deterministic forecast to determine route or flow. Decision support systems can also be adapted to use probabilistic information to provide efficient route and altitude selections, as well as time maintenance alerts, based on user's dosage thresholds.

For decision makers (i.e., operators, flight crew, air traffic control) to effectively use probabilities for the initial and ongoing evidence based qualitative risk assessments, a thorough understanding of the output from the VAAC is needed by the users. This will require educational/training efforts that will be suitable for all decision makers. It is envisioned that probabilistic information will be used pre-tactically to plan flight routes until the aircraft comes within range of an area of interest, at which time the pilot will receive higher resolution quantitative information. Also, currently the models output their recommendations in only 3 categories – INTF/NC/WKN (Intensifying/No Change/Weakening). But with a more accurate, quantitative model, several levels of warning and caution advisories can be issued. In addition to issuing status on occurrence or non-occurrence of a severe weather phenomenon, the extent of prediction can be increased from ±1000 km in 70% of the instances.

## 3. Role of Numerical Weather Prediction Models in Ash Dispersion Simulations

Numerical Weather Prediction (NWP) modelling is often at a disadvantageous situation, wherein, huge geographic regions must be simulated separately for lateral and vertical spaces. The physical parametrizations associated with certain small scale weather phenomenon are largely approximated or even totally ignored due to the complexity and the need for large computational resources. For example, grid cells in weather/climate models, such as NCEP/GFS are upwards of hundreds of kilometres whereas a typical cumulus cloud has a scale of less than 1 kilometre. As a result, finer grid sizes are required to accurately model the microphysics of normal and ash clouds.

Although Environment Lapse Rates (ELR) recommend 6.5-degrees to 9-degree Celsius difference in temperatures for every 1000 feet based on real data, it is a typical recommendation meant for normal weather scenarios. During severe weather, the atmosphere is unstable and turbulent. Sub-grid scale variations in processes need to be considered to yield accurate predictions during severe weather scenarios.

Of the various dispersion models discussed in the workshop report [8], the NAME model (Nuclear Accident Model/Numerical Atmospheric Dispersion Modelling Environment) has been taken for a short analysis as it was heavily used by UK Met Office during 2010 eruption to provide regulatory recommendations to mark safe airspace zones.

i. Case Study: London VAAC NAME VAFTD and UK Met Office NWP

The UK Met Office has international commitments to provide emergency response dispersion modelling services for release of hazardous gases and pollutants into the atmosphere. It is identified by World Meteorological Office and International Civil Aviation Organization to serve as a VAAC as part of the IAVW (International Airways Volcano Watch). In the last few decades, it has modelled radioactive releases at Chernobyl, Kuwait Oil fires, major industrial fires, chemical spills, 2 volcanic eruptions at Iceland and long term environment analysis.

NAME, discussed in the Jones et al., (2007), is the VAFTD model used by London VAAC to issue volcanic ash advisories. The impact to closure of the Air Routes, as predicted by NAME model, is shown in the *Figure 27*. The losses incurred across the world are discussed by Kristiansen et al., (2012), due to the overlap of the airspace in the path of Eyjafjallajokull eruption ash dispersion.

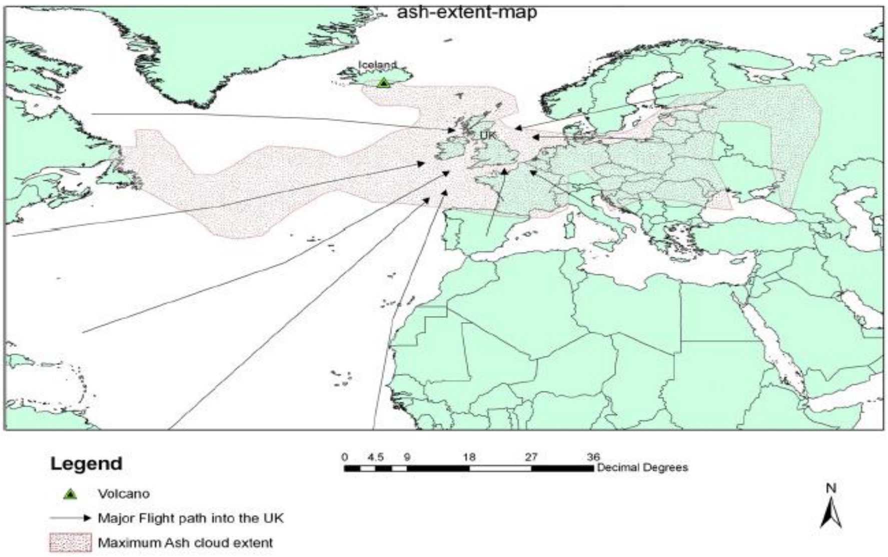


*Figure 27: Maximum Extent of Volcanic Ash Cloud that created No-Fly Zone in UK Airspace*

*(Source: UK Met Office, April/May 2010)*

The NAME model includes additional parametrizations for atmospheric processes which are unresolved in the NWP, but which influence the transport of pollutants, including deep convection, horizontal mesoscale motions, and turbulence. NAME is a local to global scale, general purpose model developed by UK's Met Office, in 1986. It is an integrated Lagrangian 3d model that includes boundary layer dispersion modelling. Random walk techniques using empirical turbulence profiles are utilized to represent turbulent mixing. It estimates pollutant concentrations using Monte Carlo simulation methods rather than solving equations.

NAME uses a puff technique when modeling dispersions over short range which reduces the needed time for computations. It is capable of computations for a wide variety of atmospheric conditions and can generate maps. The Gaussian model-based process assumes that the air pollutant dispersion has a Gaussian distribution, meaning that the pollutant distribution has a normal probability distribution. Gaussian models are most often used for predicting the dispersion of continuous, buoyant air pollution plumes originating from ground-level or elevated sources. They may also be used for predicting the dispersion of non-continuous air pollution plumes (called puff models). The primary algorithm used in Gaussian modeling is the Generalized Dispersion Equation for A Continuous Point-Source Plume.

NAME assimilates meteorological data from different NWP models and datasets, as shown in *Figure 28*.

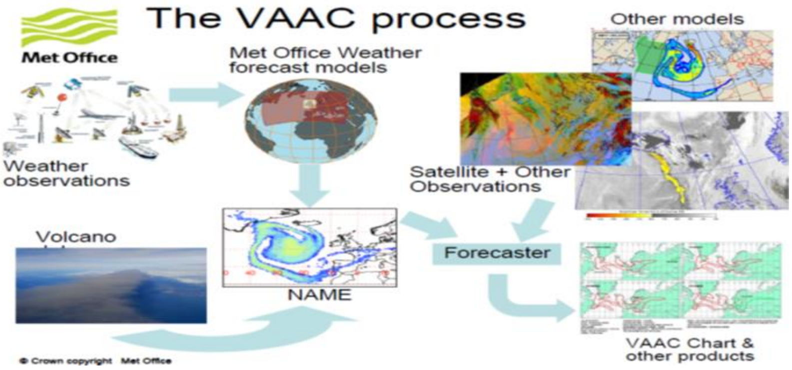


*Figure 28: The VAAC Process*

*(Source: https://journals.openedition.org/belgeo/docannexe/image/16399/img-1.jpg)*

Some of the NWPs utilized include:

- UK Met Office Unified Model (MetUM) – 1.5 km grid
- ECMWF Integrated Forecasting System (IFS) (for real time forecasts)
- ECMWF Re-Analysis (ERA)
- Single site met observations of surface weather stations for short range applications
- Rainfall Radio Detection and Ranging (RADAR) data & Subset of data from other sources such as 2d surface fields and 3d model level fields.

In the *article* by Miller, (2011), it is noted that the accuracy of NWP relevant to the ash dispersion model is very important to ensure proper response to volcanic eruptions, not just to the aviation industry but also society at large too.

The UK Met Office's main NWP model is the Unified Model (UM). The UM is initialized using observation data blended with a previous forecast, through the process of data assimilation, to give a best estimate of the state of the atmosphere. NWP variables: pressure, density, potential temperature, and wind vectors are then evolved through time by solving the dynamical equations of motion. Physical processes such as orographic drag which occur on a sub-grid scale are usually parametrized as discussed in Crown, Met Office (2010). In the follow up paper, Beckett et al., (2020), the state of the art systems are reviewed in detail.

There are several model configurations of the UM which produce output at different resolutions, over different regions, and for different purposes. The meteorological data used to run NAME operationally during 2010 was taken from the Global configuration, a grid-point model using a standard latitude-longitude coordinate system which provides weather forecasts for the whole globe. At this time, forecast met data had a horizontal resolution of 25 km at mid-latitudes, and a four-Dimensional Variational data assimilation (4DVar) method was used to combine observations with previous forecasts to initialize the model as discussed in Beckett et al., (2020).

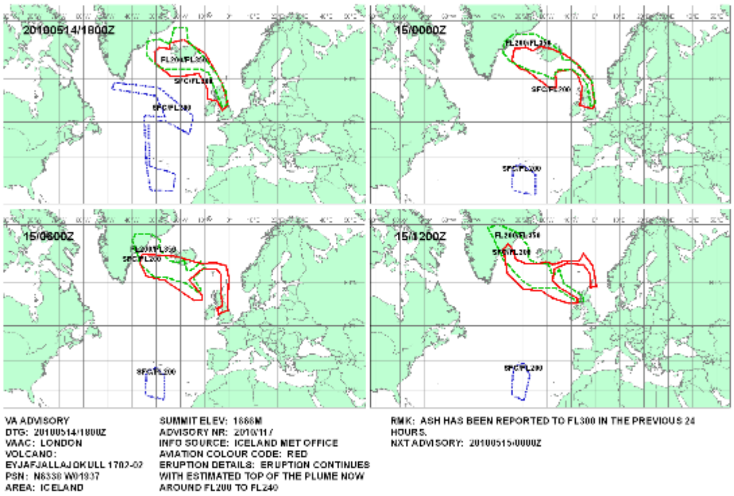


*Figure 29: Forecast ash concentration chart (Sample) of Eyjaf eruption in 2010*

*(Source: UK Met Office, April 2010)*

The forecast ash concentration chart, shown in *Figure 29* was introduced during the eruption of Eyjafjallajökull, showed six-hour averaged concentrations over three flight levels (FL000–200, FL200–350, FL350–550), where flight level (FL) represents aircraft altitude at a standard air pressure, and is approximately expressed in hundreds of feet, e.g., FL200 is 20,000 feet. However, observations of the Eyjafjallajökull ash cloud using ground-based Light Detection and Ranging (LIDAR) and research aircraft indicated that ash layers in the atmosphere were only a few hundred meters deep.

The ability to resolve the fine structure of an ash cloud in the modelling was limited by the explicit averaging of the output concentrations, and uncertainties also arose due to the assumed uniform vertical profile of the effective source, the time resolution of variations in the plume height and Mass Eruption Rate (MER), the temporal and spatial resolution of the driving meteorological factors and the sub-grid scale parametrizations applied.

ii. A Note on Recent Developments in NWP to Generate Met Data

Scientific and technological developments mean that weather forecast skill out to 3–10 days has increased by about one day per decade: in 2015, the 6-day forecast was as accurate as the 5-day forecast in 2005. Under the umbrella of the UM, in addition to the Global configuration, there are higher resolution regional configurations, referred to as Limited Area Models (LAMs). During 2010, meteorological data at a resolution of 12 km was generated for the North Atlantic and Europe region (NAE configuration). Unfortunately, the NAE configuration had a domain boundary that was very close to Iceland and therefore could not be used to track ash clouds arising from Icelandic eruptions.

Although both Global and NAE configuration forecasts suffered with decreasing accuracy with increasing forecasting time, it was clear that Global model output was the most appropriate dataset to use with NAME to simulate the transport and dispersion of volcanic ash clouds and was chosen to be the default met dataset used by the London VAAC.

To improve NWP forecasts by utilizing initial atmospheric state observations, the Global configuration now uses a hybrid ensemble/four-dimensional data assimilation system (Hybrid 4DVAR). This update considers the spread of observations over time and space and includes data from the Met Office's ensemble prediction system MOGREPS-G. The horizontal resolution of the Global configuration has therefore increased, from 25 km (in the mid-latitudes) to 17 km in 2014, and then further to 10 km in 2017.

iii. Accuracy Issues in Latest UK NWP Models due to Atmospheric Processes

The horizontal resolution of the NWP met data has increased significantly over the last decade, with higher resolutions expected to give better results. However, when the temporal resolution of the output met data is not increased inline with any increase in spatial resolution, the improvements seen in the accuracy of the dispersion modelling are only marginal. The Met Office is therefore currently considering whether there are benefits to using higher temporal resolution global met data (1 hourly) with our volcanic ash dispersion modelling.

The ability of dispersion models to represent thin and patchy ash structures is still limited by the representation of the released ash at the source, the horizontal and temporal averaging of the model output, the fact that dispersion models (both Lagrangian and Eulerian) present an average representation of the possible unresolved motions, and by the vertical resolution of NWP met data; the vertical resolution of the Unified Model (UM) Global configuration has not increased since 2010.

To predict the concentration of ash in the atmosphere, turbulent weather processes which act to disperse the ash must be represented. Currently, a uniform value for turbulence intensity is assumed in the free troposphere in NAME. Due to the intermittent nature of turbulence in the free troposphere, this assumed uniform value could lead to, in most cases, instances where turbulence is over-estimated, and excessive vertical mixing of material in the model, resulting in an underestimation of peak air concentrations. Dacre et al. found that by applying a parametrization for varying free tropospheric turbulence the representation of the depth of volcanic ash layers from the Eyjafjallajökull eruption was improved. This turbulence scheme has been further developed and included in the latest version of NAME. Work is now underway to consider the use of this parametrization in the set-up used by the London VAAC.

iv. Other NWP Strategies Explored for Ash Dispersion Modeling – Use of Ensembles

The concept of ensemble modeling is widely experimented in non-vulcanological severe weather scenarios such as the Ensemble Prediction Systems (EPS) as discussed in Biondi and Todini, (2018). The EPS acts as input to a hydrological and/or hydraulic model to produce river discharge predictions, often supported by some kind of Decision Support System. On these lines, VATDM developers were tasked to identify the best ensemble strategies, (such as, the ENSEMBLE project that could optimize ash forecasting and also NWPs themselves.

In particular, four different types of ensemble strategies were envisaged:

- Ensemble of different input conditions (according to eruption scenarios and data uncertainty ranges),
- Ensemble of different VATDMs (multi model) (on a single NWP),
- Ensemble of different NWP forecasts (on a single VATDM) and
- Combination of one or more strategies above.

It was also noted that there are several logistical constraints needed to be overcome if ensemble forecasting is to be operational during volcanic crises. This clearly shows that there is a pressing need for identifying a suitable methodology to accurately volcanic ash parameters.

As Earth's atmosphere is chaotic, even small perturbations to its current state can lead to significant changes to our future weather. The future state of the atmosphere therefore cannot be completely described with a single deterministic model forecast; instead, an ensemble of model runs is needed to fully predict all the possible outcomes. A good volcanic ash forecast should use an ensemble of met data to communicate a probabilistic assessment of the expected location and concentration of ash in the atmosphere.

The Met Office's MOGREPS-G system produces ensemble forecasts for the whole globe up to a week ahead. It generates 18 different weather forecasts and also attempts to represent uncertainty which arises due to errors in the NWP model itself by making small random variations to the forecast model. Therefore UK, Met Office is currently exploring possible approaches for using ensemble met data in the operational VAAC system. Stefanescu et al., (2014), discuss about the development of a probabilistic forecast for Eyjafjallajokull ash location with time that involves investigating the effects of aleatoric uncertainty associated with volcanic eruption source parameters and the wind field using suitable ensembles, and epistemic uncertainty associated with the advective equations of motion by investigating outputs of both multiphysics and spectral ensembles. Such ensemble supported analysis are claimed to be much needed in complex environments to provide Operational Decision Support using a Dynamic Data-Driven Application System (DDDAS) paradigm.

In addition, the chaotic nature of our atmosphere means that small errors in temperature, winds or other NWP variables can be amplified with time. Errors in the Global UM met data used by the London VAAC during their response to the 2011 Grímsvötn volcanic eruption's ash cloud caused the NAME simulations to forecast the transport of the plume further south than was observed. Post-event comparison to simulations with other NWP models pointed to the need to consider using ensemble met data, which are generated from running the NWP model multiple times with perturbed starting conditions. This would allow the operational meteorologists to assess the uncertainty associated with forecast met data in the volcanic ash model simulations.

v. Other NWP Strategies for Dispersion Modeling - Coupled NWP-VAFTD Approaches

The VAACs use offline coupled modelling systems in which the NWP is run independently to generate the met fields needed by the dispersion models. An alternative approach is to use an online strategy whereby the dispersion model is embedded within the NWP model. This approach has the advantage that it can directly incorporate the impact of the volcanic ash on the weather, including its effect on radiative heating and cloud formation. Furthermore, the particle transport is directly tied to the temporal and spatial resolution of the NWP model. This helps to avoid inaccuracies associated with the handling of atmospheric processes occurring on timescales smaller than the typical coupling intervals used between offline dispersion and NWP models. However, online approaches are computationally demanding and not without a range of as yet poorly constrained and only partially researched challenges.

For operational use, an offline approach would likely be configured over a limited area to manage computational cost and run time. It can be challenging to set the extent of the domain when the transport of the plume is not yet known, and this approach would also suffer from the same problems associated with the use of regional configuration data that were discussed earlier.

To reduce temporal resolution errors associated with its offline application, the London VAAC performs a linear interpolation in time to the meteorological fields, and it should be noted that data assimilation in the NWP necessarily incorporates the impact of the volcanic ash on future weather predictions, which are updated every 6 h. Further research, evaluation of the impact of greater coupling across a range of scenarios and model inter-comparison studies are needed to fully constrain the impacts associated with using offline versus online modelling strategies for the generation of operational forecasts of volcanic ash clouds.

In summary, although there are several Volcanic Ash Forecast Transport and Dispersion (VAFTD) models to forecast the dispersion contours and concentrations of a variety of weather and ash related variables, nearly all models rely on Numerical Weather Prediction (NWP) model outputs for accurate prediction estimates. In the absence of any well-defined ash signatures, any small error in the initialization stages of the NWP weather variables, can magnify the errors in subsequent iterations drastically and severely impact the quality of the decisions to be taken.

Most NWP models used in the context of ash dispersion rely on ensemble approach to simulate various combinations of predictions and finally decide based on the ensemble average. Also, most of these NWP models have larger grid sizes and as a result do not capture the small-scale spatial variations commonly occurring in ash concentrations. Therefore, modeling weather parameters accurately is critical to the success of any model that estimates the concentration or transport or dispersion of volcanic ash in the atmosphere.

## 4. Why is Air Temperature a good proxy for Ash Dispersion Modeling?

Weather is the state of the atmosphere, describing the degree to which it is hot or cold, wet or dry, calm or stormy, clear or cloudy. Weather is primarily indicated by 3 components: temperature, air pressure, and moisture differences between one place and another. Even among these three prime variables, surface pressure is caused chiefly due to difference in temperature values arising in differential heating of the earth's surface. Even in the absence of water bodies on the ground, elevation gradients in terrains can give rise to different air temperatures at a given altitude. Therefore, temperature differences due to presence or absence of sunlight is the single most important external factor that causes variations in weather on earth.

The temperature variable is also largely consistent across spatial scales. Very rarely, it is abnormally variant at shorter distances in the absence of natural disasters. For example, the images in *Figure 30* shows a 2.5-mile-long hail swath observed by a pilot at Northern Colorado, USA despite a high temperature of 80 degree Fahrenheit on 14th May 2015.

*Figure 30: Hail Swath observed from aircraft platform on May 14th, 2015*

*(Source: https://weather.com/storms/severe/news/2018-05-17-colorado-hail-swath-from-the-air)*

Up to 2 feet accumulated hail was observed on ground. The same hail swath, shown in *Figure 31*, was observed using satellite imagery clearly only due to lack of clouds.

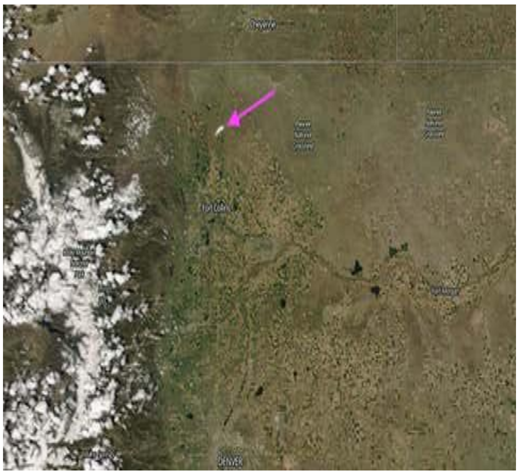

*Figure 31: Hail swath shown by arrow as observed from NASA Terra Satellite on 15th May 2015*

*(Source: https://weather.com/storms/severe/news/2018-05-17-colorado-hail-swath-from-the-air)*

This shows that, even more, in the case of severe weather scenarios, smaller spatial events are not best observed using traditional remote sensing methods due to turbulent conditions of the atmosphere. Although vog, shown in the *Figure 32* created due to sulphurous gases from volcanic eruptions serve as a proxy for ash detection, it cannot be used as a consistent marker in the case of resuspended ash and for ash clouds dispersed far away from the vent and are in negligible quantities. Because vog is a combination of fog, smog in addition to other volcanic gases. So, there is a need for consistent weather phenomenon to be identified as a proxy for the presence of volcanic ash in the atmosphere, irrespective of distal or concentrated quantities.

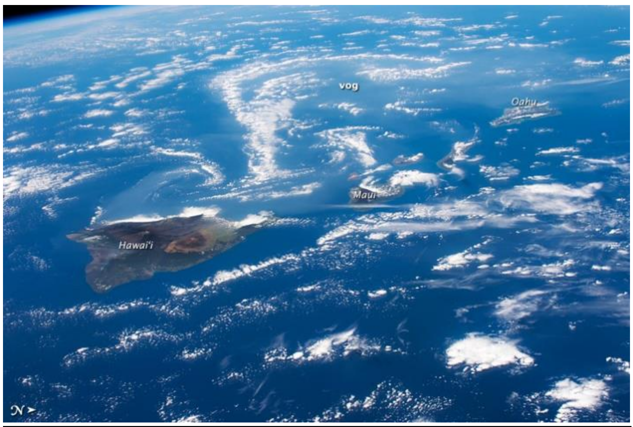


*Figure 32: Similarity between ash and Sulphurous vog in Hawaii, USA as seen from International Space Station in February 2015*

*(Source: https://earthobservatory.nasa.gov/images/85456/volcanoes-vog-and-vortices)*

The above example shows that a parameter like temperature despite which is usually assumed to be a static component in the case of normal weather scenarios and found to vary inversely only across large latitudes, can, in fact, vary significantly even in very short spatial scales during severe weather. While the occurrence of severe weather such as hail are at least limited to certain latitudes and can be detected by RADARs, volcanic ash eruptions are neither bounded by such geographical limitations nor detected using such sensors readily. In fact, ash particles have the potential to turn into Ice Nuclei/Cloud Condensation Nuclei due to their hygroscopic nature and pose additional threats, as discussed in the Martucci et al., (2012), O'Dowd et al., (2012), Martucci et al., (2012). So, any sudden changes in air temperature serves as a good proxy for potential ash cloud for detection and can thus be used to prevent inadvertent flight into such plumes.

Secondly, weather variables such as wind speed, humidity etc are measured for real time, in-situ weather monitoring via airborne platforms. This involves sampling and then processing the air drawn through pitot static in the aircraft, which would get rapidly and densely clogged with ash if aircrafts were to inadvertently entry into ash rich regions, especially at high speeds. On the other hand, air temperature (especially outside air temperature or true air temperature) is typically measured by a thermometer probe fitted on the surface of the aircraft, as shown in *Figure 33*. As a result, even in the event of losing information from all the onboard weather sensors, due to the electrical and chemical properties of ash, temperature input alone is largely unaffected.

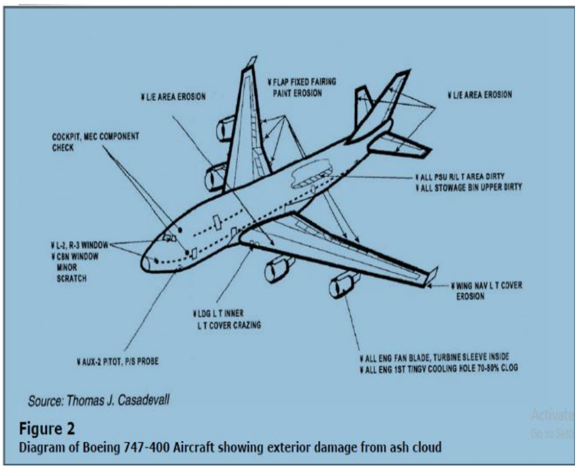


*Figure 33: Typical Flight Surfaces that experience friction with particles like Sand only at ground*

*(Source: https://www.aerohabitat.org/airmanshiponline/marzo2003/21-Volcanic%20Hazards%20and%20Aviation%20Safety.pdf)*

Thirdly, even a big jet aircraft such as Boeing 747, can glide safely for half an hour under most wind speed conditions. But even a marginal change in the temperature of the jet engine due to heavy rains or icing or ash melt can immediately cause flame out. As a result, temperature fluctuations act as a very critical, early warning proxy for detecting potential volcanic ash exposure.

Fourthly, while every platform and sensor to detect ash directly or indirectly has disadvantages such as the need for low pressure/environment for their functioning in the first place, there is a need for an approach that is fundamentally built to turn the very disadvantage itself into an advantage and thereby uses it to detect ash. By using temperature anomalies, the ash detection problem can be near accurately identified. The problem of false positives reported by other prediction and modeling methods with respect to normal ice clouds, desert sand etc are also neatly categorized by using the well-established signatures of such regular severe weather phenomenon and excluding the possibility of such phenomenon causing abnormal temperature values in the atmosphere.

Fifthly, since estimating the density of the ash is critical to shutdown of engines mid-air, temperature profiles, as shown in *Figure 34*, can be used as the perfect input for modeling and prediction of airborne ash densities and distributions.

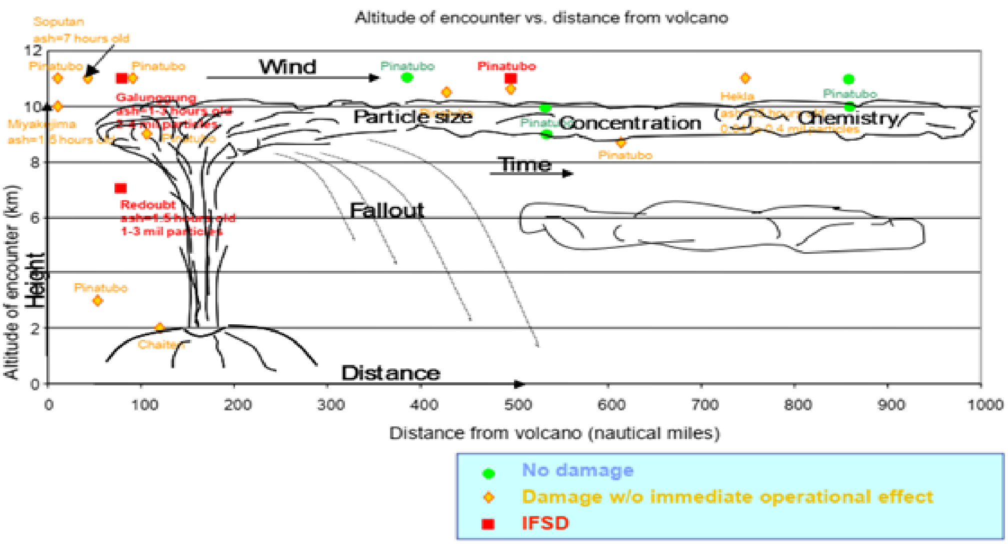


*Figure 34: Engine Damage Correlates with Cloud Age, Particle Size*

*(Source: GE Aviation Report, January 2019 - https://www.itafsc.org/wp-content/uploads/2019/07/Caso_Studio_-_I._Oddone__Air_Dolomiti.pdf)*

Apart from classifying any matter based on physical or chemical properties, they can also be studied using their intrinsic or extrinsic nature. Intrinsic or intensive properties are properties that are within the substance and do not depend on the amount of material that you have. Whereas extrinsic or extensive properties are properties that depend on the amount of the substance you have. All size measurements depend on amount, so all size measurements are extrinsic properties. Ash being microscopic particles, it is impossible to measure their size, as shown in the *Figure 35* or their shape as shown in *Figure 36* as they are amorphous in nature.


*Figure 35: Ash Particle Size in Comparison with other Particulate Matters – Electron Micrograph of a single ash particle shown together with some other common materials, US EPA.*

*(Source: Dmochowska, Anna. (2018). Hazards associated with municipal waste storage Vol. II. MATEC Web of Conferences. 247. 00033. 10.1051/matecconf/201824700033);*

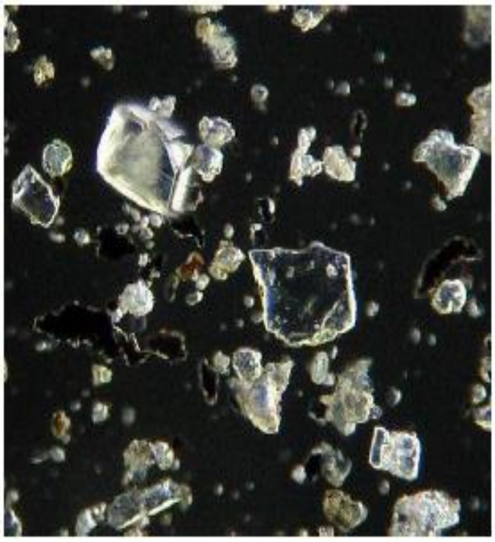

*Figure 36: Irregular Shape of Ash Particles*

*(Source:https://grrlscientist.medium.com/how-are-birds-affected-by-volcanic-ash-grrlscientist-d93451850c9)*

At the same time, it is very essential to establish the quantum of ash that can be tolerated to declare a safe airspace, as shown in *Figure 37* and *Figure 38*. Thus, the rate of change in temperature values can be supported using other quantities humidity to predict density thresholds to maximize the available airspace during volcanic eruption events.

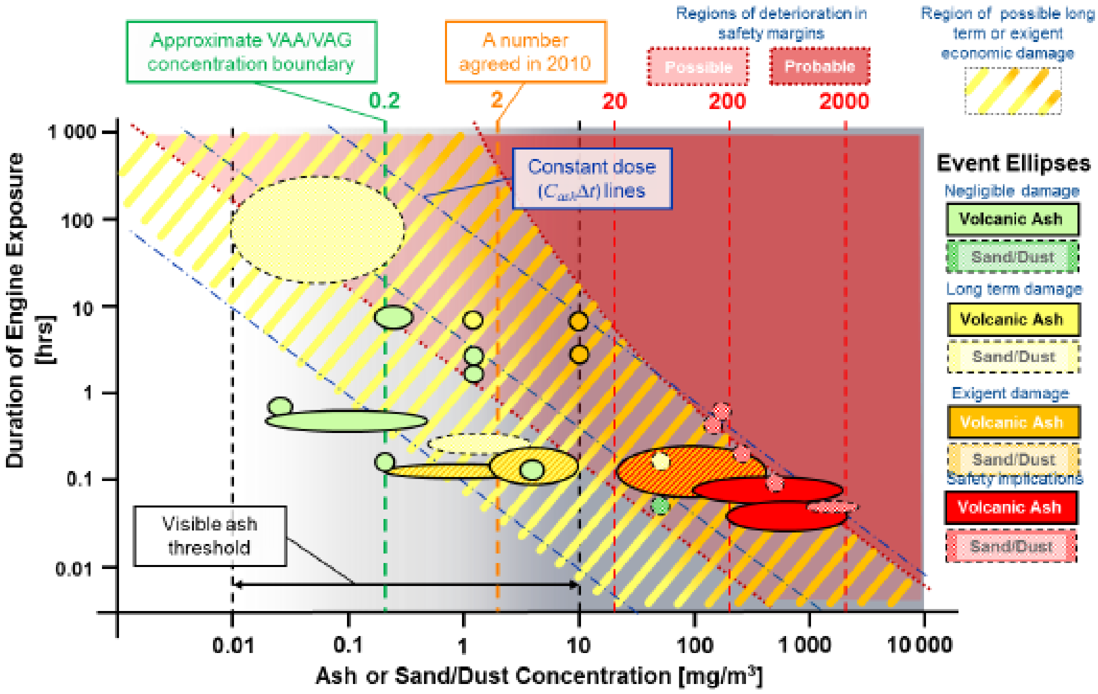


*Figure 37: Duration of Exposure versus Ash Concentration Chart by Rolls Royce*

*(Source: Volcanic Ash Impacts on Jet Engines and Developments Since 2010)*

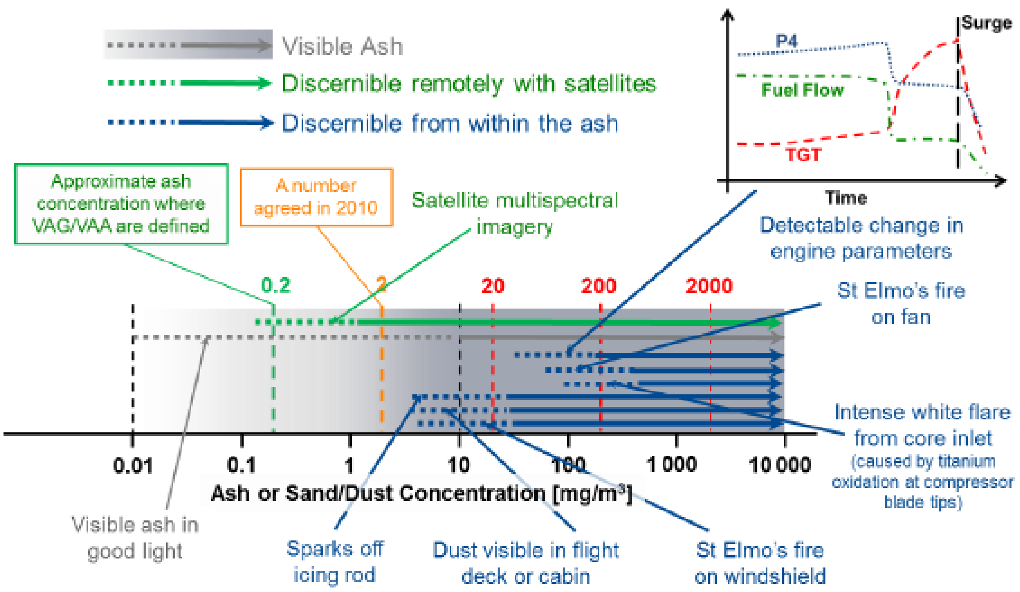


*Figure 38: Rolls Royce Engine Exposure Studies: Visible and Discernible ash plotted against ash concentration*

*(Source: Volcanic Ash Impacts on Jet Engines and Developments Since 2010)*

Lastly, temperatures can be measured in a variety of scales. Even if Celsius representation has zero and negative values, the readings can be converted to Kelvin scale to avoid numerical processing issues. So, the linear nature of temperature is yet another advantage while processing unlike precipitation which varies in units of metre and is tied to the area of measurement and the duration of the event. While rainfall, snowfall or hail are highly directional, their measurement units vary and are at times even reported using temperature units. Whereas temperature is the single unit that is used at terrain level and at atmospheric level irrespective of the gases present and presence of different forms of water in the atmosphere. Although temperature is a 3-dimensional in nature, it is not reported with different values in each direction in a given parcel of air. On the other hand, a variable like wind direction is resolved into x, y and z directional components and is cyclic in nature.

While air the temperature of the buoyant ash closer to the eruption column might be significantly higher than far away from the volcanic vent, the quantum of ash (diluted/concentrated) can significantly affect the temperature of the atmosphere even far away from the source. As a result, it is all the more essential to study this phenomenon using air temperature, since it is the best variable that can be used to understand the neighbourhood airspace in the event of volcanic eruptions to identify various dispersion patterns. Thus, irrespective of desiring to reduce the duration of exposure to ash or to decrease exposure to particulate concentration, air temperature can be used as a proxy property to model the spatial dispersion of airborne volcanic ash.

## 5. Problem Formulation

The aim of this research is to propose a methodology to generate the spatial distribution of volcanic ash spread using temperature as a proxy variable to understand the dispersion patterns of airborne ash in the neighbourhood airspace in the event of an eruption. To model and create a gridded air temperature map, which is as close as, to the actual dispersion of airborne volcanic ash, over synoptic scales, in terms of averages and variances, is an open issue. This is because, the accuracy of the model outputs, have a significant impact on decisions pertaining to safety and livelihood of humans across continents on air and ground. Traditionally, an extensive variety of geostatistical methods and simulation techniques have been experimented to model weather variables. Map generation based on model outputs from samples can be achieved by two methods. While Grid based techniques aggregate local observations into average values on a regular grid, Interpolation methods use values at target locations (eg: grid points) to create models.

NCEP is a grid-based NWP method that uses Ensemble Kalman Filter (EnKF) to prepare daily composites of weather data sourced from different sensing platforms. EnKF technique is equivalent to geostatistical conditional simulation, and it implicitly assumes Gaussian model. On the other hand, in this research, we present a geostatistical method, known as Kriging, to ascertain that, embracing a pure spatial analysis approach is a powerful framework to supplement grid-based methods to generate highly accurate prediction estimates, even in severe weather scenarios over synoptic scales. To demonstrate the same, initially we propose to use a Linear Regression Model to interpolate the air temperature data. Subsequently, we have experimented, Kriging which is a Non-Linear Regression technique. We chose two variants of Kriging, namely Simple Kriging (SK) and EBK (Unconditional Simulation – with &without transformation) techniques to generate prediction maps.

We intend to investigate if with sparse, heteroskedastic datasets, can a technique like Kriging be an effective method to model and understand the volcanic ash dispersion. Severe weather events are significantly different from normal weather scenarios because the environment is rapidly changing due to turbulence across the horizontal and vertical extents of the atmosphere. Applying classical statistics with the assumption that variables are independent of each other and that Gaussian distribution models are appropriate to model severe events requires to be challenged. With Gaussian models, the concept of averages is rendered meaningless since the variability of the sample data points is similarly distributed before and after mean values. When there are no well-defined means and variances in a spatial domain under study, additive models that have both positive and negative variations induces constant effects across the study region. On the other hand, multiplicative models such as Power Law distributions have only positive deviations and are highly directional towards infinity. As a result, power laws with no average and no finite standard deviation and therefore can be used to model heavy tailed (fat /long and cluster) scenarios. Instead of assuming that events are interdependent of factors like location, spatial statistics helps correlate the influence of location patterns across events and realizations.

While near-homogenous dispersions and randomness can be easily identified, it is extremely difficult to model clusters using frequentist approaches. So, a combination of partitioning approaches using Bayesian methods is inevitable to accurately model a given natural phenomenon.

Conditional simulation techniques that support multiple realization approaches, such as Turning Bands, EnKF etc mostly produce global estimates of the random field honoring the means and variances. On the other hand, traditional kriging methods (such as Simple Kriging, Ordinary Kriging, Universal Kriging) require the assumption that the random field under exploration belongs to a single realization.

As a result, there is a need to identify algorithms that are most suited to interpolate samples even from clustered spatial distribution patterns to produce both global and local means and variances with minimal errors, for a given region without assuming, that, the samples originate from a single realization.

## 6. Use of GIS and Geostatistics in Interpolation of Temperature

Geospatial analysis is an approach to applying statistical analysis and other analytic techniques to geographic or spatial data using Geographic Information System (GIS) software to render maps. Since the aim is to generate a spatial model to understand the natural phenomenon, the first step involves understanding the association between the attribute and location data. Since the analysis to be performed is purely spatial in scope, there is a need to quantify the spatial patterns and then use it to make predictions of variables at unsampled locations. Also, many datasets from real world scenario have inherent randomness, a stochastic approach is largely required to deal with uncertainties. Since non-normality in data is to be expected, regression technique was chosen over Analysis of Variance (ANOVA). If the data samples have groups of unequal variances, then they give rise to unbalanced design due to crossed random effects. In which case, the dataset needs to be analysed by both transforming the data to normality and without applying any transformations.

Among the 12 VATDMs benchmarked in the Volcanic Ash Workshop held in 2010, 7 models required some form of data interpolation algorithm to estimate ash concentrations. Also, 9 of those models required temperature as an input weather variable for their respective NWP model. In particular, NCEP NWP is used by the following VAFTDs: Hysplit, Modèle Lagrangien de Dispersion de Particules d'ordre zero (MLDP0) and Volcanic California Puff (VOL-CALPUFF) Model.

Regression based techniques have been traditionally to interpolate weather variables. For this study, we initially evaluate the suitability of Linear Regression method. In addition, Geostatistics based non-linear regression interpolation technique, called Kriging, originally applied in ore mining industry, as discussed in *paper* [34] is proposed to be investigated. The cross application of Kriging method for atmospheric problems is a novel exploration in the context of volcanic ash events. In particular, a Bayesian variant of Kriging using the concept of Generalized Covariance Functions is being rigorously validated against international Numerical Weather Prediction Model outputs in this study to generate risk maps for aviation safety.

Geospatially enabled tools using Kriging on temperature as proxy variable will enable preparation of surface outputs at least an hour before ash potentially impacts a FIR or other VAAC areas. Even in the absence of any eruption, such spatial models can be run to simulate potential disasters at a lesser cost for various combinations of weather variables and intensities of the chosen variables. This methodology could be used to even simulate scenarios where no known or named volcanoes exist in both single realization and ensemble models.

In this study, only the horizontal component of weather, expressed in latitude/longitude coordinates are initially considered. The vertical component (altitude) of the sampled data is averaged and assumed to be at a single pressure level. This is assumed rightly so, because the environment is anyhow in a state of flux during such events.

## 7. Defining Go/No-Go Regions

While the primary objective of the research is to model past eruption to understand the phenomenon better spatially, this research can also be applied directly and indirectly in related problems. As part of this research, we intend to propose a validated method to define and visualize the go and no-go regions by generating risk maps that can aid in improving the safety air traffic management during such disasters.

## 8. Objectives

The following objectives are chosen for this research:

1. Study and analysis of different interpolation techniques to determine which method of spatial interpolation is suitable for 3D ash cloud modeling.
2. Evaluate different kriging methods along with error estimations to validate if Geostatistics can provide good estimate of temperature values at different altitudes
3. Arrive at a method to visualize the ash temperature distribution for categorizing Go/No-Go regions and to classify the patterns and bands around a set of observations.

The application of a relatively new variant of a geostatistical technique called Empirical Bayesian Kriging in the context of volcanic ash, which hitherto, has not been attempted in any of the research till date. Through this, we address the chief debate in this field, which is to identify a reliable, probabilistic method that is capable of estimating both predictions and uncertainties to augment the deterministic methods currently in use for the International Volcanic Ash Task Force (IVATF) authorities to aid in robust decision making.

## 9. Structure of thesis

In Chapter 1, the problems due to airborne volcanic ash is introduced, supported by a review of literatures pertaining to the modeling of ash, how Numerical Weather Prediction models play key role in ash dispersion models, formulate a specific problem statement related to inadequate accuracy in air temperature modeling observed in NWPs and propose how a geostatistical approach would be appropriate to address the gap. In Chapter 2 the study site chosen is described along with validation datasets and exploratory spatial data analysis. Chapter 3 discusses two methodologies to generate spatial distribution of ash temperature - viz Linear Regression and three variants of Non-Linear Regression technique, namely, Kriging. The prediction and error estimates are verified, global profiles are analysed and compared to validate against the NCEP NWP validation dataset. Chapter 4 discusses in detail the point and block grade errors observed at global and local scales in kriging estimates to identify the most appropriate ash temperature modeling strategy among the three chosen methods. Chapter 5 deals with a potential application of the chosen kriging method in the aerospace industry. Finally, in Chapter 6, the benefits, limitations and scope for future work are discussed in conclusion.

# II. Study Area and Study Sites

## 1. Study Site

The European airspace shutdown from 14th April 2010 due to the explosive eruption of the Icelandic volcano, Eyjafjallajokull marked the beginning of the largest shut-down of air traffic since the Second World War. The effusive eruption started on March 20$^{th}$ and lasted till April 12th. But the ash plumes from the explosive eruption phase travelled around 900 miles within 24 hours and blanketed Northern Europe. In the ensuing six days 95,000 flights were cancelled across Europe, costing airlines an estimated £1.1 billion. The UK Treasury lost £30m of revenue from air passenger duty, with British hotels, restaurants and shops also taking a significant financial hit. It has been estimated London's economy alone was left £100m out of pocket by the end of the flight ban.

Initially, within the area at risk from ash, the ban was absolute, leaving up to one million British passengers marooned abroad. However, as the threat continued there was mounting pressure to remove the blanket ban and get some flights moving again. As a result, aircraft engine manufacturers released details of a maximum concentration of ash that their engines could withstand. The issue was that ash concentration is hard to measure directly. Meteorologists at the Met Office's Volcanic Ash Advisory Centre (VAAC) were included in decision making by mathematically modelling the ash cloud. Wilkinson et al., (2012) discusses the extent of disruptions caused in European Airspace in 2010. The map of various regions in Europe affected during April 2010 is depicted in *Figure 39*.

*Figure 39: Impact to European Airspace in 2010 - Open (light green) and closed (grey) FIR in Europe on 15th April, 18th April and 21st April 2010*

*(Source: https://www.researchgate.net/figure/Open-light-green-and-closed-grey-FIR-in-Europe-ie-airspace-for-a-15th-April-b_fig1_251417365)*

In particular, Thordarson and Larsen, (2007) and Sturkell et al., (2010) discuss about the nature of two specific volcanoes that can disrupt air traffic due to widespread ash dispersal. While the Hjaltadóttir et al., (2015) discuss the history of past eruptions of Eyjafjallajokull, Saltykovskii, (2012) discuss in detail the specific eruption of 2010. Although there are several meteorological stations present close to the vent, Denlinger et al., (2012) and Gislason et al., (2011) discuss the issues in detection of ash due to various factors related to weather.

During the resurgent May 2010 eruption of Eyjafjallajokull volcano, as shown in *Figure 40*, ash was dispersed across the European airspace for several days (Latitude: 54.2992 to 63.633333 and Longitude: 3.557819 to 19.6). Facility for Airborne Atmospheric Measurements (FAAM) aircrafts, shown in *Figure 41*, were flown in sync with satellite overpasses for multiple days, near potentially hazardous ash laden regions to collect a variety of scientific data. British Atmospheric Data Centre (BADC) released a subset of the weather data for academic research purposes.

*Figure 40: Photo of Eyjafjallajokull Eruption in Iceland on 8th May 2010 during clear weather conditions*

*(Source: [https://phys.org/news/2010-04-iceland-volcanic-ash-halts-flights.html](https://phys.org/news/2010-04-iceland-volcanic-ash-halts-flights.html))*

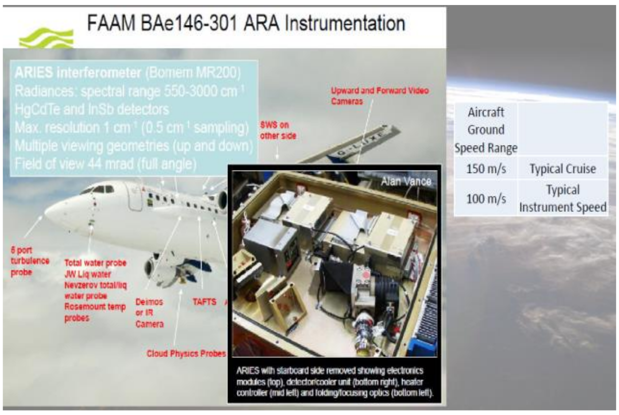


*Figure 41: FAAM Bae 146-301 ARA Instrumentation*

*(Source:https://cimss.ssec.wisc.edu/itwg/itsc/itsc18/program/files/newman_volcanic_ash_itsc18.pdf)*

The data from "Dataset Collection Record: Eyjafjallajokull Volcanic Ash Cloud Measurements and Imagery," n.d.(2010) collected using a BOMEM Michelson interferometer, on four days (May 14, May16, May 17, May 18) was chosen for this study. While the field sampling durations extended several hours, a small portion of the recorded data, considered to be ash-significant region, was handpicked for this research. The dataset for this research was created by mapping univariate temperature data against the flight path information and by referring to the discussions made amongst the scientific crew about the intensity of ash spread during the sorties.

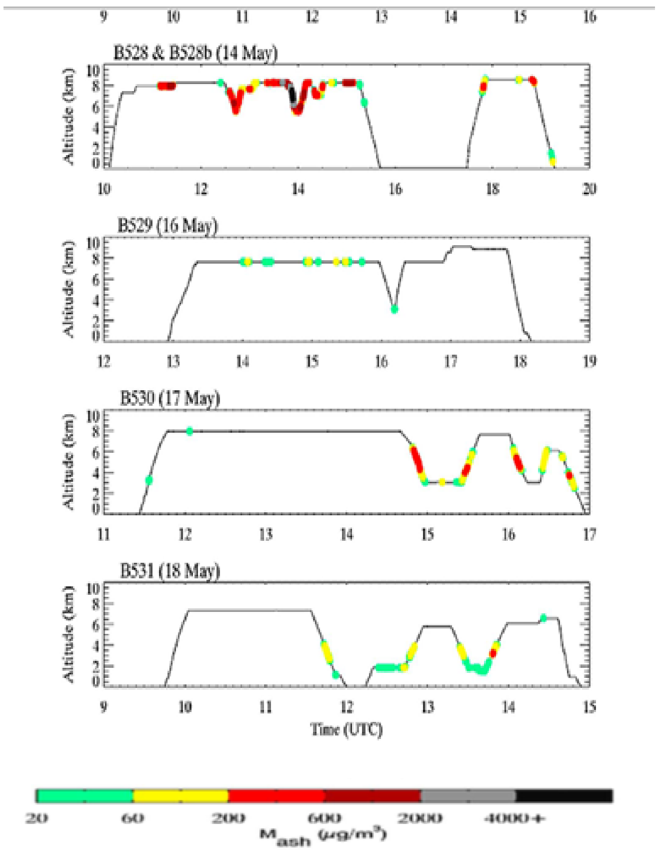


*Figure 42: Location, Timestamps and Density of Ash Distribution*

*(Source: https://agupubs.onlinelibrary.wiley.com/doi/full/10.1029/2011JD016760)*

It is interesting to note the legend for the above graphs is left open on its higher limits (4000+ microgram of ash), as shown in the *Figure 42*. Data collection experiment for volcanic ash dispersion has been primarily conducted with sole aim to determine the jet engine tolerance thresholds. As a result, the sampling process cannot be stated to be adequate or appropriate for predictions over large areas and which areas are affected to which extents. It is not just enough to identify significantly high ash areas, but the sampling strategy must also be able to bring out patterns of ash concentrations.

The data collected is shown in the below map within the Minimum Bounding Region (MBR) which includes the vent location as shown in the *Figure 43*. Although 4 days datasets were available for this research, only 3 days (May 16th – 221 points, 17$^{th}$ – 288 points and 18$^{th}$ – 240 points) data were used to develop the model. 14$^{th}$ May data (122 points) was reserved for model validation needs. A unique sample for vent and 3 dummy points were included in the dataset to mark the minimum bounding region comprising totally of 875 data points.

*Figure 43: Map showing the MBR with Data Locations w.r.t. Volcanic Vent over Europe*

For the 4 days of flight data, 16th, 17th and 18th were used as input, while 14th data was considered as test dataset for evaluating the accuracy of estimations. The MBR encompasses around 5 lakh square Kilometres of area. The temperature distribution across those days were compared and plotted as shown in *Figure 44*.

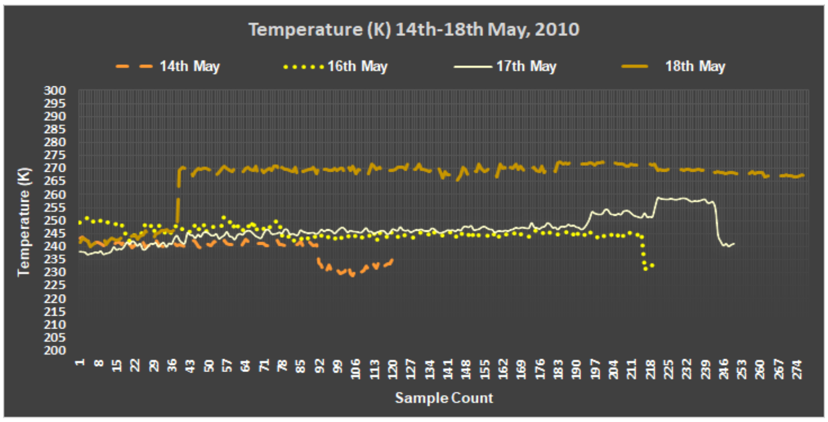


*Figure 44: Temperature Distribution Plot of Data Samples*

The spatial distribution of the data points across each day varies significantly. Although the total distance covered each day for sample collection is around 40 km, the leg velocity varies between 0.03 m/s (on 18$^{th}$ May) to 740 m/s (on 14$^{th}$ street).

Also, the dataset reveals clustering phenomenon and complex anisotropic processes. The map shown in *Figure 45* reveals for each point, the direction in degrees, to the nearest source and a complex anisotropy is observed for the chosen dataset.

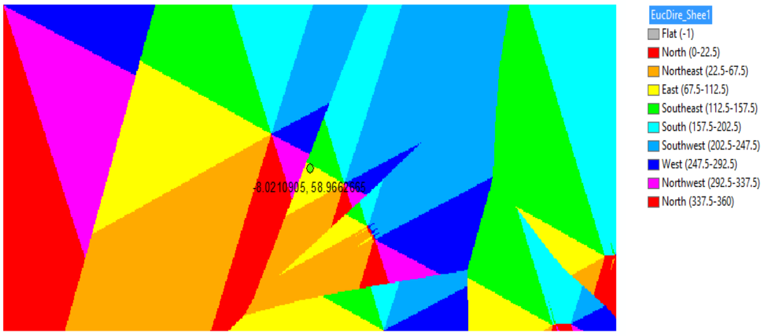


*Figure 45: Euclidean Map revealing high degree of anisotropy observed in the study site*

## 2. Validation: NCEP NWP Gridded Reanalysis

\

An Ash Dispersal Forecast and Civil Aviation Workshop was conducted post eruption to benchmark 12 dispersion models based on ash & weather data from the Hekla eruption in 2000. Ash concentration contour maps were generated at different flight levels. While all the operative models were tested and compared based on properties of ash, this study focuses on temperature variable as a proxy to model the ash dispersion.

The input climate/weather data used in these VATDs included only reanalysis datasets: ECMWF ERA-40 and NCEP/NCAR reanalysis-1. ECMWF stands for European Center for Medium Range Weather Forecasts while NCEP/NCAR stands for National Center for Environmental Prediction/National Center for Atmospheric Research. The former is available only for the period 1957- 2002 while the latter from USA is continuously updated from 1948 to present. Since this research involves modeling of 2010 eruption at synoptic scales, NCEP/NCAR was therefore chosen as validation dataset.

Although the workshop used only reanalysis version 1, this research used the updated dataset Compo et al., (2011) from version 2c of NCEP/NCAR reanalysis since it is available for the given region under study for the said time period. Although, v3 based dataset was also released by NCEP/NCAR, the interpolation algorithm used between version 2c versus version 3 with respect to generation of daily composites did not have significant changes. So, v2c, being closer to v1 was finalized as validation dataset for this study.

Data for each day was downloaded from the as referenced in the *repository by* Compo et al., (2011) according to the pressure altitude of the flight routes (350 mb/400 mb/700 mb/800mb), and required time slots (set to European Projection configuration). The Air Temperature weather variable daily composites were downloaded for the period of 14th May 2010 to 18th May 2010 for this study.

## 3. Analysis of Validation Dataset

The initial step was to understand the temperature profiles simulated by NWP models such as NCEP, theoretically, over continental, and oceanic Europe for the same period and region of interest. Daily composites for the period between May 14th to May 18th were compared annually from 2008-2011. From the minimum and maximum temperature values predicted at 350/400/700/800 mb Pressure Altitudes, it was observed that there were no variations in temperature greater than 8K in total. Contrastingly, May 17th, 2010, samples (collected by flight) revealed a variation of up to 22K even at very short spatial scales. Further, up to a 27K drop in air temperature was observed on May 17th when compared against the usual Environment Lapse Rate (ELR) (expected at 700 mb). From the *Table 3*, it is observed that there is no significant difference in temperature values (in Kelvin) between the input days (161718) and validation days (14161718) with respect to NCEP.

| **Year (Date)** | **Pressure Altitude** | **Minimum Temperature** | **Minimum Temperature** | **Maximum Temperature** | **Maximum Temperature** |
|---|---|---|---|---|---|
| Fused - 2008 | | 1415161718 | 161718 | 1415161718 | 161718 |
| | 350 mb | 228 | 234 | 244 | 252 |
| | 400 mb | 232 | 234 | 252 | 252 |
| | 700 mb | 258 | 255 | 282 | 285 |
| | 800 mb | 264 | 265 | 291 | 295 |
| Fused – 2009 | 350 mb | 232 | 232 | 244 | 242 |
| | 400 mb | 238 | 238 | 250 | 250 |
| | 700 mb | 262 | 262 | 280 | 282 |
| | 800 mb | 267 | 267 | 291 | 291 |
| Fused - 2010 | 350 mb | 234 | 234 | 246 | 246 |
| | 400 mb | 240 | 240 | 254 | 254 |
| | 700 mb | 264 | 264 | 285 | 285 |
| | 800 mb | 270 | 270 | 294 | 294 |
| Fused - 2011 | 350 mb | 230 | 230 | 246 | 248 |
| | 400 mb | 234 | 234 | 254 | 254 |
| | 700 mb | 256 | 255 | 282 | 285 |
| | 800 mb | 265 | 265 | 290 | 295 |

*Table 3: Comparison between Input Days (14161718) & Validation Days (161718) By Overlaying Individual Days*

But when NCEP temperature values was compared against flight data for 2010, as shown in *Table 4*, it is observed that for the samples collected on May 17th and May 18th the values signal very turbulent atmosphere, with a deviation of up to 27K from usual Environment Lapse Rate which the NCEP NWP is designed to faithfully honour.

| Year | Pressure Altitude | NCEP – Minimum Temperature (K) | NCEP – Maximum Temperature (K) | Flight – Minimum Temperature (K) | Flight – Maximum Temperature (K) |
|---|---|---|---|---|---|
| Fused - 2008 | 350 mb | 228 | 244 | - | - |
| | 400 mb | 232 | 252 | - | - |
| | 700 mb | 258 | 282 | - | - |
| | 800 mb | 264 | 291 | - | - |
| Fused - 2009 | 350 mb | 232 | 244 | - | - |
| | 400 mb | 238 | 250 | - | - |
| | 700 mb | 262 | 280 | - | - |
| | 800 mb | 267 | 291 | - | - |
| Fused - 2010 | 350 mb | 234 | 246 | 229 | 244 |
| | 400 mb | 240 | 254 | 231 | 252 |
| | 700 mb | 264 | 285 | 237 | 259 |
| | 800 mb | 270 | 294 | 266 | 273 |
| Fused - 2011 | 350 mb | 230 | 246 | - | - |
| | 400 mb | 234 | 254 | - | - |
| | 700 mb | 256 | 285 | - | - |
| | 800 mb | 265 | 294 | - | - |

*Table 4: Comparison between Flight Averages (14161718) and Validation Days (161718) for Individual Days*

The individual and fused NCEP air temperature (in kelvin) dataset for various days are plotted over World Map in the below figures for the required Minimum Bounding Region. The individual days NCEP values were overlayed for a common scale of values to diverse and dissimilar inputs to create an integrated analysis. The input rasters were transformed into a 0/1 scale, indicating the strength of a membership in a set, based on a specified fuzzified algorithm. Alternatively, a weighted overlay can be generated using a common measurement scale and weights each according to its importance. *Figure 46* shows that coarse grid sizes used in NWP models do not accurately represent the state of the atmosphere even during large volcanic eruptions in any given region. The average temperature of the overlay created from using rasters of each day was ~253K.

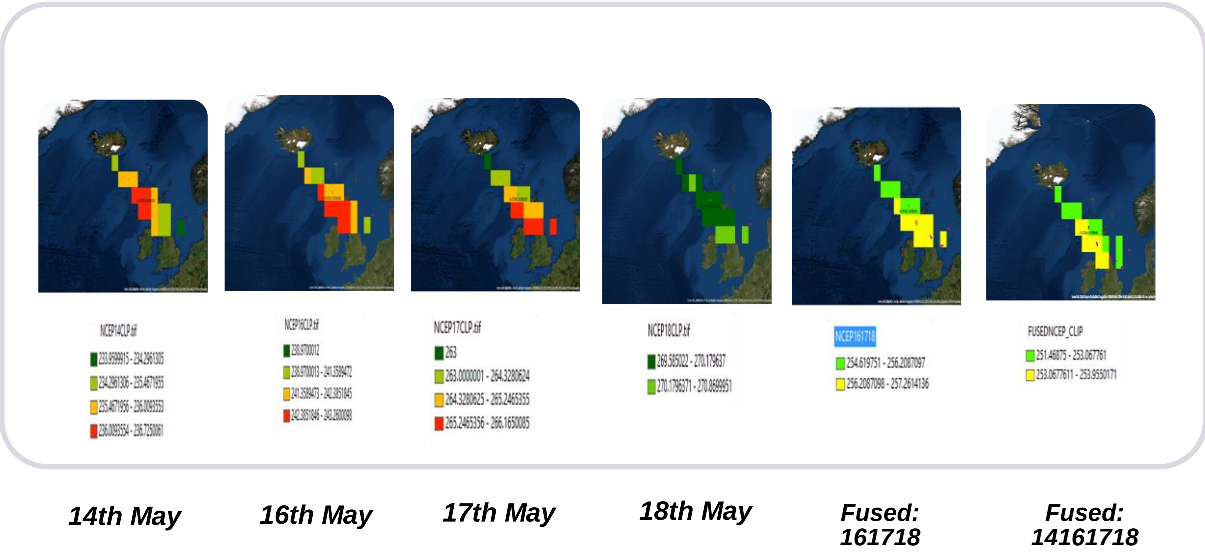


*Figure 46: Map showing Overlay of Grids of NCEP Rasters from Individual Days & Composites across Days*

Using the NCEP temperature values given in *Table 5* and *Table 6*, probability density graphs were generated, to visualize and study various statistical aspects related to the datasets.

| **Altitude (Feet)** | **NCEP14 (8K)** | **Input 14** | **NCEP16 (7K)** | **Input 16** | **NCEP17 (3K)** | **Input 17** | **NCEP18 (1K)** | **Input 18** |
|---|---|---|---|---|---|---|---|---|
| **Min** | 233 | 229 | 238 | 231 | 263 | 237 | 269 | 266 |
| **Max** | 236 | 244 | 243 | 252 | 266 | 259 | 270 | 273 |
| **Mean** | 235 | 239 | 241 | 245 | 264 | 246 | 270 | 270 |
| **Range** | 3 | 15 | 5 | 21 | 3 | 22 | 1 | 7 |

*Table 5: NCEP Temperature values against Input Data of Individual Days (in Kelvin)*

| Altitude (Feet) | Input 161718 | NCEP 161718 | Input 14161718 | NCEP 14161718 |
|---|---|---|---|---|
| **Min** | 231 | 254 | 228 | 251 |
| **Max** | 272 | 257 | 300 | 253 |
| **Mean** | 253 | 256 | 251 | 253 |
| **Range** | 41 | 2 | 71 | 2 |

*Table 6: NCEP Temperature values against Input Data of Overlayed Composites (in Kelvin)*

*Figure 47* shows the following plots that depict the temperature distribution on individual days and across days from May 2010.

i. Input Data: Individual 4 Days vs Combined 3 Days (16th, 17th, 18th May 2010)
ii. NCEP: Individual 4 Days vs Combined 3 Days (16th, 17th, 18th May 2010)
iii. NCEP vs Input Data: Combined 3 Days

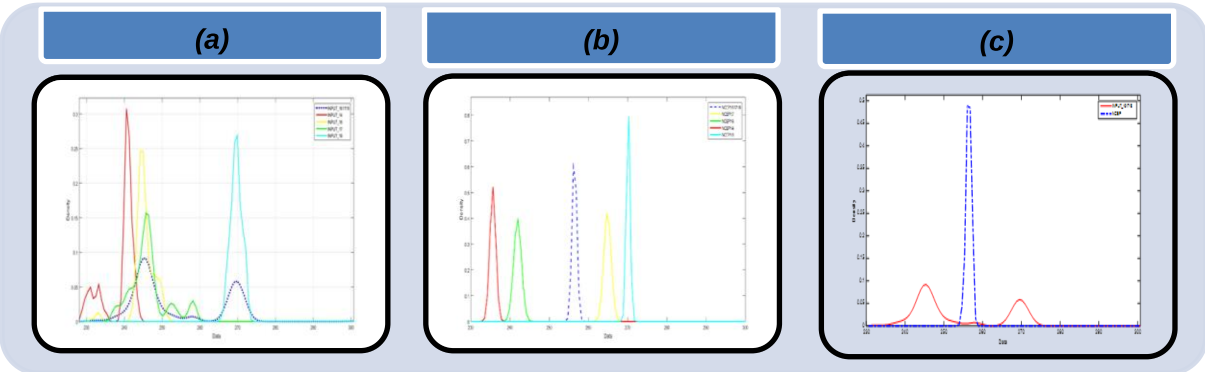


***Figure 47: Plots showing temperature distribution on individual days and across days from May 2010***

The reason why NCEP estimates do not capture the small-scale spatial variations is discussed in (Compo et al., 2011). The paper describes the interpolation approach used in NCEP models and discusses the limitations arising in accuracy of model outputs when EnKF is applied in the context of large geographic regions.

*In particular, the paper notes that: "As discussed by, e.g., Anderson and Anderson (1999) and Whitaker and Hamill (2002), sampling and model errors prevent the ensemble-estimated background error covariances from being optimal in the Kalman update equation (1). Such issues must be addressed to prevent 'filter divergence' wherein the update equations (1)–(4) weight the background too much and the observations too little. Cycling during such a condition reinforces the background and causes the filtered 'analysis' estimate to drift farther and farther from observations. Two methods are used to account for these sources of error: covariance inflation (Anderson and Anderson, 1999) and distance dependent covariance localization (Houtekamer and Mitchell, 2001; Hamill et al., 2001). Covariance localization (Houtekamer and Mitchell, 2001; Hamill et al., 2001) is a spatial filter that smoothly sets the ensemble covariances to zero beyond a specified distance. This reduces the potential for filter divergence arising from spurious long-distance correlations obtained using finite ensemble sizes."*

The assumption that there is poor correlation in long distance contexts and weighing the observations lesser than the background, constrains the accuracy of the NCEP model outputs since they are obligated to honor the mean and variances for a fixed geographic extent in 2D and 3D. As a result, Power Law based spatial interpolation models are also investigated. This is required so that both spatial factors and attribute properties in various clusters in any given random field is given appropriate weightage by constructing semivariogram of distances and variances.

## 4. Exploratory Spatial Data Analysis

Exploratory Spatial Data Analysis is performed as the initial step to get familiarized with the data and to detect patterns of regularity. Datasets are usually checked for three criteria primarily, namely, presence of normal distribution, stationarity and absence of trends. The summary statistics for the input dataset are captured below:

| | |
|---|---|
| Count | 753 |
| Minimum | 231.25 |
| Maximum | 300 |
| Mean | 253.46 |
| Standard Deviation | 11.785 |
| Skewness | 0.59215 |
| Kurtosis | 1.8588 |

i. Normal Distribution Check

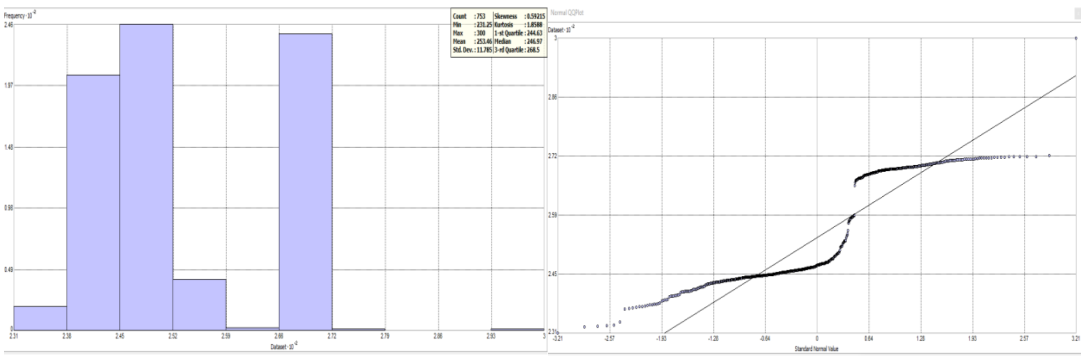

***Figure 48: Normal Distribution Check Using Histogram and Normal QQ Plot***

Since the histogram, shown in *Figure 48* has a bimodal peak, Gaussian Normality criteria is not met. Usually, log or box transformations. The mean is also expected to be close to median (253.46 vs 246.97). Skewness is expected to be close to 0 and was found to be ~0.59215. Kurtosis is expected to be close to 3 but was observed to be ~1.8588. There are no explicit outliers. The Normal QQ Plot generated shows that data does not follow 1:1 line. In such scenarios, applying Normal Score Transformation fits a smooth curve to the data to perform a quantile transformation to the normal distribution which is then transformed back at the end.

ii. Stationarity Check

Stationarity is defined as the statistical relationship between two points depends only on the distance between them. It means that statistical properties do not depend on exact locations. Therefore, the mean (expected value) of a variable at one location is equal to the mean at any other location. Voronoi maps (symbolized by Entropy or Standard Deviation) are used to assess stationarity by looking for randomness in the symbolized Thiessen polygons. Usually, if data is not stationary, then, transformations can stabilize the variances after removing trends to make the data constant. Since the dataset had significant heterogeneity, Voronoi maps could not be effectively generated. As a result, EBK technique was chosen to process the non-stationarity observed in the data. Empirical Bayesian Kriging can be used to treat local variance separately. Instead of variance being similar in a whole extent, EBK performs kriging as a separate underlying process in different areas. It still performs kriging but is done at a local scale. In this context, it is important to calculate another metric named, Global Moran's Index (I), as shown in *Figure 49*.

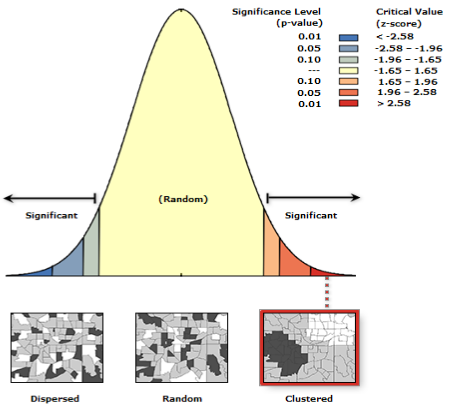


*Figure 49: Global Moran's Index*

---

- Given the p value, which is the probability of value zero, it could mean that it is very unlikely (small probability) that the observed spatial patterns is the result of random processes.
- Given the z-score, which is the standard deviation, of 63.3883332056, there is a less than 1% likelihood that this clustered pattern could be the result of random chance.
- This combination of (low p values and high z values) indicates a spatial clustering of high values since higher z scores indicates a more intense spatial clustering. It is usually found at the tails of the normal distribution.

---

*The default neighbourhood search threshold was 673070.9000 Meter computed using Chordal distances (Earth modelled as sphere instead of Ellipsoid as found in Geodesic distances).*

iii. Absence of Trends Check

Trends are systematic change in data across an entire study area i.e. Mean is not same/similar everywhere. They are often indistinguishable from autocorrelation and anisotropy. Large trends are removed using functional transformations to remove the relationship between data variance and data trend. The trend analysis graph provides a 3D perspective of the data. Above each sample points, the value is given by the height of a stick in the Z dimension with input data points on top of the sticks. Then the values are projected on the XZ plane and the YZ plane, make sideways view through the 3D data. Polynomial curves are then fit through the scatter plots on the projected planes. In *Figure 50*, the green line shows the trend in the E-W direction and the blue depicts the trend in N-S direction. It is observed that there are lower temperature values in the centre in E-W direction and higher values in N-S direction indicating the presence of different trends in different directions.

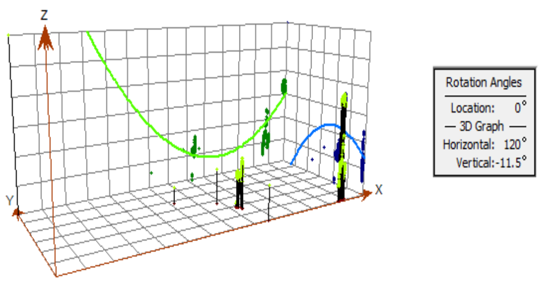


*Figure 50: Trend Analysis Check*

iv. Spatial Autocorrelation Check

The Spatial Autocorrelation check is used to examine the local characteristics of spatial autocorrelations within a dataset and look for local outliers. The semivariogram cloud shown in *Figure 51* provides the empirical semivariogram values for all pairs of locations within a dataset and plots them as a function of the distance that separates the two locations. Each dark red dot shows the squared difference between the values of two data points making up a pair plotted against the distance separating the two points.

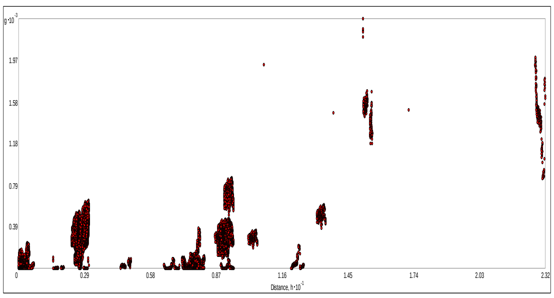

*Figure 51: Semivariogram Cloud*

The semivariogram surface, shown in *Figure 52* is generated including the search direction. With search direction is included, the values in the semivariogram cloud are put into bins based on the direction and distance between a pair of locations. These binned values are then averaged and smoothed to produce the semivariogram surface. The lag size determines the size of bins and the number of lags determines the number of bins. The extent of the semivariogram is controlled by lag size and number of lags. If the lag size is too large, the short-range autocorrelation may be masked. If the lag size is too small, there may be empty bins and sample sizes within bins with be too small to get representative average for bins.

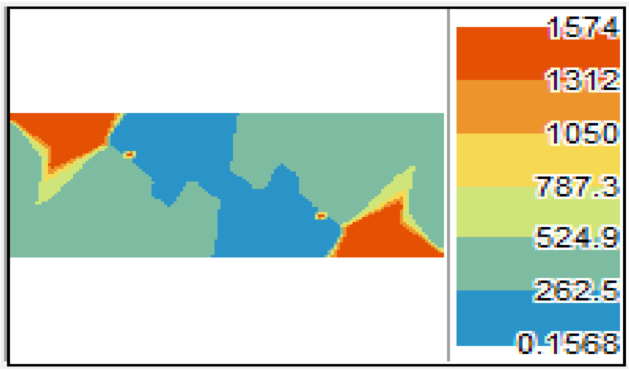


*Figure 52: Semivariogram Surface (Lag Size: 2.3158; No. of lags: 10)*

When sample sizes are located on a sampling grid, grid spacing is usually a good indicator for lag size. However, if data is using irregular or random sampling scheme, a simple rule can be followed to determine lag size. The lag size can be multiplied by the number of lags, which should be about half the largest distance among all points. If the range of the fitted semivariogram model is large relative to the extent of the semivariogram, one can increase the lag size. Another approach widely used to determine lag size is to find the average nearest neighbour value using Euclidean distance.

Having checked the dataset for a variety of criteria for spatial aspects, initially a simple linear regression technique, widely used in the context of time series analysis is experimented to understand the patterns from yet another perspective.

# III. Estimation of Spatial Spread of Temperature

## 1. Methodology #1: By Multiple Linear Regression (MLR)

In statistical modeling, regression analysis is a set of statistical processes to estimate the relationships between a dependent variable and 1 or more independent variables (also called predictors or covariates). The most common regression analysis form is linear regression. In linear regression, one finds a line or a more complex linear function that most closely fits the data. It is based on a specific mathematical criterion. Regression analysis is chiefly used for two theoretically different purposes.

- Widely used for prediction and forecasting.
- In some scenarios, it is used to infer causal relationships between the predictors and dependent variables.

In either case, it is essential to justify why existing relationships have predictive power for a new context or why a relationship between two variables has a causal interpretation using observational dataset. Prediction *within* the value range for a given to fit models is known as interpolation. Prediction *outside* this data range is called as extrapolation. Extrapolation generally relies on few assumptions. Although, the parameters of a regression model are usually estimated by method of least squares, some of the other notable methods include: Bayesian methods, % regression, Least absolute deviations (LADs), Nonparametric regression, Scenario optimization, Distance metric learning to name a few.

Linear regression is a linear approach to modeling the relationship between one dependent variable and 1 or more independent variables. When one explanatory variable is used, it is known as simple linear regression. If more than one explanatory variable is used, the process is then known as multiple linear regression. This is different from multivariate linear regression, wherein, multiple correlated dependent variables are predicted, rather than a single dependent variable. From the available dataset comprising 4 days of temperature data, collected during May 2010, in the vicinity of the eruption, 3 days's data has been considered for this analysis. Although a significant assumption, it is presumed that the different day's data originate from same altitude and from same time during the day. This facilitates in utilizing three days samples to be studied and used in the prediction of temperatures of the $4^{th}$ day. The datasets available for $14^{th}$ May, $16^{th}$ May, $17^{th}$ May & $18^{th}$ May 2010.

From this dataset, the last 3 days have been chosen as inputs owing to the logical continuity in dates. From the complete dataset, the following outlier values, listed in *Table 7* (eg: Vent data, data points from other time slots, dummy values etc) are ignored.

| **Lon (dd)** | **Lat (dd)** | **Alt (m)** | **Temp (K)** |
|---|---|---|---|
| -9.47537 | 59.9374 | 8048 | 266.753918 |
| -19.6 | 63.633333 | 4000 | 300 |
| -6.72907 | 58.5211 | 7487 | 274.057838 |
| -5.21287 | 54.2992 | 8061 | 273.5359 |

*Table 7: Key outlier values along with their location*

The temperature correlation between pairs of days, namely, 16th vs 17th, 17th vs 18th and 16th vs 18th are depicted in Figure 53 (a), 53(b) and 53(c), respectively.

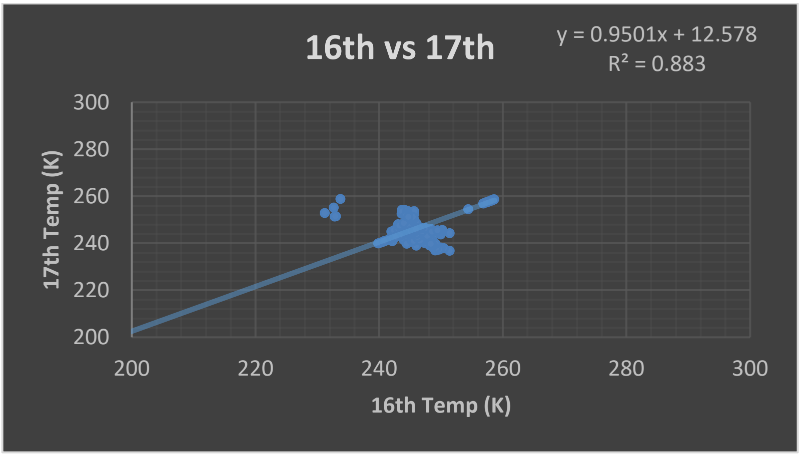


*Figure 53 (a): Correlation of temperature between 16th and 17th May 2010*

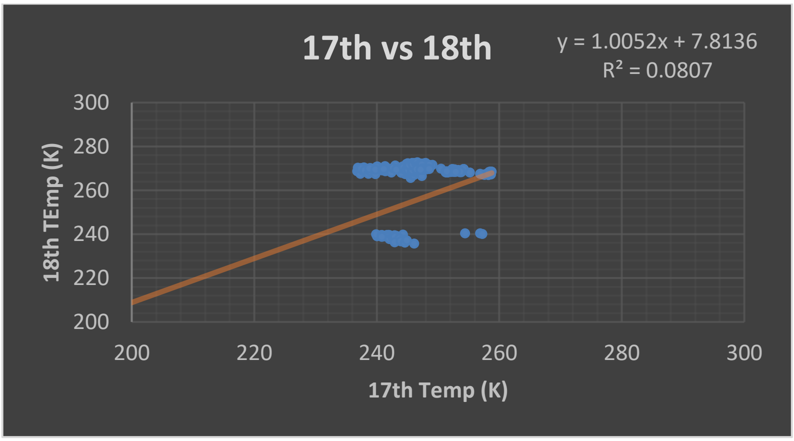


*Figure 53 (b): Correlation of temperature between 17th and 18th May 2010*

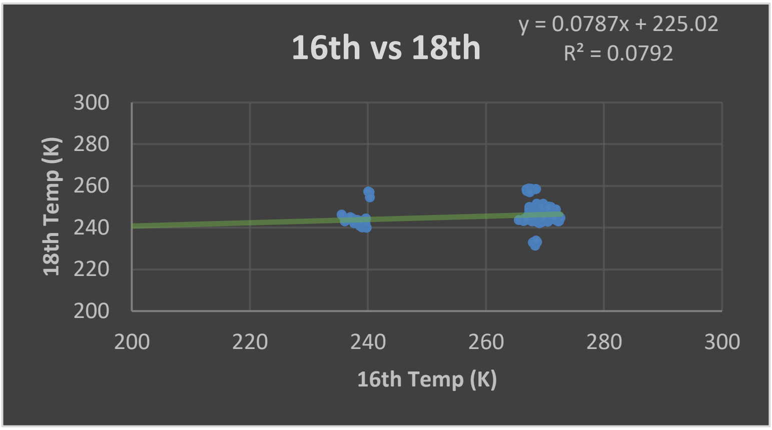


*Figure 53 (c): Correlation of temperature between 17th and 18th May 2010*

*Figure 53: Plots showing correlation of temperature between: (a) 16th and 17th May 20201 (b) 17th and 18th May 2010 (c) 16th and 18th May 2010*

From the plots in Figure 53, it is observed that while May 16th and 17th seems to be highly positively correlated, May 18th temperature values do not reveal any significant correlation with May 16th and 17th.

i. Modeling Using MLR Technique

The combined correlation among the three days, as shown in *Figure 54*, is observed to be very insignificant since the Correlation Co-efficient, R value is found to be 0.000005.

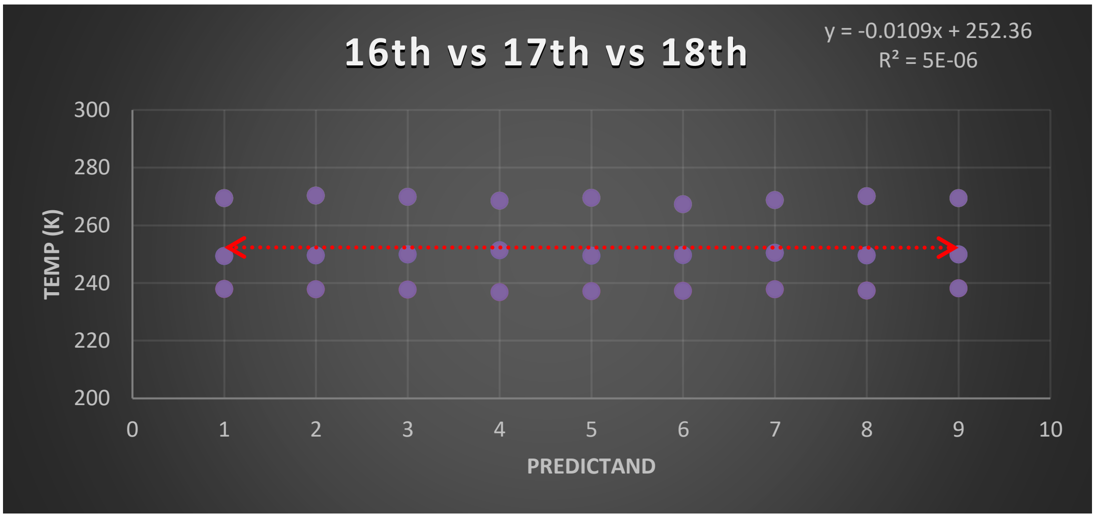


*Figure 54: Combined Correlation Analysis of May 16th to May 18th*

With this line of trend, the values are predicted for 4th day. The predicted temperature estimates are compared against input data to show the differences in *Figure 55*.

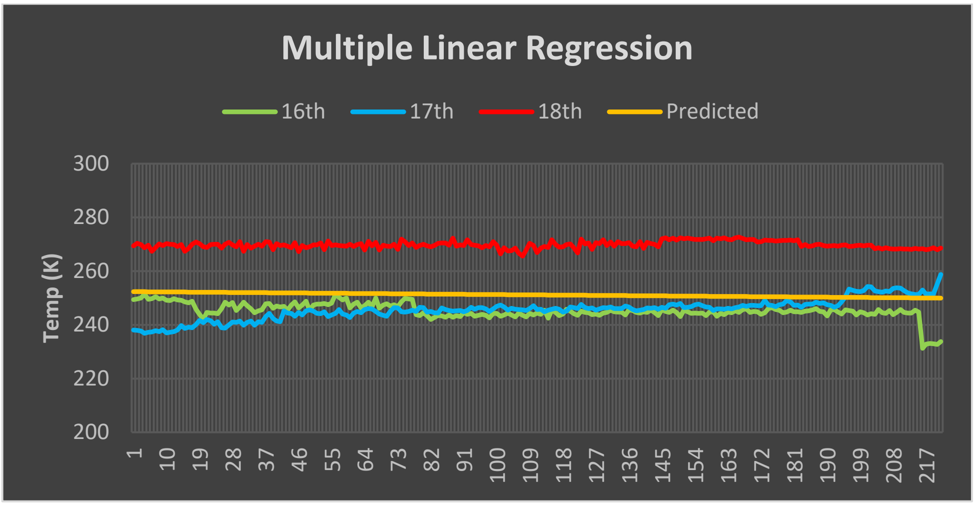


*Figure 55: Modeling Using Multiple Linear Regression*

The summary of statistics of the predicted values are compared against the summary statistics of the input data in *Table 8*.

| ***Temp (Kelvin)*** | **Input (16,17,18)** | **Predicted** | **Difference (Error)** |
|---|---|---|---|
| **Mean** | 253.435 | 250.785 | 2.65 |
| **Max** | 272.672 | 252.35 | 20.322 |
| **Min** | 231.248 | 249.221 | -17.973 |
| **Range** | 41.424 | 3.129 | 38.295 |

*Table 8: Summary of Statistics of Predicted Values*

From *Figure 56*, it is inferred the prediction estimates appear positively correlated with input values but not consistently or significantly in magnitude across the 3 days. This implies that Linear Regression Techniques can produce good estimates of global mean but are not very effective in modeling local variations correctly.

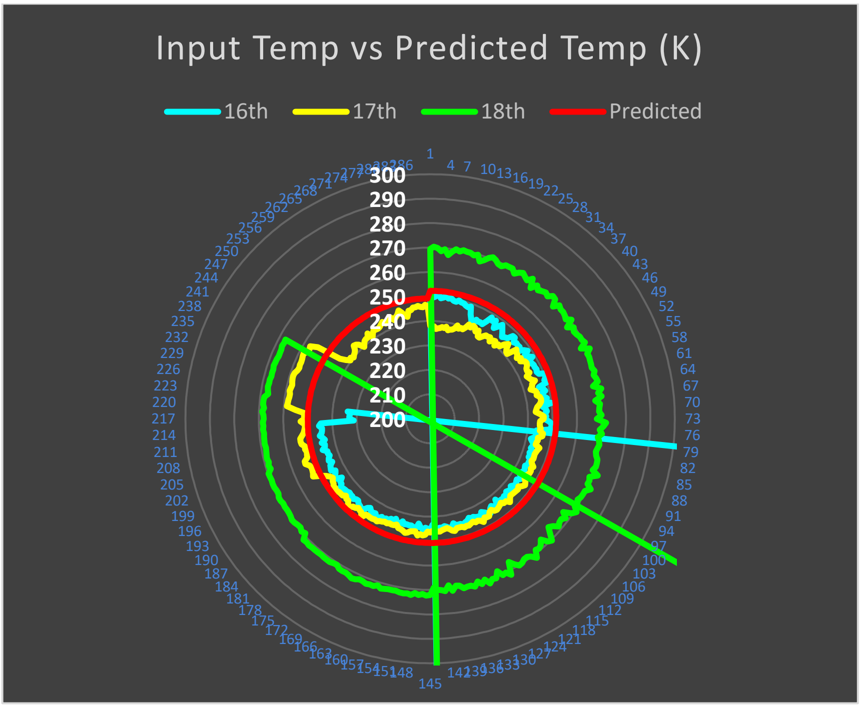


*Figure 56: Comparison of Input Data against Predicted Temperature Estimates*

The unbiasedness in the estimation of the mean (average) and variance using MLR technique is assessed by comparing the correlation of predicted value with each day's temperature data. It is observed that, although the correlation of temperature values is positive, it is not significant in magnitude (0.01 to 0.3).

ii. Validation of MLR Predictions against Input Dataset

From the correlation plots between temperature values from input data and predicted estimate for each day, as shown in *Figure 57(a), Figure 57(b) and Figure 57 (c)*, it is inferred the prediction estimates appear positively correlated with input values but not consistently or significantly in magnitude across the 3 days. This implies that Linear Regression technique can produce good estimates of global mean but are not effective in modeling local variations.

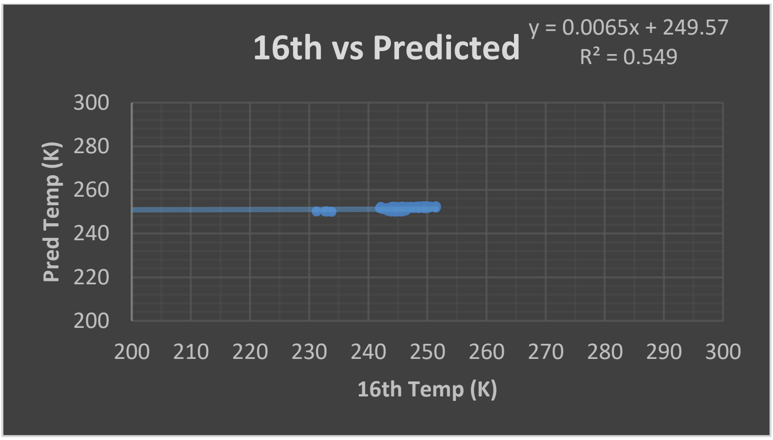


*Figure 57 (a): Plot showing correlation between temperature of 16th May against predicted estimates*

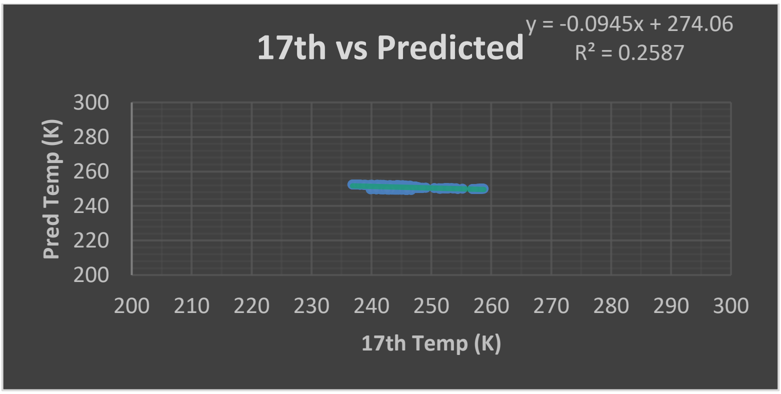


*Figure 57 (b): Plot showing correlation between temperature of 17th May against predicted estimates*

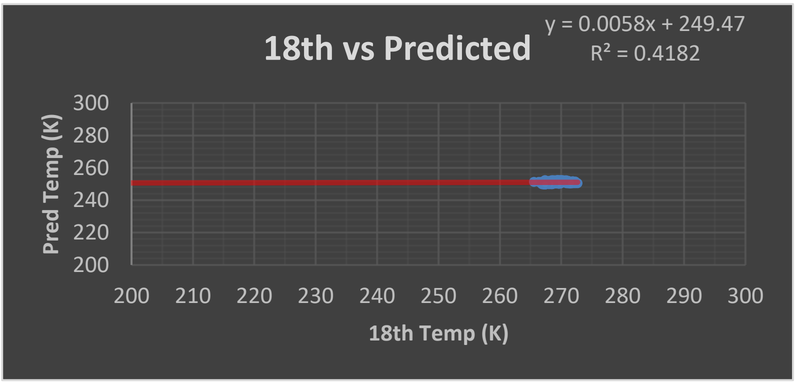


*Figure 57 (c): Plot showing correlation between temperature of 18th May against predicted estimates*

*Figure 57: Comparison of Individual Days vs Predicted Temperature Estimates (a) 16th May 2010 vs Predicted Estimates (b) 17th May vs Predicted Estimates (c) 18th May 2010 vs Predicted Estimates*

iii. Validation of MLR against NCEP

From *Table 9* and *Table 10*, it is observed that the over estimation error observed using MLR technique in comparison against the NCEP model for the same 3 days is around 5K in magnitude. The range (min/max) also varies roughly by 5K. But these values are global in nature. To identify and model variations in smaller scales, MLR technique is not useful. So, using non-parametric regression (distribution free methods) models, the predictor can be constructed according to information derived from the data (instead of predetermined apriori).

| **Temp (K)** | **Input 161718** | **NCEP 161718** | **Predicted 4$^{th}$ day** | **NCEP 14th** | **Validation Input 14$^{th}$** |
|---|---|---|---|---|---|
| **Min** | 231.248 | 254.62 | 249.221 | 233 | 228.76 |
| **Max** | 272.672 | 257.26 | 252.35 | 236 | 243.84 |
| **Mean** | 253.435 | 256.41 | 250.785 | 235 | 238.84 |
| **Range** | 41.4 | 2.64 | 3.129 | 3 | 15.08 |

*Table 9: Comparison of Composite Input, Composite NCEP, and MLR Predicted for 14th May, NCEP 14th May and Input 14th May Statistics*

With respect to each validation dataset, the accuracy of prediction using MLR is given below:

| **Temp (Kelvin)** | **Predicted 4$^{th}$ day vs Input161718** | **Predicted 4$^{th}$ day vs NCEP161718** | **Predicted vs NCEP 14th** | **Predicted 4$^{th}$ day vs Input 14$^{th}$** |
|---|---|---|---|---|
| **Error in Min** | -17.973 | 5.399 | -16.221 | -20.461 |
| **Error in Max** | 20.332 | 4.91 | -16.35 | -8.51 |
| **Error in Mean** | 2.65 | 5.625 | -15.785 | -11.945 |

*Table 10: Comparison of Predicted Estimate for 14thagainst Validation Datasets*

In summary, since the residual plots exhibit "heteroscedasticity," meaning that the residuals get larger as the prediction moves from small to large (or from large to small). This doesn't inherently create a problem, but it's often an indicator that the model can be improved. The most frequently successful solution is to transform a variable. Often heteroscedasticity indicates that a variable is missing. The most common way to transform one or more variables, usually using a "log" or other functional transformation. Transforming a variable changes the shape of its distribution. In general, regression models work better with more symmetrical, bell-shaped distributions. So, it is essential to try different kinds of transformations until one is found to give this type of distribution.

## 2. Methodology #2: By Non-Linear Regression – Kriging

Kriging or Gaussian Process Regression, discussed in the *paper* [34], is a stochastic, kernel based, spatial, geostatistical interpolation model similar to regression. It can be used in analysing, predicting (by interpolation) and surrogate model-based optimization processes for modeling even complex natural phenomenon. Unlike Support Vector Machine (SVM) or Radial Basis Function (RBF) or IDW, it provides uncertainty estimates too. The spatial dependence at various distance of spatial point reference data can be captured by a covariance function/semivariogram. Real world spatial data often show inherent variation sin measurements of a relationship over space, due to influence of spatial context on the nature of spatial relationships. The spatial dependency is captured by the spatial covariance matrix, which is estimated through spatial variogram. The accuracy of the model lies heavily on the modeling of the variogram. Conventional methods require specialized and in-depth domain knowledge about the field. By automating the estimation of single/multiple theoretical variogram for even fields that are anisotropic (not uniform in all directions), and exhibiting any type of stationarity phenomena (heterogeneous/non-stationary or intrinsically stationary or weak stationarity where in only some statistical properties do not change with locations), investigations can be performed with and without removal of trends alongside analysis of the spatial continuity of the field (i.e. dependence across locations). Non-normal data can be transformed using methods such as log transformation (which is a special case of Box Cox Transformation processes) to assume that the dataset is normally distributed post transformation.

Geospatial Kriging technique is a combination of mathematical and statistical models. The addition of a statistical model that includes probability separates kriging from deterministic methods. Kriging is a weighted moving average technique, similar in some ways to Inverse Distance Weighting (IDW) interpolation. Comparing the two techniques provides insight to the benefits of Kriging. With IDW, each grid node is estimated using sample points which fall within a circular radius. The degree of influence each of these points will have on the calculated value is based upon the weighted distance of each of sample point from the grid node being estimated. In other words, points that are closer to the node will have a greater degree of influence on the calculated value than those that are farther away.

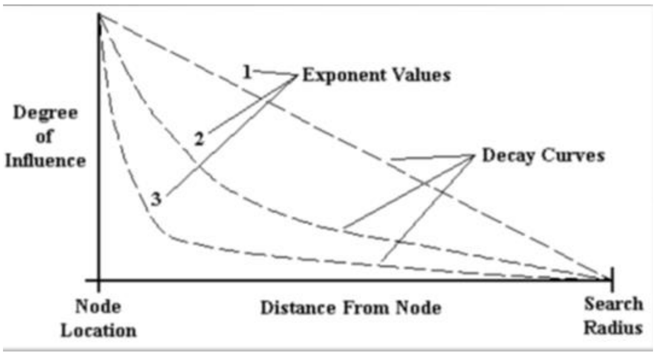


*Figure 58: Decay Curves – IDW Interpolation*

The disadvantage of the IDW interpolation technique is that it treats all sample points that fall within the search radius the same way. For example, if an exponent of 1 is specified, a linear distance decay function is used to determine the weights for all points that lie within the search radius, as shown in *Figure 58*. This same function is also used for all points regardless of their geographic orientation to the node (north, south etc.) unless a sectored search is implemented. Kriging on the other hand, can use different weighting functions depending on,

- the distance and orientation of sample points with respect to the node, and
- the manner in which sample points are clustered.

Kriging is a weighted average technique that assigns higher weights on nearby observations. The predictions ("kriges") at a given location (encompassed by a grid of locations over the geographic area of interest) are calculated on the basis of weighted average of the sample values (sample points near the prediction location are given larger weights than those that occur further away), with weights usually assigned as the straight line (Euclidean) distance between actual sample sites and the target location.

Weights are determined empirically by 'semivariogram analysis" (below). The latter models the similarity of sample values, in pairs, as a function of distance (or "lags") between the sampling sites (Little et al.1997). Kriging uses the following weighted linear combination estimator:

$$\hat{z} = \sum_{i=1}^{n} w_i z_i$$

Where, $z_i$ is the sample value at location i, $w_i$ is a weight, n is the number of samples.

Kriging is such a method that determines the weights so that the mean squared error (MSE) is minimized:

$$MSE = E\left((\hat{z} - z_0)^2\right)$$

Subject to the unbiasedness constrain:

$$\sum w_i = 1$$

Kriging is the optimal interpolation method, since it:

- Estimates the true value, on average,
- Produces lowest expected prediction error,
- Can use extra information, such as covariates,
- Filters measurement error,
- Can be generalized to polygons (Areal interpolation, Geostatistical simulations),
- Estimate probability of exceeding a critical threshold.

i. A Note on Partition Modeling

Partition models can be useful modelling tools as, unlike standard spatial models (e.g., kriging) they allow the correlation structure between points to vary over the space of interest. Typically, the correlation between points is assumed to be a fixed function which is most likely to be parameterised by a few variables that can be estimated from the data. Partition models avoid the need for pre-examination of the data to find a suitable correlation function to use. This removes the bias necessarily introduced by picking the correlation function and estimating its parameters using the same set of data.

Spatial clusters are, by their nature, regions which are not representative of the entire space of interest. Therefore, it seems inappropriate to assume a stationary covariance structure over X. The partition model relaxes this assumption by breaking up the space into regions where the data are assumed to be generated independently from locally parameterised models. This can naturally place in a single region those points relating to an unusual cluster, and these points do not necessarily have to influence the response function in nearby locations. Further, by assuming independence between the regions the response function at the cluster centre tends not to be over smoothed.

Considering the large volumes of traffic in modern scenarios, even small countries that do not have their own NWP can still be part of International Aviation Volcano (IAV) watch activities and tasks with our proposed model. This method can support multiple disjoint cloud clusters and not just single dispersed samples of a large ash cloud. This is critical from a collaborative analysis, forecasting and decision-making perspectives and to report with uncertainties in parallel.

ii. Kriging Techniques – Chosen for Study

Three variants of kriging were experimented for this comparative study, namely – Simple Kriging, Empirical Bayesian Kriging (with and without applying transformation). Chilès and Desassis, (2018) discuss the technique of Simple Kriging while Krivoruchko and Gribov, (2014), (Gribov & Krivoruchko, 2020) and Krivoruchko and Gribov, (2019) discuss Empirical Bayesian Kriging technique in detail. *Table 11* lists the key differences in the theoretical aspects among the three chosen methods.

| **Type** | **Kriging** | **Empirical Bayesian Kriging** | **Empirical Bayesian Kriging** |
|---|---|---|---|
| **Sub-Type** | Simple Kriging | Without Transformation | With Transformation – Simple Kriging |
| **Data Type** | Stationary Stochastic Process | Moderate Non-stationarity | Moderate Non-stationarity |
| **Assumption** | Data – Normally Distributed | Normal Distribution, ideal | Transformations applied |
| **Coordinate Systems** | Uses Euclidean Distance – Inaccurate, especially from the equator | Uses Chordal distance – 3D straight line distance between points on a spheroid - Accurate approximation to geodesic distance upto 30 degrees | Uses Chordal distance 3D straight line distance between points on a spheroid<br><br>Accurate approximation to geodesic distance upto 30 degrees |
| **No. of semivariogram** | One (theoretical) | Multiple | Multiple |
| **Definition** | Simple kriging is used for spatial interpolation when the mean and spatial correlation model are constant and known. SK is applied in conditional simulation | Empirical Bayesian Kriging is a Kriging-based interpolation method that accounts for uncertainty in semivariogram estimation by simulating many semivariograms from the input data. In addition, EBK builds local models on subsets of the input data. | Empirical Bayesian Kriging is a Kriging-based interpolation method that accounts for uncertainty in semivariogram estimation by simulating many semivariograms from the input data. In addition, EBK builds local models on subsets of the input data. |

*Table 11: Table comparing chosen Kriging techniques*

The reason for choosing these 3 variants of Kriging are discussed below. Going by the First Law of Geography, as discussed in Zhu et al., (2019), which is also known as, Tobler's Law, that states "Everything is related to everything else, but near things are more related than distant things", the following 4 scenarios are identified in *Table 12*:

| | **Nearer Things** | **Farther Things** | **Spatial Concept/Theme** | **Comment** |
|---|---|---|---|---|
| **1st Scenario** | Similar | Dissimilar | Spatial Autocorrelation | 1st Law of Geography |
| **2nd Scenario** | Dissimilar | Dissimilar | Spatial Heterogeneity - (Every point on earth is varying uncontrollably) | 2nd Law of Geography – Pure random process |
| **3rd Scenario** | Similar | Similar | Everywhere Homogenous | Very unlikely |
| **4th Scenario** | Dissimilar | Similar | Spatial Structure/Fractal Theory | Spatial autocorrelation at various spatial scales |

*Table 12: Combinations of Tobler's Law*

The approximate distance and temperature ranges from this dataset are provided to help quantitatively interpret the terms near, distant/far, more related, less related. Although Kriging creates semivariograms based on distances between every pair of points, irrespective of the patterns in distribution, here, the distance and relation terms are interpreted from the vent perspective for the analysis since the samples are spatially clustered on each day and the distance between the samples is unique within each cluster (ranging from ~1m to ~700m), as shown in *Table 13* and *Figure 59*.

| **Location 1** | **Altitude (Feet)** | **Location 2** | **Altitude (Feet)** | **Distance (km)** | **Average Temperature (Kelvin)** | **Pressure Alt (mb)** |
|---|---|---|---|---|---|---|
| Vent | 4,000 | 16th | 7,530 | 1054 | 300-246 | 400 mb |
| Vent | 4,000 | 17th | 3,144 | 1553 | 300-246 | 700 mb |
| Vent | 4,000 | 18th | 1,799 | 1480 | 300-269 | 800 mb |
| Vent | 4,000 | All data points | 4,000 | - | 300-253 | - |
| Vent | 4,000 | 14th | 8,120 | 1359 | 300-238 | 350 mb |

*Table 13: Distance between Vent location and Individual Sampling Locations*

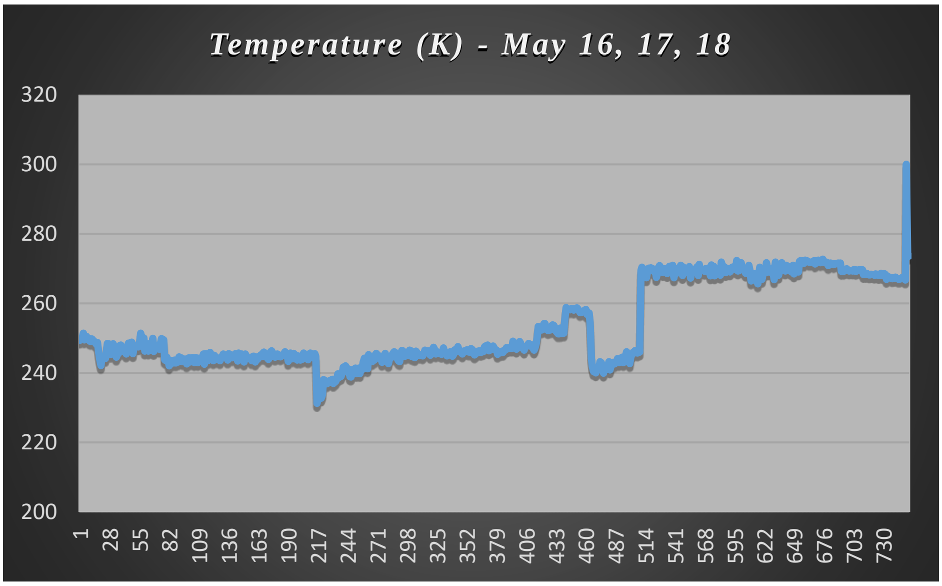


*Figure 59: Plot showing graph of attribute (air temperature in Kelvin) values in the input dataset*

In addition, the temperature values observed in each day (Cluster) is also unique since they are sampled from different altitudes, as shown in *Table 14* and *Figure 60*. Therefore, this dataset is highly heteroskedastic in nature as given in *Table 15*. Also, this perspective helps us to compare and analyse the profiles generated from kriging estimates.

| **Location 1 (May '10)** | **Altitude (Feet)** | **Location 2 (May '10)** | **Altitude (Feet)** | **Distance (km)** | **Average Temperature (K)** |
|---|---|---|---|---|---|
| 16th | 7,530 | 17th | 3,144 | 558 | 246-246 |
| 16th | 7,530 | 18th | 1,799 | 575 | 246-269 |
| 17th | 3,144 | 18th | 1,799 | 270 | 246-269 |

*Table 14: Distance between Pairs of Sampling Locations*

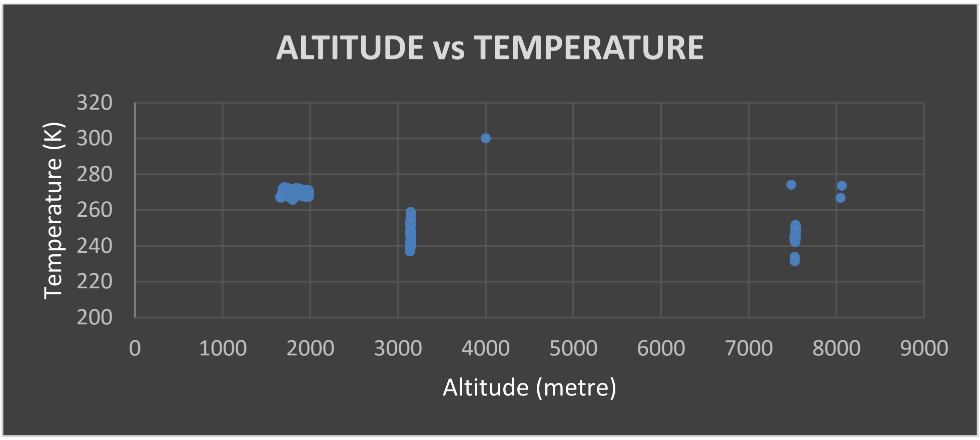


*Figure 60: Scatterplot showing Altitude vs Temperature on May 16, 17, 18*

| Date | Max Temperature | Min Temperature | Avg | Range |
|---|---|---|---|---|
| 16th | 251 | 231 | 246 | 20 |
| 17th | 258 | 236 | 246 | 22 |
| 18th | 272 | 265 | 269 | 7 |

*Table 15: Comparison of Temperature Values - Across Sampling Locations*

| Location 1 | Altitude (Feet) | Location 2 | Altitude (Feet) | Distance (km) | Average Temperature (K) |
|---|---|---|---|---|---|
| Vent | 4,000 | Center of Map | - | 807 | - |
| 16th | 7,530 | Center of Map | - | 268 | - |
| 17th | 3,144 | Center of Map | - | 784 | - |
| 18th | 1,799 | Center of Map | - | 743 | - |

*Table 16: Distance between key Sampling sites and Center of map*

In *Table 16*, the distance between key sampling sites and the center of the map are also tabulated. Based on the above details, the following aspects can be **"assumed"**:

a. That "nearer things" correspond to the distance between the ash samples collected during experimentation.

b. That "farther things" correspond to the distance between the vent and the regions were the ash samples were collected as part of the experimentation.

c. And that distances mentioned in Point (ii) are twice than the distances mentioned in Point (a), ignoring the altitude component.

iii. Possible Postulates Based on Tobler's Law

The following postulates are envisaged based on Tobler's law: (Considering the Center of the map to be corresponding to the origin in the semivariogram graph).

- **Scenario #1:** Going by Tobler's Law, with the vent assumed to be at 300K and the sampled data (average) at 253K, the intermediate regions are expected to be largely comprising of 2 sets of temperature ranges.
  - Area in and around data points
  - Area excluding the region covered in above mentioned point
- **Scenario #2:** Going by Second Law of Geography, each point must be unique with the entire field having a mixture of temperatures.
- **Scenario #3:** Going by the third scenario, the interpolated region has to appear homogenous irrespective of the temperature differences at the vent and at the sampled locations.
- **Scenario #4:**
  - Regions closer to the sampled regions should exhibit several minor (value related) variations even at shorter spatial scales, and,
  - The region between the vent and the area covered in point (i) must exhibit fewer, large variations at larger spatial scales.

Although scenario 1 and scenario 4 are evaluated using the same dataset, the effectiveness of the Simple Kriging (SK) technique (which relies heavily only on the belief of stationarity) is compared against that of EBK technique (which has been developed on Spatial Autocorrelation theory and modified for modeling non-stationary processes). 2$^{nd}$ and 3$^{rd}$ scenarios are ignored for analysis due to their extreme positioning with respect to variable intensity/behaviour.

To validate 4$^{th}$ scenario, two types of methods are used. While Empirical Bayesian (RMEL) approach is common to both the methods, the use of semivariogram model applied varies.

(i) EBK Without Transformation (EBK): Uses Power Model (Intrinsic Random Function)

(ii) EBK With Transformation (EBKT): Uses Models allowed for Simple Kriging

So, it is a critical criteria to be checked – whether the variations appear to change gradually (smoothly) or abruptly in each of the above discussed scenarios, as discussed in Krivoruchko and Mateu, (2020), van Stein et al., (2020) and Thakur et al., (2018). Whichever method provides a near-accurate variation in the region around sampled data points shall then be considered for validation, thereby, it can be considered to be reliable even for the predicted values region wherein sampled data points are not available.

iv. Results – Global Prediction and Error Estimates

i. Prediction Estimates

The maps in the below figure show the different patterns in the predicted values produced by various Kriging methods. Figure 61 (a) shows the predicted values of Simple Kriging, Figure 61 (b) shows estimates of Empirical Bayesian Kriging and Figure 61 (c) shows the values of EBK when dataset was transformed. While Simple Kriging predicts all range of values at all regions in almost equal proportions, EBK technique is able to predict location specific variations more accurately. Irrespective of EBK and EBKT being approximately closer values, the dispersion pattern varies drastically, visually/graphically.

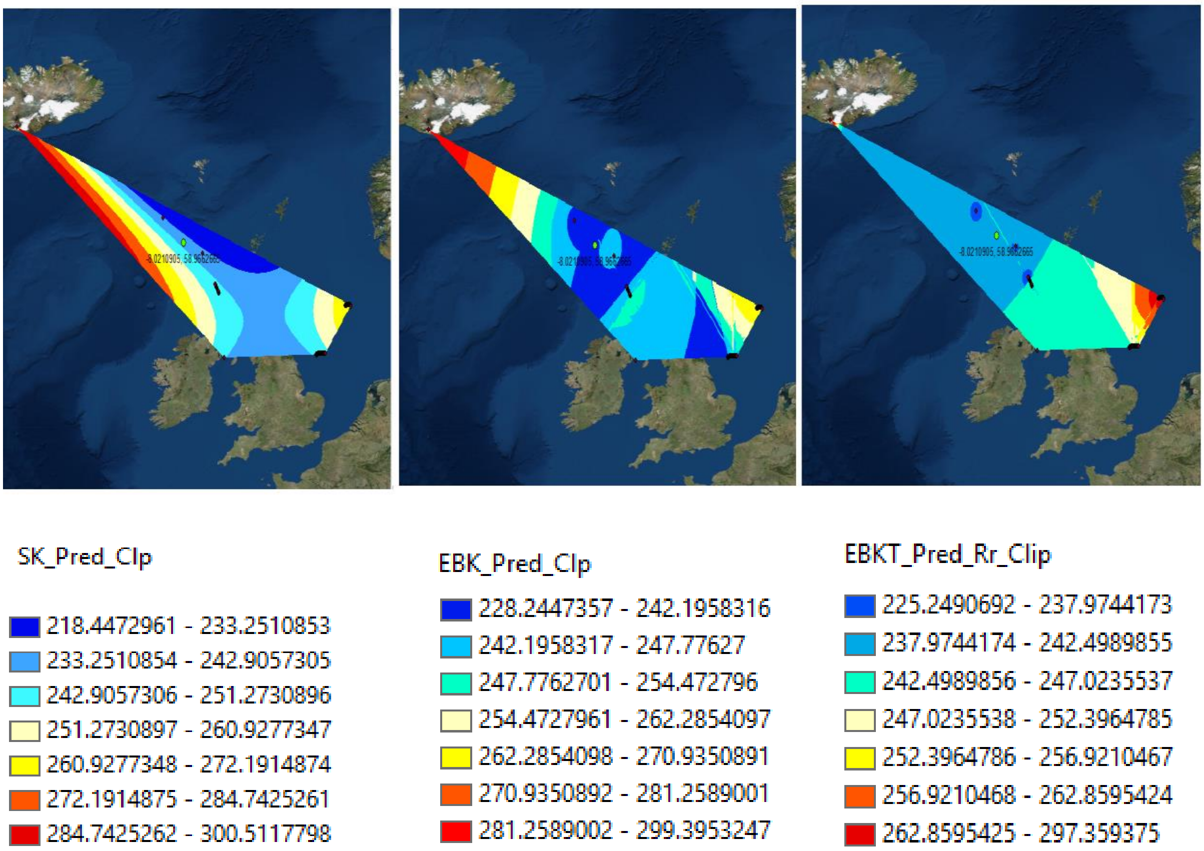


*Figure 61 (a) SK Estimates* *Figure 61(b) EBK Estimates* *Figure 61(c) EBKT Estimates*

*Figure 61: Maps showing Prediction Estimates by SK, EBK, EBK (Transformed) methods*

ii. Error Estimates

The maps in the below figure show the different patterns in the error values produced by various Kriging methods. Figure 62 (a) shows the predicted values of Simple Kriging, Figure 62 (b) shows estimates of Empirical Bayesian Kriging and Figure 62 (c) shows the values of EBK when dataset was transformed.While Simple Kriging reports no error for the entire region, higher magnitude of errors are concentrated in sparse data region with EBK and all ranges of errors are fairly distributed across the MBR region using EBKT. Again, irrespective of EBK and EBKT error magnitudes being almost similar, the dispersion pattern varies drastically, visually/graphically.

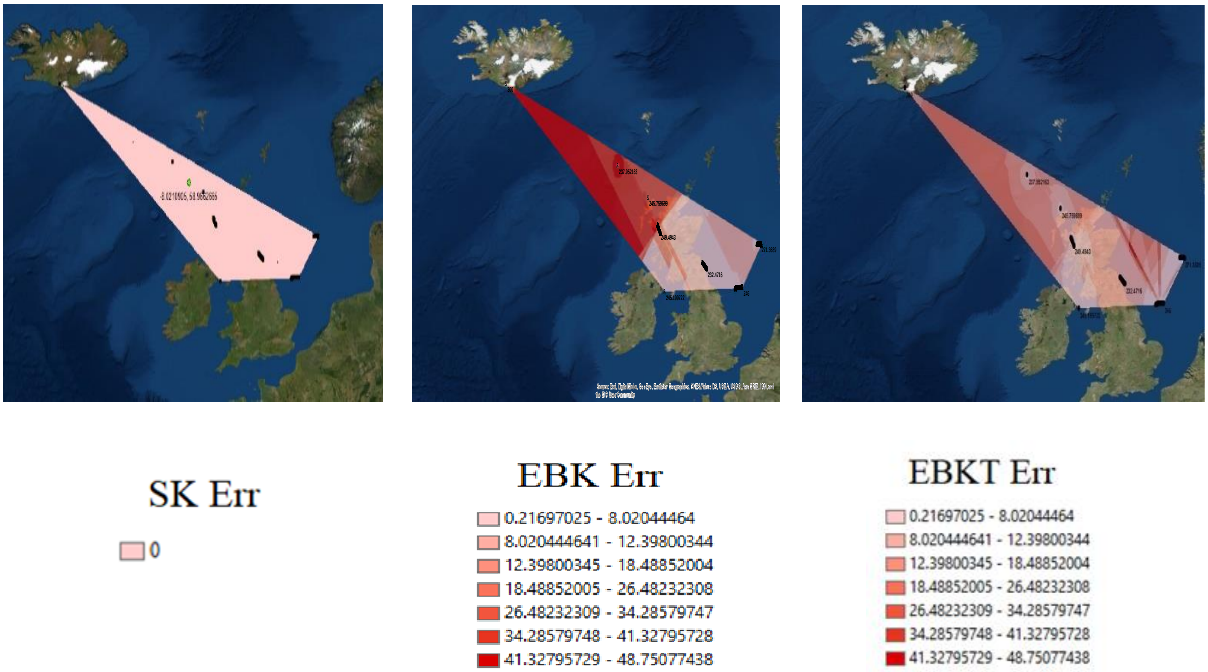


*Figure 62(a) SK Error* *Figure 62(b) EBK Error* *Figure 62(c) EBKT Error*

*Figure 62: Maps showing Prediction Estimates by SK, EBK, EBK (Transformed) method*

**Key Inferences**:

- The MBR covers approximately 5,00,000 square kilometre of area
- Using EBK method, 60% of MBR contains prediction overestimation errors ranging between +0.2 K::+24 K
- Area wise, 1.25L sq km of region lies within +8K error range

Both SK and EBK/EBKT methods estimate nearly the same average prediction temperature values, but there is a notable difference in the standard errors of the predictions. This is because simple kriging almost always underestimates standard errors due to the usage of a single theoretical semivariogram for the entire geographical extent. While a larger standard error in EBK seems to imply that EBK has larger uncertainty than simple kriging, the truth is that it captures even the small-scale variations accurately. This also clearly shows that the standard errors of simple kriging are incorrectly low.

iii. Verification of Kriging Results Using Geostatistics

Kriging is a distance based but not location-based interpolation algorithm. In addition to interpolated values, kriging can provide an estimate of the uncertainty in the interpolated values, which is known as the kriging variance or standard error. Kriging Models can be assessed based on two major aspects: (i) Numeric (prediction error statistics) and (ii) Qualitative (behaviour of phenomenon). Two questions that are applicable to modelling techniques that produce approximate estimations include:

i. Model Convergence: Can more data improve the model?

ii. Model Sensitivity - If data is modified, how much do the errors get magnified?

The objectives measure of success which constitute the basis for obtaining optimum predictors (also estimators) in the field of geostatistics include:

a. Unbiasedness (Mean of Error = 0)

$$E\left[\hat{Z}\ (s_0) - Z\ \ (s_0)\right] = E\ [p(Z, s_0) - Z\ (s_0)] = 0$$

b. Minimum Mean Square Error of prediction (estimation)

$$E\left[[\widehat{Z}\ (s_0) - Z\ \ (s_0)]^2\right] = E\ [[p(Z, s_0) - Z\ (s_0)]^2] \rightarrow min$$

To compare different interpolation techniques, the difference between the known data and the predicted data using the Mean Error or Mean Bias Error (ME/MBE), the Root Mean Squared Error (RMSE), the Average Kriging Standard Error (AKSE), the Root Mean Square Standardized Prediction Error (RMSP) and the Mean Standardized Prediction Error (MSPE) are traditionally used. Other commonly used criteria include Mean Square Error (MSE), Mean Absolute Error (MAE), Average Standard Error (ASE), Mean Square Reduced Error (MSRE), Root Mean Square Standardized Error (RMSSE), Mean Standardized Error (MSE) etc.

| **Comparison Parameters** | | **SK** | **EBK (Non-Transformed)** | **EBKT (Transformed)** |
|---|---|---|---|---|
| **Prediction Errors** | **Target Values** | | | |
| **RMSS** | 1 | 4.523536399830001 | 0.9387761153709571 | 0.9271949442684004 |
| **MS** | 0 | 0.07202474449353798 | 0.01834833637396241 | 0.0008108897593434113 |
| **RMS** | As low as possible | 3.570262293188187 | 2.59698926266238 | 2.3744524182584796 |
| **ASE** | As close to RMS Error as possible | 0.7892635269437307 | 2.0837038030126807 | 2.9657089460361927 |
| **Regression Function** | - | 0.941227711687841 * x + 15.2180711791894 | 0.989436793632373 * x + 2.6485023542719 | 0.992914337830346 * x + 1.76956611998676 |
| **Mean** | - | 0.05684650386619058 | 0.08815992385540611 | -0.07532375520937504 |

*Table 17: Error Estimates for SK, EBK and EBKT methods*

**Inference:** While Root Mean Square value is desired to be as low as possible for any interpolation algorithm, a special metric to assess Kriging efficiency is RMS-Standardized, which is expected to be close to 1 while mean values are preferred to be unbiased (close to zero). From *Table 17*, it is evident that EBK has the closest target value of 1 for RMSS, which is significantly lesser than SK. Although the error values of EBK (with and without transformation) are closer for RMSS and RMS, the Average Standard Error of EBK with Transformation is higher than RMS Error and therefore EBKT is a less preferred method. Also, for the given dataset, EBK has lower over estimations while EBKT has slightly higher underestimated values.

iv. Profile Analysis: Point Kriging Prediction & Error Estimates

The profiles of point kriging prediction and error estimates of SK, EBK and EBKT are compared in *Figure 63.* Profiles of SK, EBK, EBKT and NCEP values are shown as 3D plots in *Figure 63 (a)*, *Figure 63 (b)*, *Figure 63 (c)* and *Figure 63 (d)* respectively.

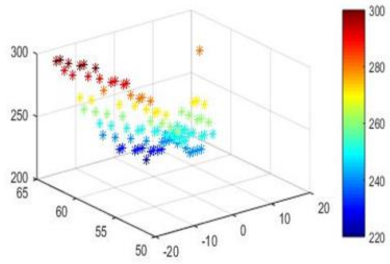


*Figure 63 (a) Prediction Profile of Simple Kriging*

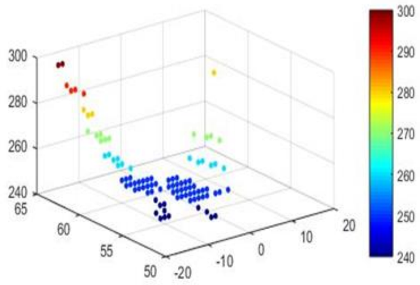


*Figure 63 (b) Prediction Profile of EBK*

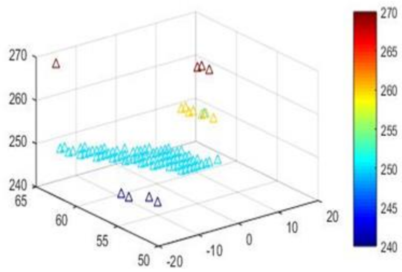


*Figure 63 (a) Prediction Profile of EBKT*

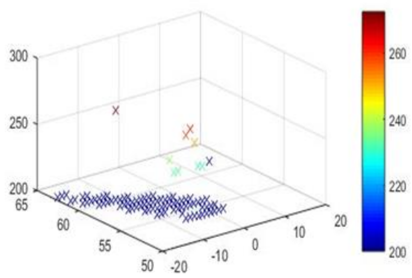


*Figure 63 (d) Prediction Profile of NCEP*

*Figure 63: Comparative 3D Visualization of Kriging and NCEP Profiles*

While kriging estimates span a range of temperature values, NCEP is largely limited to a narrow range of values. *Figure 64* compares the prediction profiles of Simple Kriging with profiles generated from EBK Point Kriging estimates, (with & without transformations).

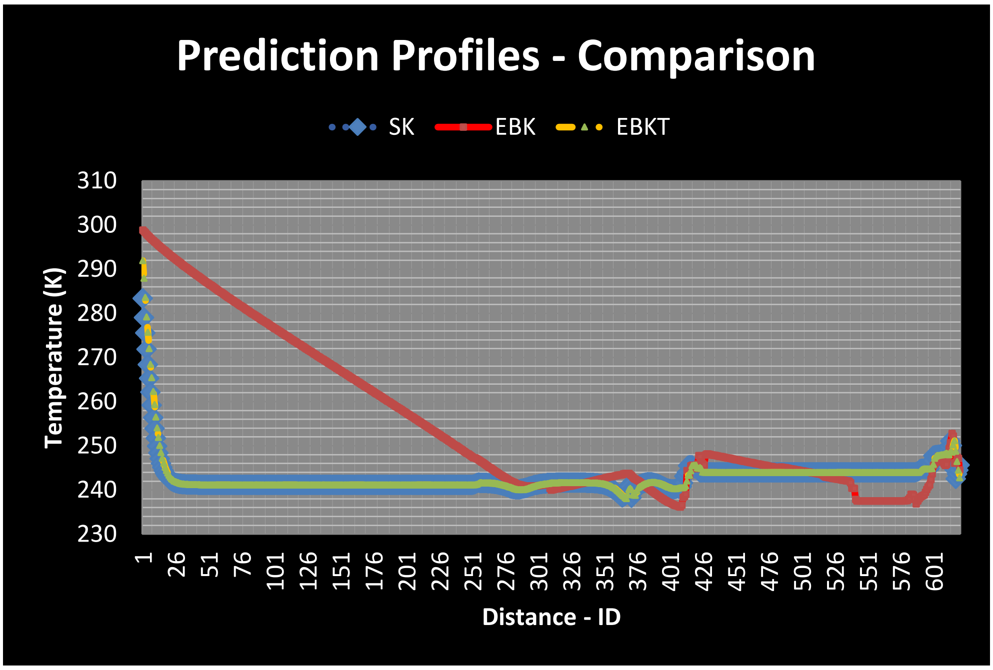


*Figure 64: Comparison of Prediction Profiles – SK, EBK, EBKT*

Among the three kriging techniques, SK and EBKT methods show similar profiles because, EBK when transformed internally uses Simple Kriging technique in Arcgis software. On the other hand, EBK when used without transformation uses random functions. As a result the profile reveals a significantly different pattern when EBK method is used. *Figure 65* compares the prediction and error profiles of Simple Kriging with profiles generated from EBK and EBKT estimates.

Figure 65 (a) and Figure 65 (b) show the prediction and error profiles of Simple Kriging.

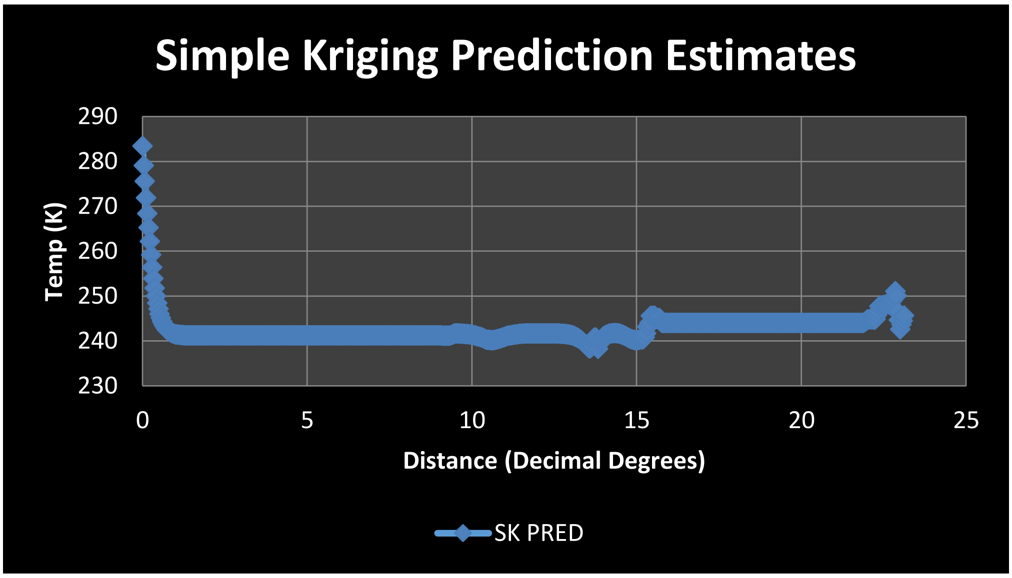


*Figure 65 (a) Simple Kriging Prediction Estimate Profile*

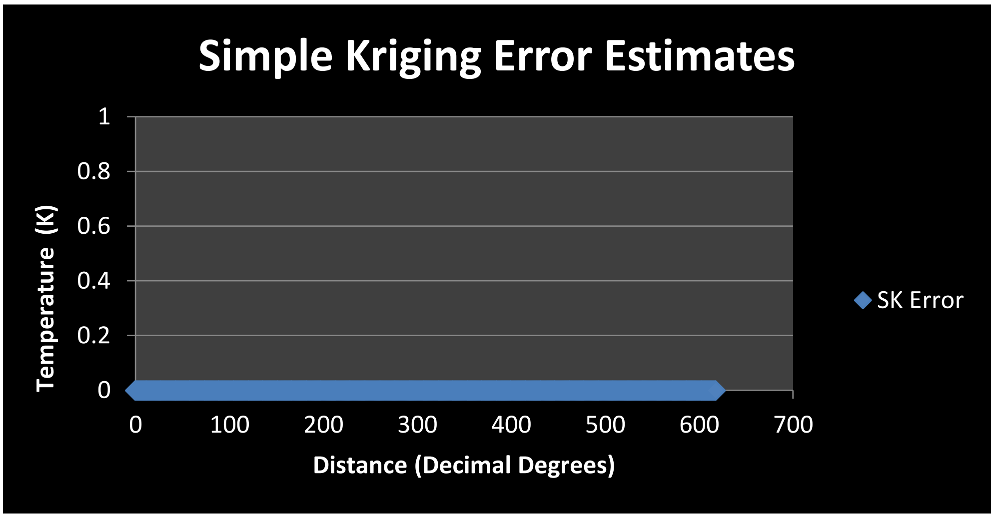


*Figure 65 (b) Simple Kriging Error Estimate Profile*

Figure 65 (c) and Figure 65 (d) show the prediction and error profiles of Empirical Bayesian Kriging.

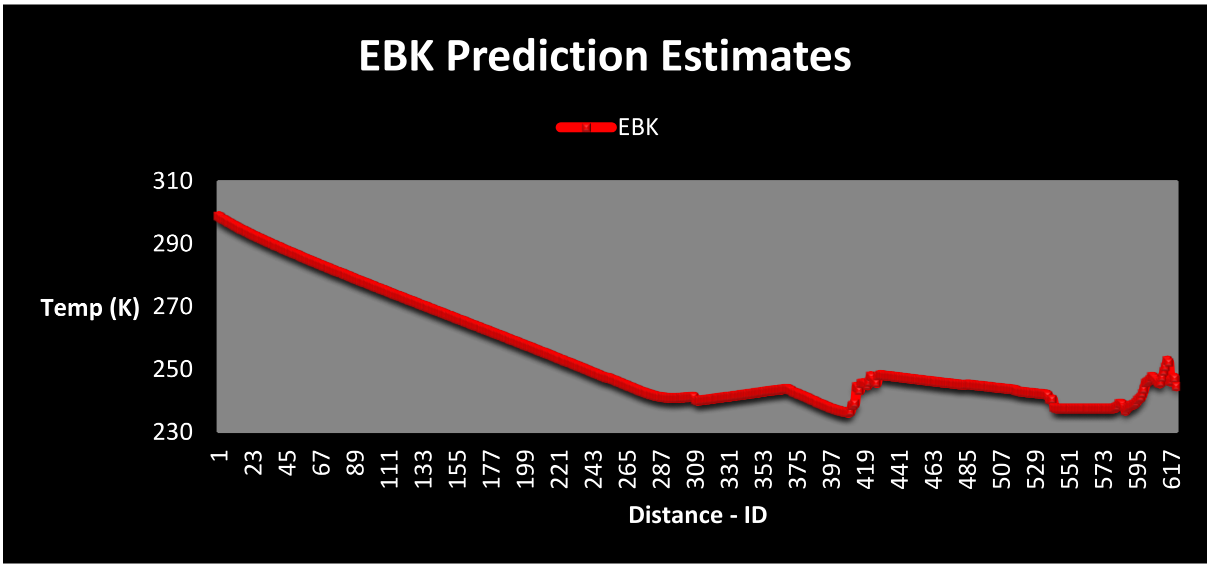


*Figure 65 (c) EBK Prediction Estimate Profile*

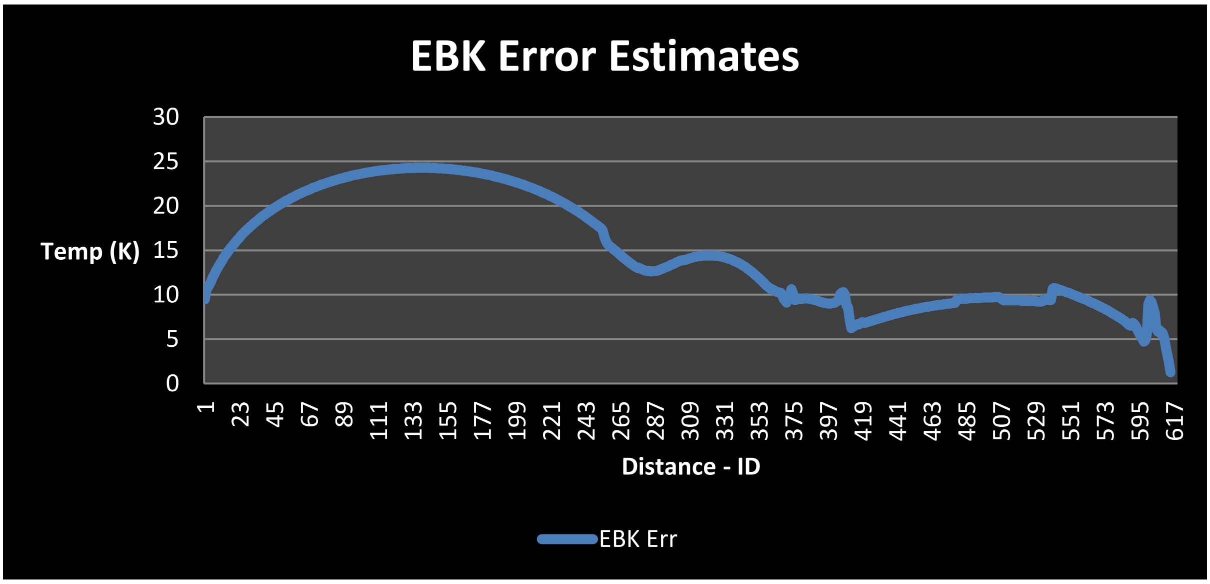


*Figure 65 (d) EBK Error Estimate Profile*

Figure 65 (e) and Figure 65 (f) show the prediction and error profiles of EBKT.

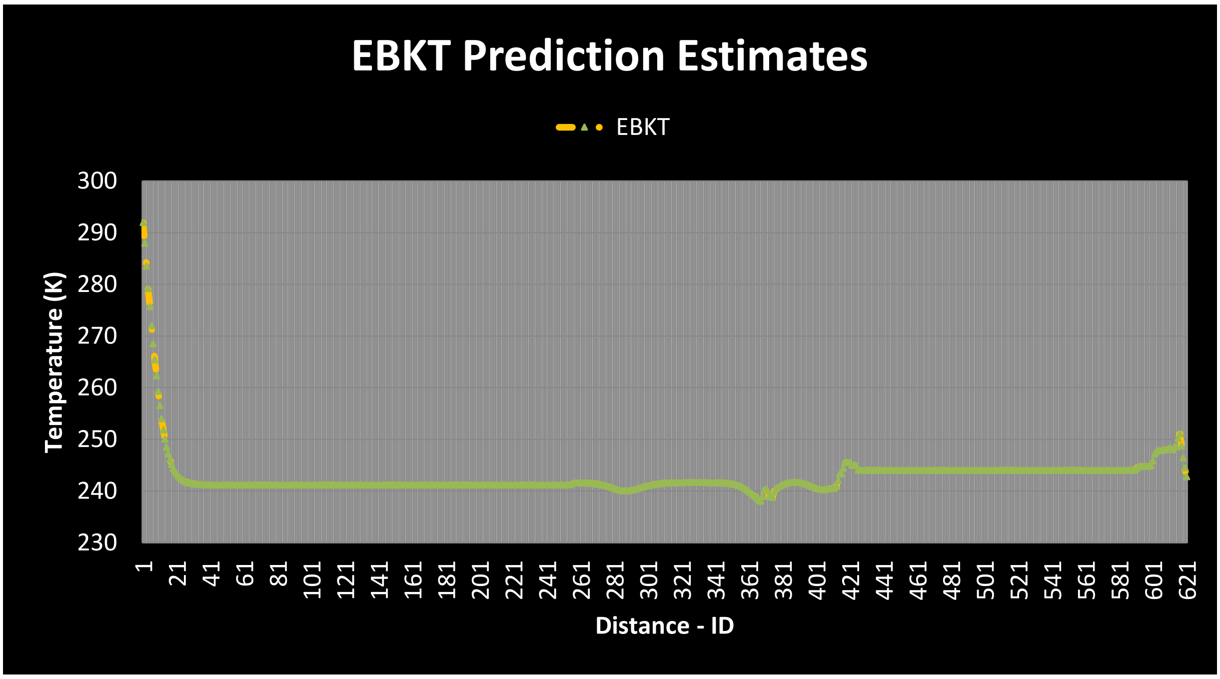


*Figure 65 (e) EBKT Prediction Estimate Profile*

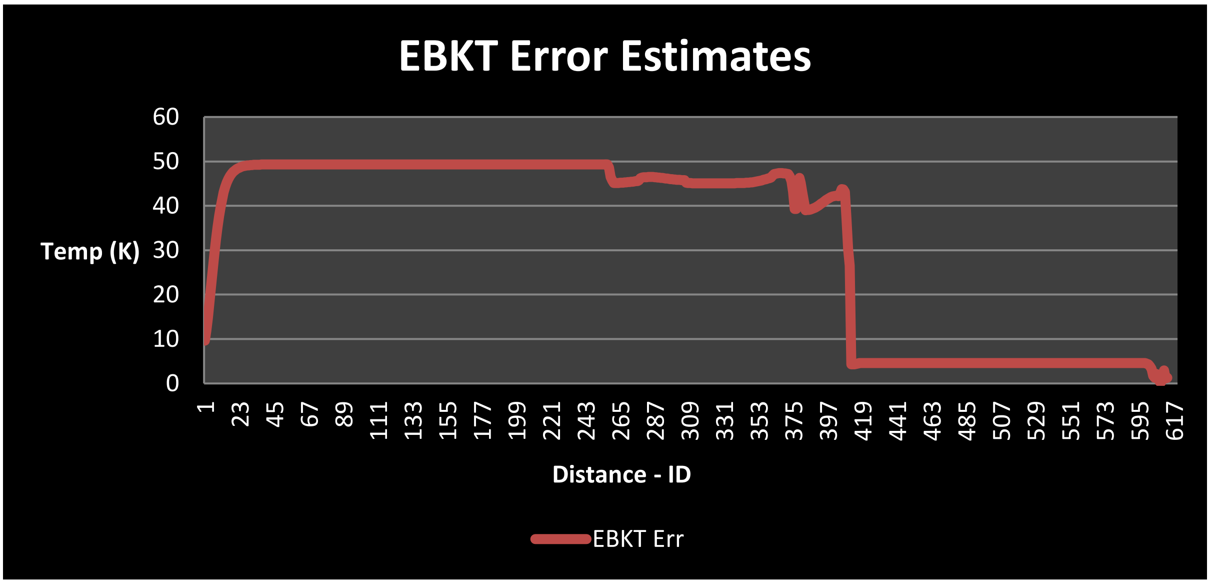


*Figure 65 (f) EBKT Error Estimate Profile*

*Figure 65: Comparison of Prediction, Error Profiles of Kriged Estimates*

Although SK and EBKT showed similar prediction profiles, the errors are not well estimated using Simple Kriging technique when compared with EBKT. Between EBK and EBKT, the latter has higher magnitude of errors in regions even in regions where input samples were not sparse for the profiles generated.

# IV. Detailed Analysis of Kriging as Interpolator

## 1. Validation of Point Kriging Results (Global Estimates)

### i. Validation of Point Kriging Estimates against NCEP

*Table 18* compares the various Basic Statistics (Col 1), for Input data on 16th&17th&18th May 2010 (Col 2), Simple Kriging Prediction (Col 3), Simple Kriging Error (Col 4), EBK Prediction (Col 5), EBK Error (Col 6), EBKT Prediction (Col 7), EBKT Error (Col 8), NCEP on all 4 days (Col 9) and NCEP on 16th&17th&18th May 2010 (Col 10). All temperature Prediction and Error values are in Kelvin.

| BAND STATS | I/P 161718 | I/P 14161718 | SK PRED | SK ERROR | EBK PRED | EBK ERROR | EBKT PRED | EBKT ERROR | NCEP 14161718 | NCEP 161718 |
|---|---|---|---|---|---|---|---|---|---|---|
| MIN | 231.25 | 228.764 | 218.4472961 | 0 | 228.2447357 | 0.21697025 | 225.2490692 | 0.197122157 | 251.46875 | 254.619751 |
| MAX | 300 | 300 | 300.5117798 | 0 | 299.3953247 | 48.75077438 | 297.359375 | 54.43642044 | 253.9550171 | 257.2614136 |
| MEAN | 253.57 | 251.544 | 250.5170935 | 0 | 248.5588341 | 14.06798523 | 243.7774291 | 26.9505363 | 253.0810213 | 256.413902941176 |
| STD DEV | NA | NA | 16.74186955 | 0 | 10.64582349 | 6.348119983 | 4.418745578 | 20.23731289 | 0.576458821 | 0.6371759 |
| RMS | NA | NA | 4.5235364 | NA | 0.938776115 | NA | 0.927194944 | NA | NA | NA |
| ERR RANGE | NA | NA | NA | NA | NA | 6 to 24 | NA | 4 to 49 | NA | NA |
| ERR CENTER PT (of Map) | NA | NA | NA | NA | NA | 9 to 14 | NA | 45 to 49 | NA | NA |
| AVG RANGE | 68.75 | 71.236 | 82.06448364 | NA | 71.15058899 | NA | 72.11030579 | NA | 2.4862671 | 2.6416626 |
| INACCURACY % | NA | NA | NA | NA | NA | 12.64922768 | NA | 62.40439492 | NA | NA |
| | | NA | NA | NA | NA | 19.6765764 | NA | 67.95145225 | NA | NA |
| MAP CENTER PT - VALUE | | NA | 229-237 | NA | 241-242 | NA | 242-244 | NA | 253.196 | 255.98595 |

*Table 18: Validation of Band Statistics of Punctual (Point) Kriging Estimates Against NCEP Estimates*

From the band statistics, it is observed that EBK (without transformation) method produces better estimates of averages and standard deviation (variance) than SK and EBKT when compared against NCEP estimates.

ii. Validation of Point Kriging against 14th May 2010 (Test Data vs 16th&17th&18th)

Out of the 4 days input data, 14$^{th}$ May samples were reserved as test dataset for verification. The input data for 14$^{th}$ May has a temperature range of 228K-243K while prediction estimates ranged between 228K–247K for all the three types of kriging. NCEP for the same period ranged between 235K-236K.

*Figure 66* shows the kernel PDF of the input (161718$^{th}$) dataset, kriged outputs (SK, EBK, EBKT), test data (NCEP14, NCEP161718 and May 14$^{th}$) values.

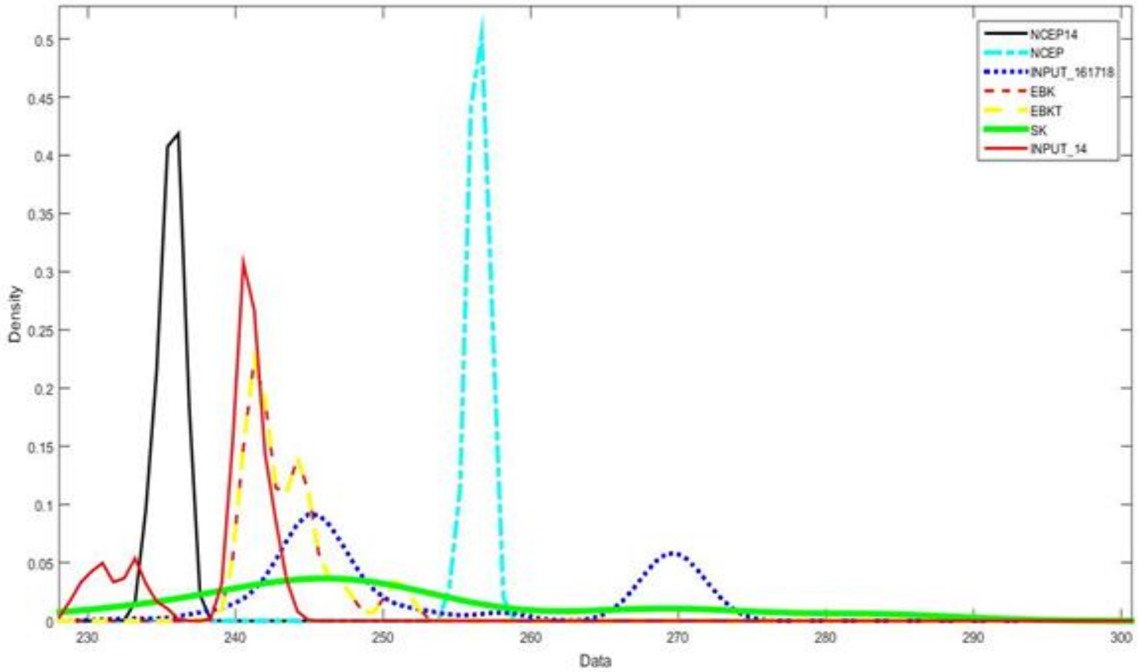


*Figure 66: Probability Density Graphs for Input, Kriged and NCEP Estimates*

Although SK predictions estimates were between 233K-242K, the errors were wide ranging and included both overestimation and underestimations (-29K to 26K). On the other hand, most of EBK and EBKT estimates were observed to lie between 242K-247K and had overestimations of about only 12K-15K.

From *Figure 67*, it is evident that 14th input temperature (TEMP variable - blue dotted line) has significant variations which are best predicted by only EBK. Both SK and EBKT (using SK technique iteratively) techniques yield poor predictions.

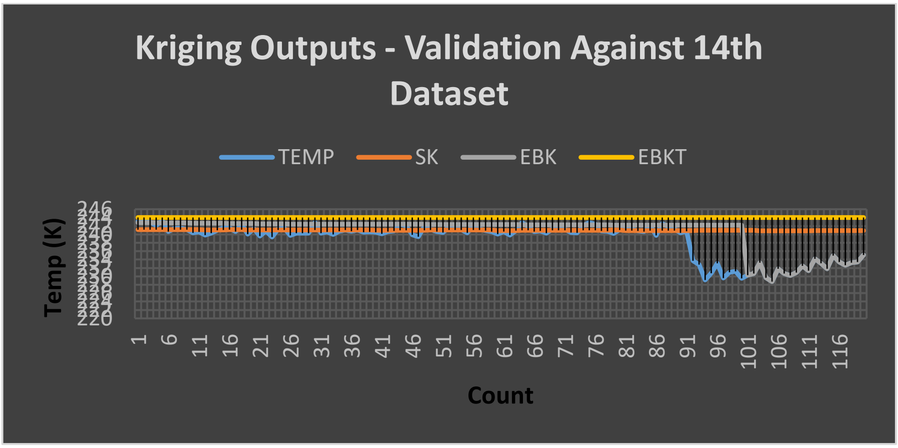


*Figure 67: Graph comparing SK, EBK and EBKT estimates against test data (14th May)*

Although the global prediction estimates of EBK using point kriging method span roughly a range of 70K, on an average, an overestimation error of only <8K was observed when tested against 14th May 2010 (test data). Thus, the error is within 10% threshold for EBK prediction estimates.

## 2. Comparative Analysis: Local Estimates - MLR, Kriging, NCEP

i. Comments on Average Estimates

*Figure 68* compares the average temperature observed on the 14$^{th}$, 16$^{th}$, 17$^{th}$, 18$^{th}$ of May 2010 among the different datasets within the range of 200 K – 300 K. Temperatures below 240K are labelled as COLDEST; values between 240K–260K are labelled as COLDER; values above 260K are labelled as HOT/HOTTER. Colder values are given in various shades of blue color while hotter values are given in shades of orange/red.

From the color codes, it is evident that although the average temperature of atleast one of the days using MLR is closer to NCEP, it is highly homogenous and hardly captures the variance observed in the input data across the other three days. On the other hand, although kriging estimates, closely follow the input data and the NCEP data, it also captures the small-scale variations accurately.

Figure 68(a) depicts the range of temperature values in the input dataset while Figure 68(b) shows the temperature estimates using MLR technique.

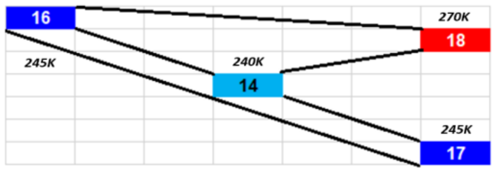


*Figure 68 (a) INPUT DATASET – BLOCK AVERAGES*

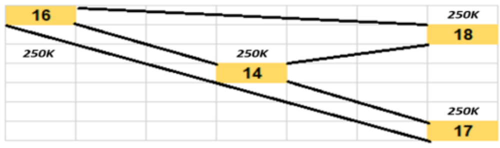


*Figure 68 (b) MLR-BLOCK AVERAGES*

Figure 68(c) shows kriged estimates (SK/EBK/EBKT – all 3 same averages) and Figure 68(d) shows values of the validation dataset from NCEP dataset for the same location.

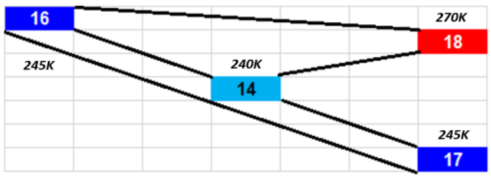


*Figure 68 (c) Kriging – SK, EBK, EBKT – BLOCK AVERAGES*

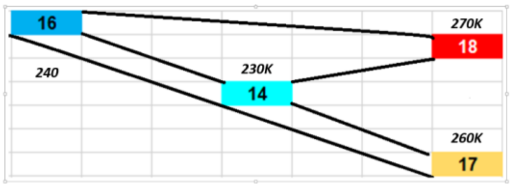


*Figure 68 (d) NCEP – BLOCK AVERAGES*

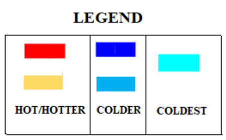


*Figure 68: Comparison of approximate averages of Input, MLR, Kriging& NCEP temperature values locally*

This proves that kriging is certainly a better technique than Multiple Linear Regression to model the block average estimates for ash dispersion.

ii. Comparative Analysis of Variation in Kriging Estimates against NCEP

*Figure 69* is a combined scatterplot that shows the correlation between kriged prediction estimates against NCEP. Simple Kriging correlations are scattered both positively and negatively with NCEP. As a result, consistency is unreliable. On the other hand, both Empirical Bayesian Kriging approaches, i.e. with and without transformation, appear to be largely negatively correlated with NCEP averages estimates.

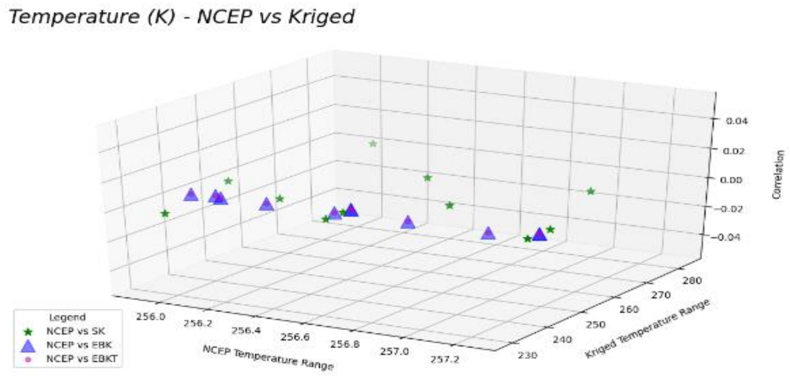


*Figure 69: Correlation of Prediction Estimates by each kriging method against NCEP*

*Figure 70* shows the correlation between error estimates using both EBK methods (with and without transformation) againt NCEP. The errors too are largely either uncorrelated or no correlation is observed with NCEP. Simple Kriging does not estimate any quantified errors and are therefore not included in this analysis.

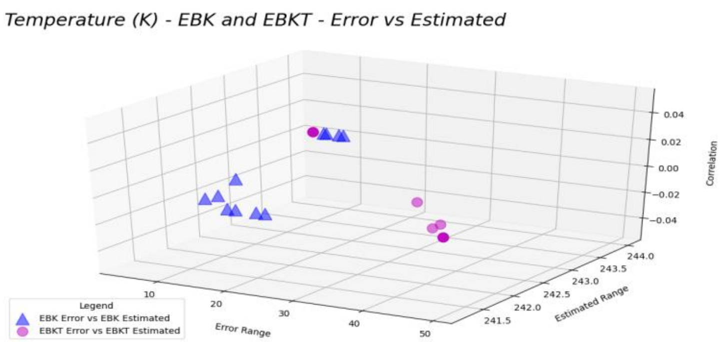


*Figure 70: Correlation of Error Estimates by EBK Methods against NCEP*

Given this significant discrepancy in correlation, further validations are performed on EBK technique to assess the suitability and efficiency of the stochastic kriging method in association with NWP algorithms.

## 3. Is EBK better than SK and EBKT?

With the same geographical extent, each day was kriged in isolation using the three techniques for a comparative analysis. The results of each kriging technique are given along with their respective PDFs below.

### *i. SK Results*

*Table 19* shows the prediction estimates by Simple Kriging method for each of the input days with respect to the minimum, maximum and average values (in Kelvin) to show the range of temperature estimate values predicted.

| Date | Max Temperature | Min Temperature | Avg | Range |
|---|---|---|---|---|
| 16th SK | 246 | 244 | 245 | 2 |
| 17th SK | 249 | 245 | 246 | 3 |
| 18th SK | 271 | 267 | 269 | 4 |

*Table 19: Comparison of SK Temperature Values - Across Sampling Locations*

*Figure 71* compares the probability density graph of prediction estimates produced by Simple Kriging method for the entire region with the estimates of NCEP and input data values for the same region.

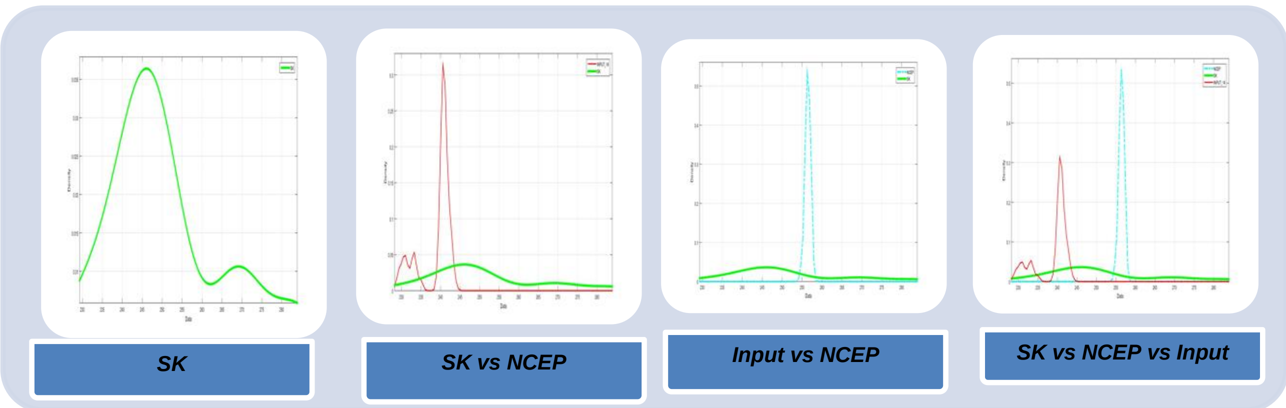


*Figure 71: Comparison of Probability Density Graphs for SK Estimates, NCEP and Input*

### ii. *EBK Results*

*Table 20* shows the prediction estimates by Empirical Bayesian Kriging method for each of the input days with respect to the minimum, maximum and average values (in Kelvin) to show the range of temperature estimate values predicted.

| **Date** | **Max Temperature** | **Min Temperature** | **Avg** | **Range** |
|---|---|---|---|---|
| 16th EBK | 249 | 233 | 245 | 16 |
| 17th EBK | 256 | 241 | 247 | 15 |
| 18th EBK | 273 | 268 | 269 | 5 |

*Table 20: Comparison of EBK Temperature Values - Across Sampling Locations*

*Figure 72* compares the probability density graph of prediction estimates produced by EBK method for the entire region with the estimates of NCEP and input data values for the same region.

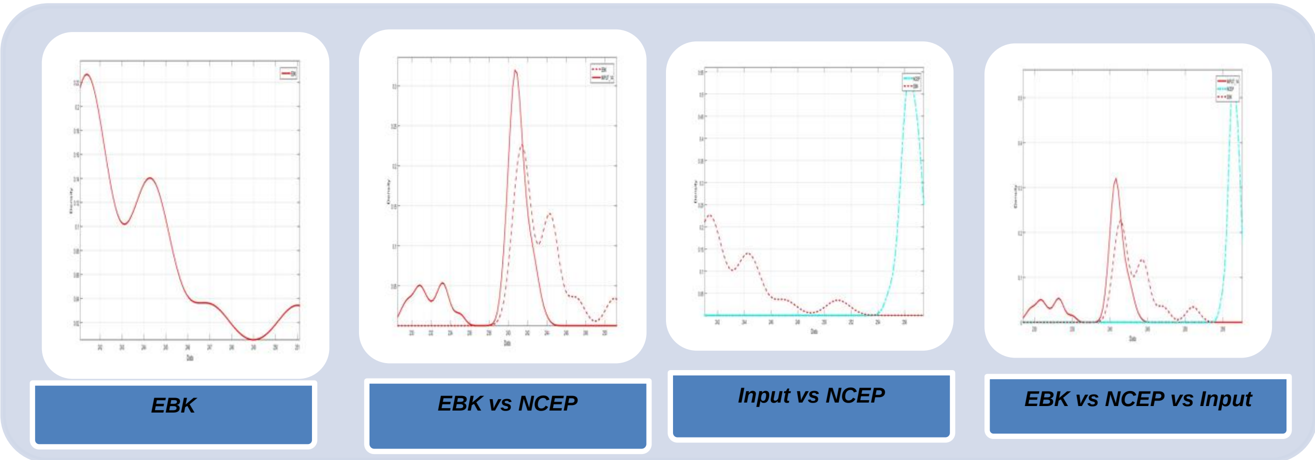


*Figure 72: Comparison of Probability Density Graphs for EBK Estimates, NCEP and Input*

### *iii. EBKT Results*

*Table 21* shows the prediction estimates by Transformed - Empirical Bayesian Kriging method for each of the input days with respect to the minimum, maximum and average values (in Kelvin) to show the range of temperature estimate values predicted.

| **Date** | **Max Temperature** | **Min Temperature** | **Avg** | **Range** |
|---|---|---|---|---|
| $16^{th}$ EBKT | 248 | 231 | 244 | 17 |
| $17^{th}$ EBKT | 254 | 241 | 247 | 13 |
| $18^{th}$ EBKT | 272 | 268 | 269 | 4 |

*Table 21: Comparison of EBKT Temperature Values - Across Sampling Locations*

*Figure 73* compares the probability density graph of prediction estimates produced by EBKT method for the entire region with the estimates of NCEP and input data values for the same region.

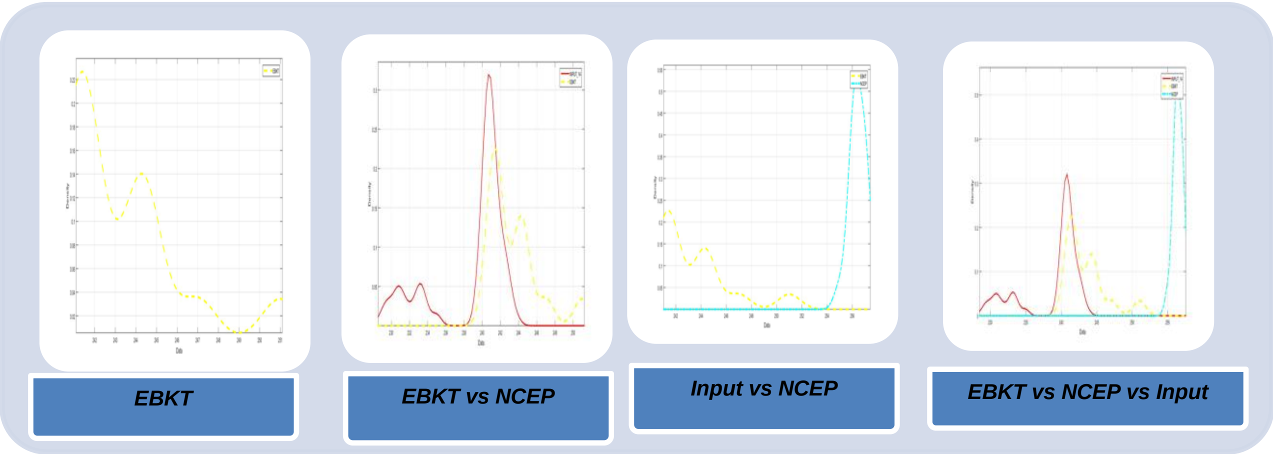


*Figure 73: Comparison of Probability Density Graphs for EBKT Estimates, NCEP and Input*

*Table 22* compares range and values of average temperature estimates predicted by each kriging method against input data for each day from input data.

| **Date** | **Avg (Input)** | **Avg (SK)** | **SK Diff_Avg** | **SK Diff Range** | **Avg (EBK)** | **EBK Diff_Avg** | **EBK Diff Range** | **Avg (EBKT)** | **EBKT Diff_Avg** | **EBKT Diff Range** |
|---|---|---|---|---|---|---|---|---|---|---|
| $16^{th}$ | 246 | 245 | 1 | -14 to 6 | 245 | 1 | -4 to 11 | 244 | 2 | -4 to 14 |
| $17^{th}$ | 246 | 246 | 0 | -8 to 11 | 247 | 1 | 1 | -5 to 11 | | |
| $18^{th}$ | 269 | 269 | 0 | -4 to 3 | 269 | 0 | -4 to 2 | 269 | 0 | -3 to 2 |

*Table 22: Comparison of each Day's SK, EBK and EBKT Average Temperature Values and Range of Temperature Values*

From the above graphs and *Table 22*, the following analysis is done. When compared against the average values of each of the days given in the input data, the following aspects are evident:

i. EBK estimates are better not only for entire region but also better when viewed in isolation for each day (i.e. $16^{th}$ or $17^{th}$ or $18^{th}$ May 2010)

ii. The range of EBK differences for each day ($16^{th}$: 15K, $17^{th}$: 16K, $18^{th}$: 6 K) is also significantly better than SK ($16^{th}$: 20 K, $17^{th}$: 19 K, $18^{th}$: 7 K) and EBKT ($16^{th}$: 18 K, $17^{th}$: 16 K, $18^{th}$: 5 K).

Therefore, even with very sparse data (less than ~300 points) of each day in isolation too, it is seen that EBK produces better estimates than SK and EBKT techniques.

# 4. Detailed Analysis of EBK Predictions and Errors

## i. Verification Using Classical Statistics

The summary statistics comparing predicted estimates using EBK (Point Kriging) method against the input dataset are given in *Table 23*:

| Statistic | Input Dataset | Predicted Dataset [EBK] |
|---|---|---|
| Standard Deviation, σ | 12.144024 | 11.37003 |
| Variance, $s^2$ | 147.47732 | 129.27759 |
| Count, n | 873 | 873 |
| Mean, μ | 251.4469 | 251.89772 |
| Sum of Squares, SS | 128600.22 | 112730.06 |

*Table 23: Summary Statistics Compared EBK Predicted Estimates against Input Dataset*

The average of prediction estimates by Empirical Bayesian Technique is 1 sigma above the mean. [(1* σ) + μ]. This implies that 68% of the data is within 1 standard deviation (σ) of the mean (μ). The confidence that the result is real is 84.13%.

## ii. Visualization of EBK Predictions On Map

The EBK (without transformation) produces two main types of surface outputs: Prediction Maps and Prediction Error Maps. Although Simple Kriging and EBK predict nearly the same global mean temperature, but there is a notable difference in the standard errors of the predictions. This is because Simple Kriging almost always underestimates standard errors due to using only a single theoretical semivariogram. While a larger standard error in EBK seems to imply that EBK has larger uncertainty than Simple Kriging, the actuality is that the standard errors of Simple Kriging are incorrectly low since large scale variations are ignored completely.

The EBK prediction estimates were split in intervals of 5 Kelvin to map to compare the variations in each day against the input samples. *Figure 74* shows the maps for entire region and for 14th May 2010. 14th data was not provided as input for kriging both locally and globally.

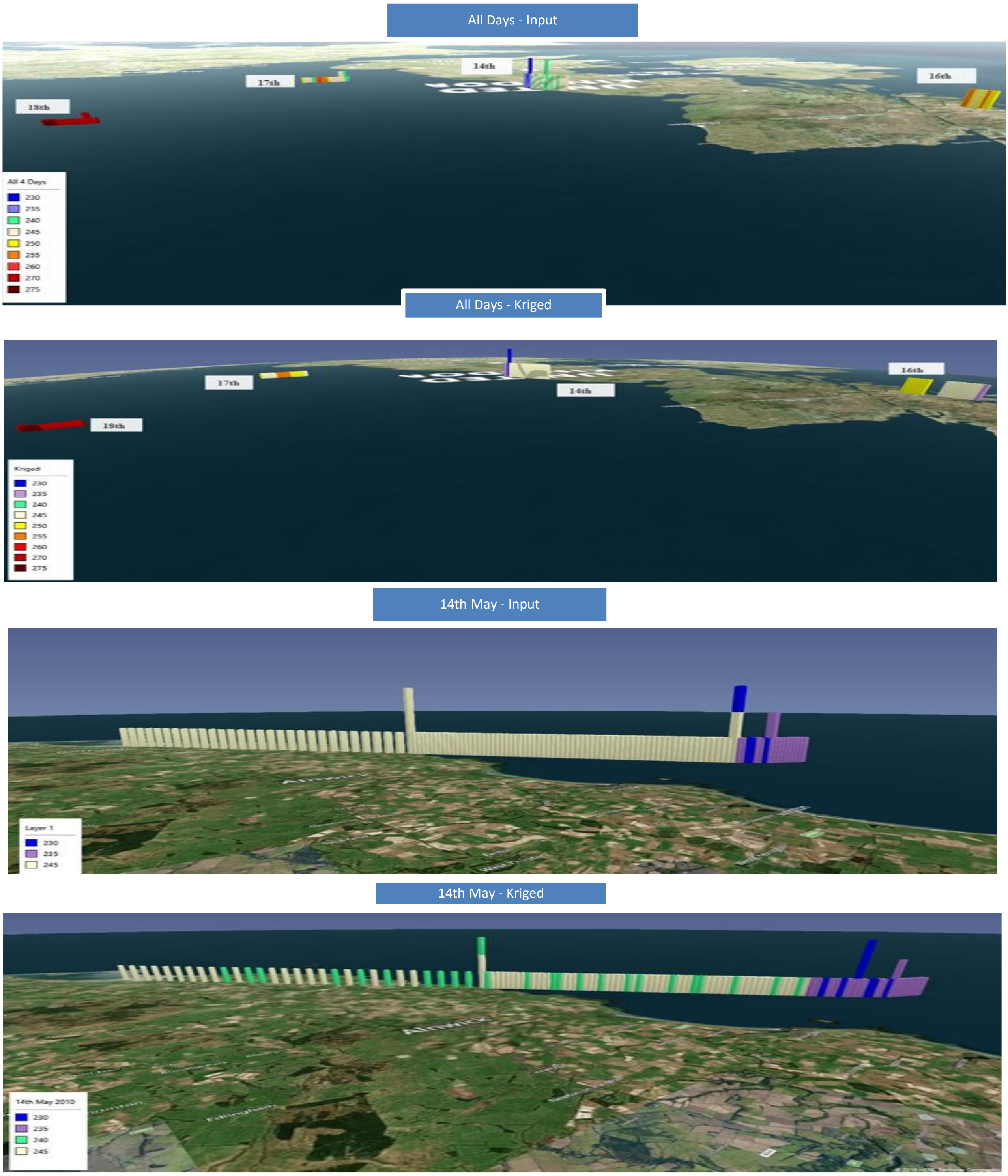


*Figure 74: Comparison of EBK Prediction Estimates Against Input Samples in 5K Intervals Using Maps For 14th May and Entire region (with no inputs for 14th May 2010)*

*Figure 75* compares the inputs and local kriged estimates of 16th, 17th and 18th May 2010 by providing the input data as samples for kriging.

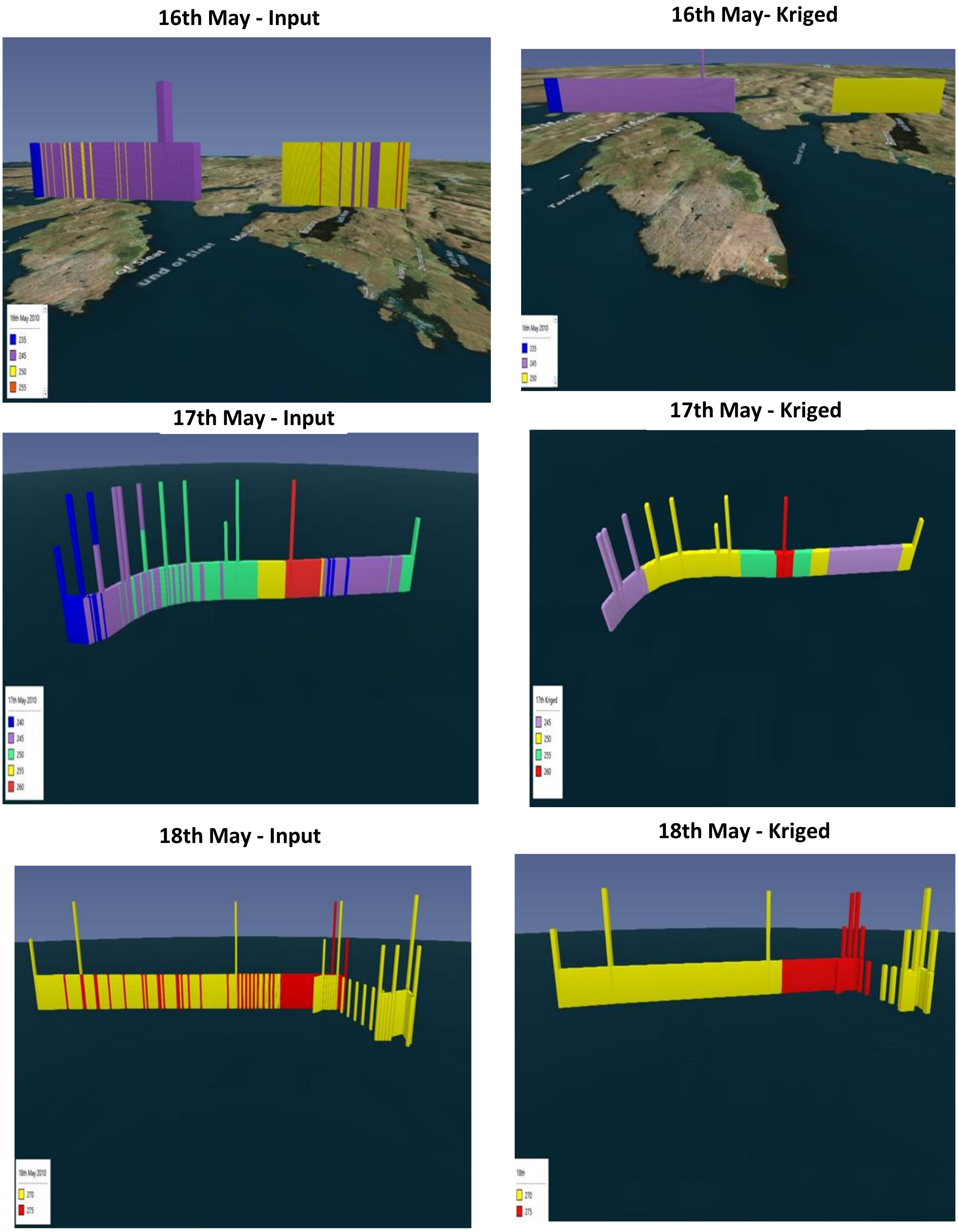


*Figure 75: Comparison of EBK Prediction Estimates Against Input Samples in 5K Intervals Using Maps For Input Locations (16$^{th}$ May, 17$^{th}$ May, 18$^{th}$ May)*

a. Prediction vs Error Visualizations on Maps

*Figure 76* compares the magnitude of prediction estimates against error estimates at each location of the input sample in intervals of 5 Kelvin. 14th May location is predicted without any input and has higher error variations. The patterns of under estimations and over estimations in other 3 days are observed from the maps. The blue color depicts predictions while red color depicts errors.

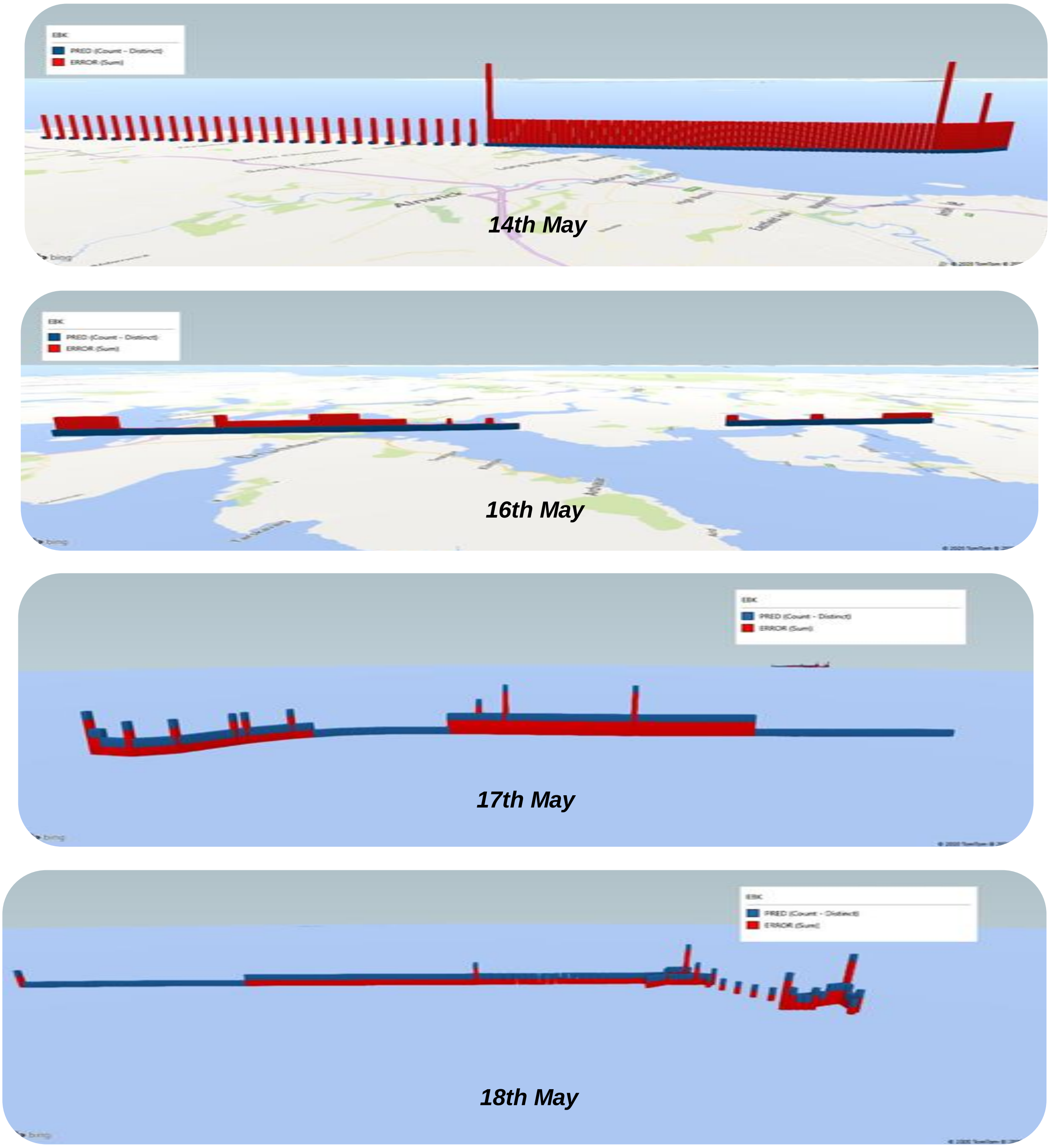


*Figure 76: Comparison of Prediction Estimates and Error Estimates for Each Day*

b. Error Analysis

Detailed error analysis is performed to support the argument why EBK is a better technique than SK and EBKT - not just in terms of prediction quality, but also in better determining the associated errors based on locations. From the EBK Prediction map earlier, it was observed that hottest temperatures (Closer to 300K) are less spread out than colder temperatures (closer to 200K), the reason being the vent is the only point with highest temperature (>280K) when compared with all the other input samples. *Figure 77* shows the 3d contour view of EBK error estimates across all temperature ranges.

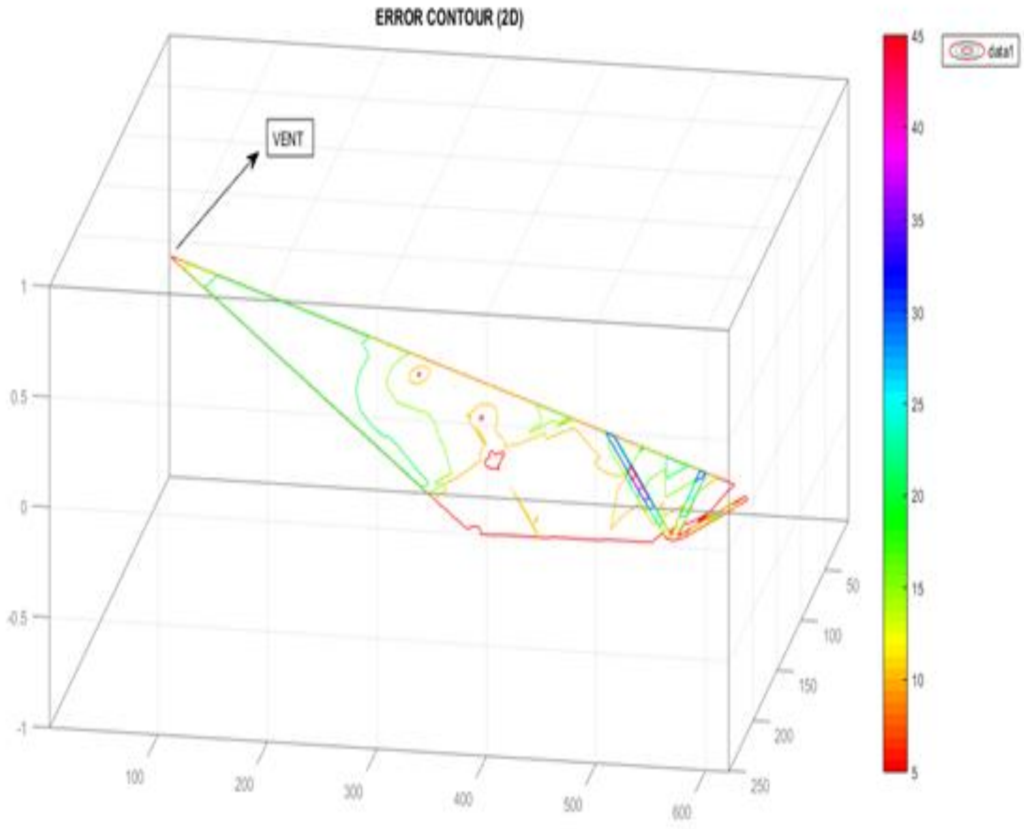


*Figure 77: 3D Contour View of EBK Error*

*Figure 78* shows the locations of regions with highest (in red) and lower (in green) magnitude of errors.

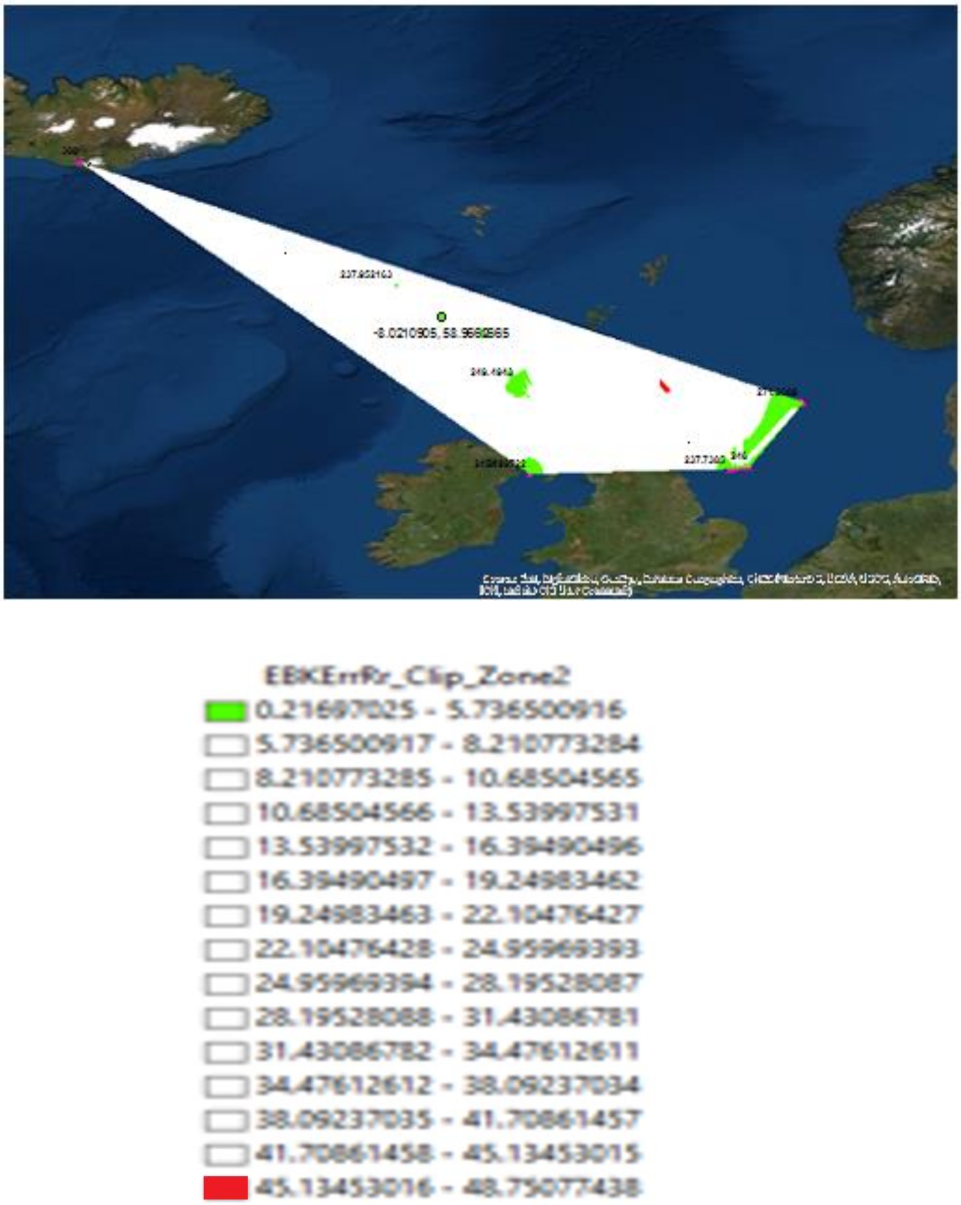


*Figure 78: Location of Extreme Low and Extreme High Errors in MBR*

It is observed that the error magnitude is significantly higher (up to +45K) near the hotter temperature areas when compared against those regions with colder temperatures. (33% of the estimates lie between 0K to 15K, 33% estimates lie between 15K-30K, 33% of estimates lie between 30K-45K error magnitudes). While this could be due to lower number of samples closer to vent and also the sample points near vent being significantly at a higher temperature than those found at other regions.

Based on the above analysis, a perspective of error map is created as shown in *Figure 79*. In this map, the intervals are chosen such that there are a maximum of 3 classes to assess the threshold of reliability of the Go/No-Go regions in the atmosphere.

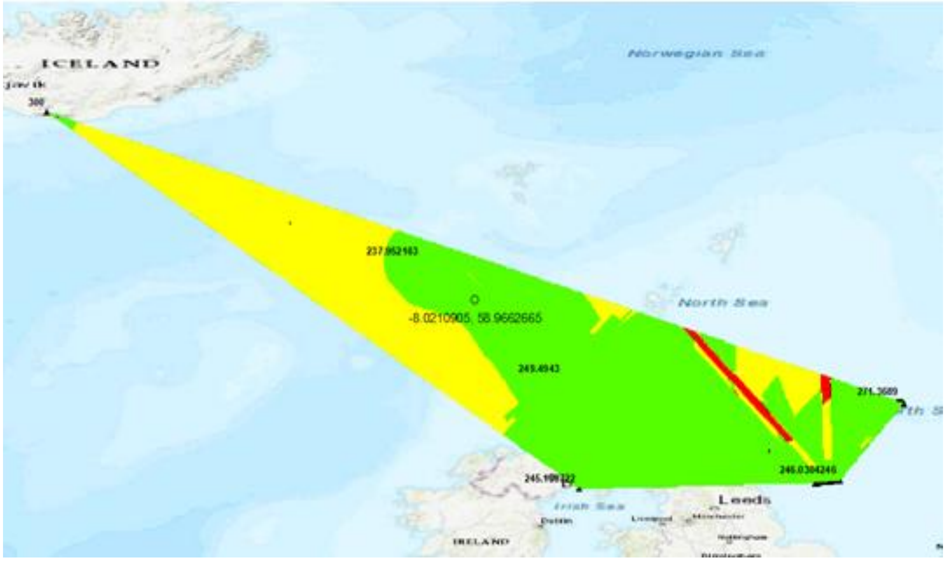


| ***EBK Error (Raster Clipped)*** | | |
|---|---|---|
| | 0.21697025 | 15.06260445 |
| | 15.06260447 | 27.43396629 |
| | 27.4339663 | 48.75077438 |

*Figure 79: Categorization of Reliability of Zones based on Errors*

Regions in green are most accurate (<5K) and regions coloured in red are least accurate (<45K) (error). Regions where adequate input data are available provide nearly most of the reliable predictions while those regions were adequate input samples were not well spread out yielded higher errors.

iii. EBK – Error Growth Pattern

In *Figure 80*, the growth pattern in errors in 8 iterations when classified into 15 classes is shown.

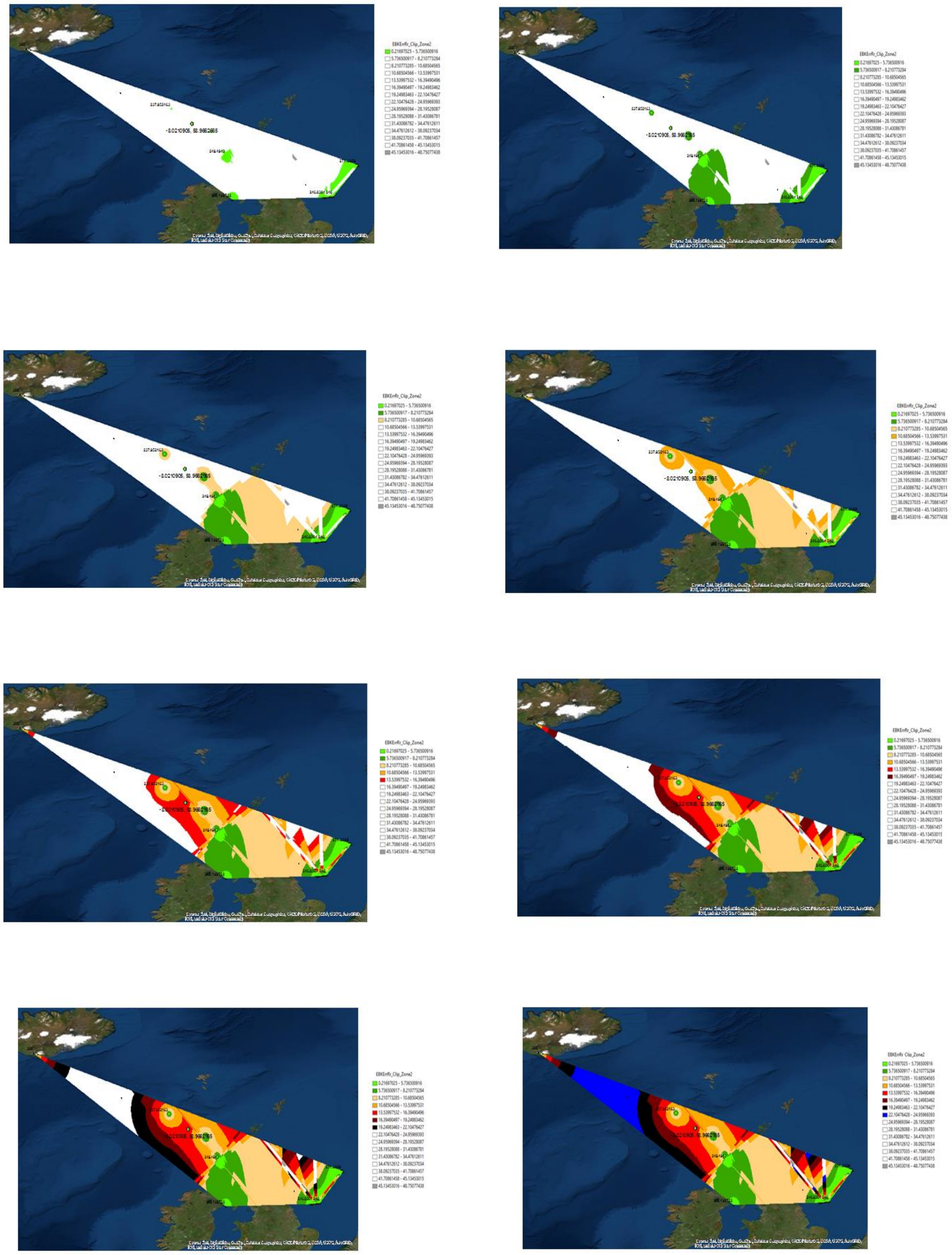

*Figure 80: Growth pattern in errors when categorized into 15 classes.*

The growth is observed to be growing from regions around the points where the samples were available. As the Kriging progresses, through each iteration, in regions where the data samples were available, error magnitudes were observed to be lower. As further iterations progressed, regions that are sparse in data are kriged based on the distance from those regions where the data is available and this leads to larger error values.

iv. EBK - Distance vs Error Analysis

For the selected locations at various distances from the Vent, the error magnitudes were grouped into intervals of 10K and analysed in detail in *Figure 81*.

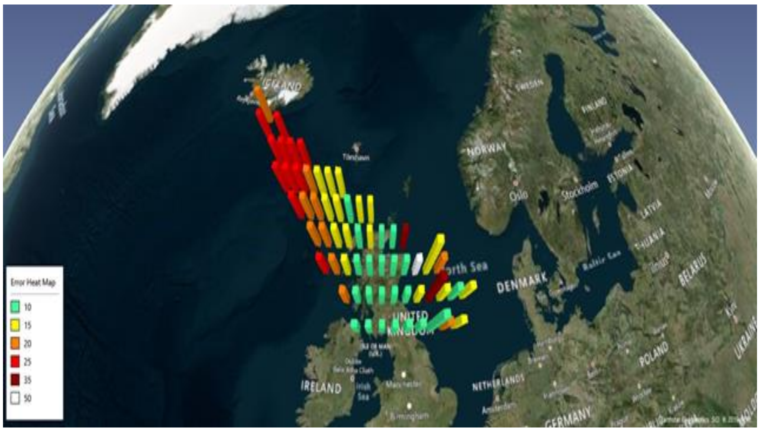


*Figure 81: Discrete representation of error values in the form of stacks*

If upto 10K error magnitude (which is 10% error) is defined to be acceptable in non-critical regions (where more data is available) then with intervals of 5K, if critical regions (regions where input data is less in number) are categorized, the following patterns are observed. i.e. For error values between 10K-45K, these categories are observed:

a. Extreme errors (>35K) account only 3% of the total region

b. Medium errors (between 15K to 35 K) account for 36% of the total region

c. Lesser errors (below 15K) account for 61% of the total region

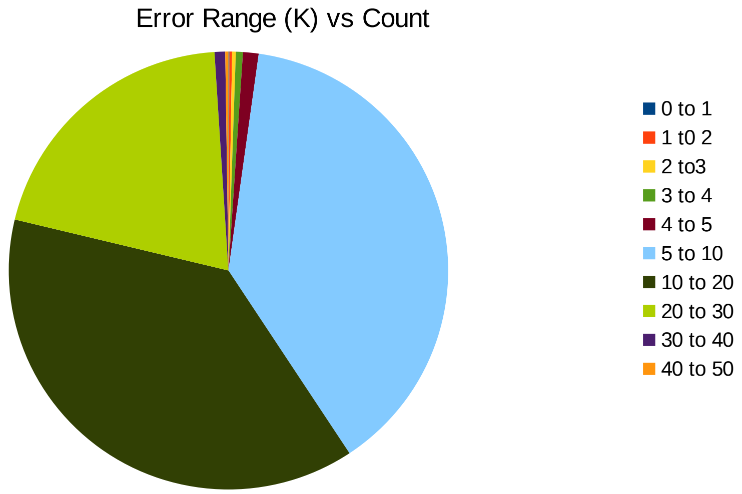


*Figure 82: Approximate Count of Error Ranges in Intervals of 5 Units*

As shown in the *Figure 82*, since error values less than 5K and above 30K are very miniscule in proportion, it can be said that to achieve lower errors using EBK method, the sampling criteria can be improved for density and distribution of the samples recorded during experiments.

v. Comparison of EBK and EBKT Prediction Maps for Accuracy

EBK and EBKT Prediction Maps were generated at 1 degree temperature intervals and zoomed for detailed analysis of two points on either side of the centre of the map, which is the origin of the semivariograms. This is done to compare the errors at these points using both techniques and then conclusively establish which method is better for interpolation of air temperature variables, as shown in *Table 24*.

| | **Left of Origin - EBK** | **Left of Origin - EBKT** | **Right of Origin - EBK** | **Right of Origin - EBKT** |
|---|---|---|---|---|
| **Latitude (dd)** | 59.9374 | 59.9374 | -6.72907 | -6.72907 |
| **Longitude (dd)** | -9.47537 | -9.47537 | 58.5211 | 58.5211 |
| **Altitude (m)** | 8048 | 8048 | 7487 | 7487 |
| **Input (K)** | 237.952163 | 237.952163 | 245.759699 | 245.759699 |
| **Prediction (K)** | 238.521103 | 231.402527 | 245.251556 | 242.355881 |
| **Max Error (K)** | 4.63958 | 25.275112 | 3.975919 | 14.778852 |

*Table 24: Comparison of error values with reference to origin by EBK and EBKT methods*

- The point chosen to the left of origin is at a greater distance (136 km) when compared to the point chosen to the right of the origin (90 km).
- As shown in *Table 24,* the errors on the left of the origin in EBK was only ~4K while it was ~25K for EBKT. Similarly, the error magnitude to the right of the origin for EBK was observed to be ~3K while EBKT value was ~14K.
- Between EBK and EBKT, EBK without transformation consistently outperforms with significantly lesser error rates (approximately 3 times lesser error) on either sides of the origin.

This proves EBK without transformation technique is superior to SK and EBK with transformation methods as it yields more accurate results consistently.

## 5. Comparative Analysis of Block Grade EBK against NCEP

i. Comparative Profile Analysis between EBK and NCEP

EBK block averages were validated against the NCEP NWP model values for the same duration in the area of interest. *Figure 83* shows a consistent deviation of 10K of EBK values from NCEP estimates. However, the small-scale spatial variations were better estimated using the EBK method with a maximum deviation of ~12K.

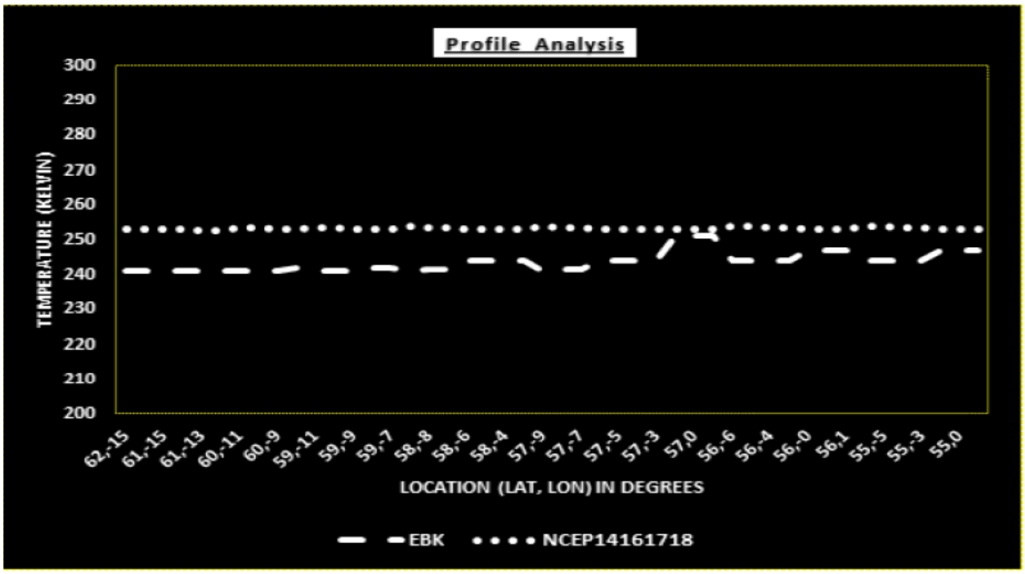


*Figure 83: Plot Validating EBK Prediction Profile against NCEP Profile*

ii. Comparative Probability Density Analysis between EBK and NCEP

*Figure 84* shows the non-parametric probability density estimation for NCEP and EBK block averages. While EBK estimates had a Standard Deviation of ~3K, NCEP measured at ~0.57K.

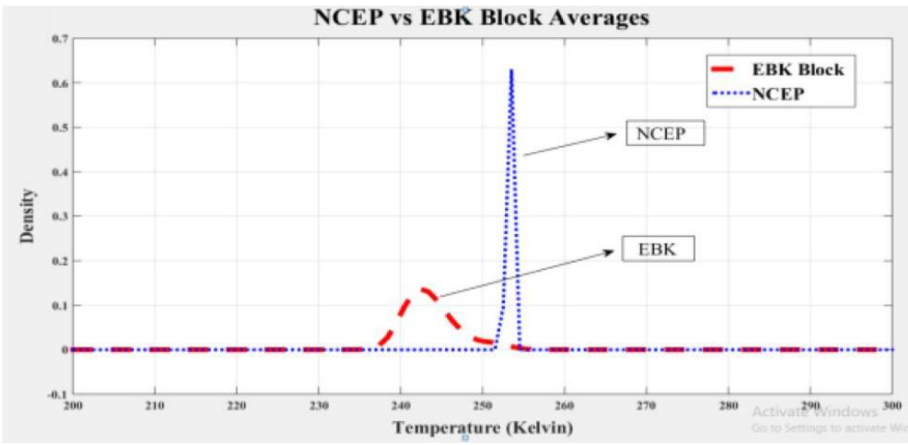


*Figure 84: Plot of Probability Density Estimates - EBK Prediction vs NCEP*

Given the above analysis, the MBR depicted in the *Figure 85* was coarsely split into two categories based on the error magnitude of EBK estimates. These 2 categories roughly get mapped into two zones – one is a region where abundant input data samples were available and other region had sparse input data samples. These were labelled as “Rich Regions” and “Poor Regions”, respectively. A comparison was drawn for these two zones among three set of outputs, viz EBK estimates in Punctual Kriging mode, EBK estimates in Block Kriging mode and NCEP model, outputs, to assess the similarity of the estimates across the 3 methods as part of equivalence class testing approach.

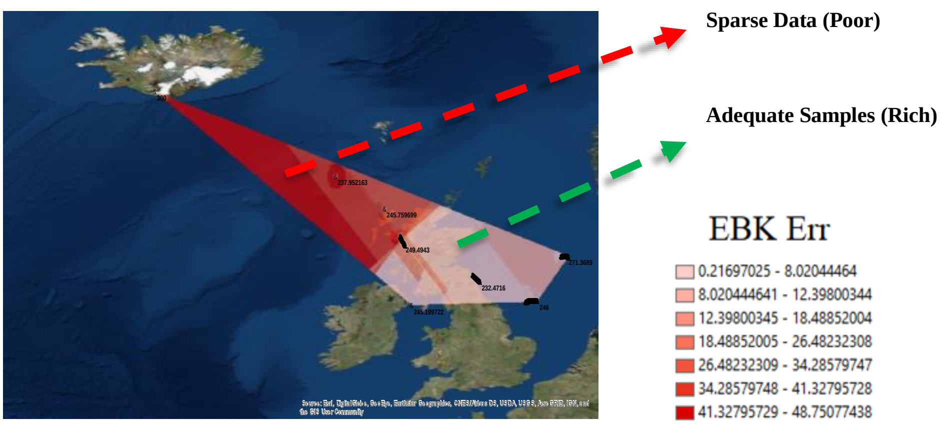


*Figure 85: EBK Map Showing Total MBR, Data Rich and Data Poor Regions*

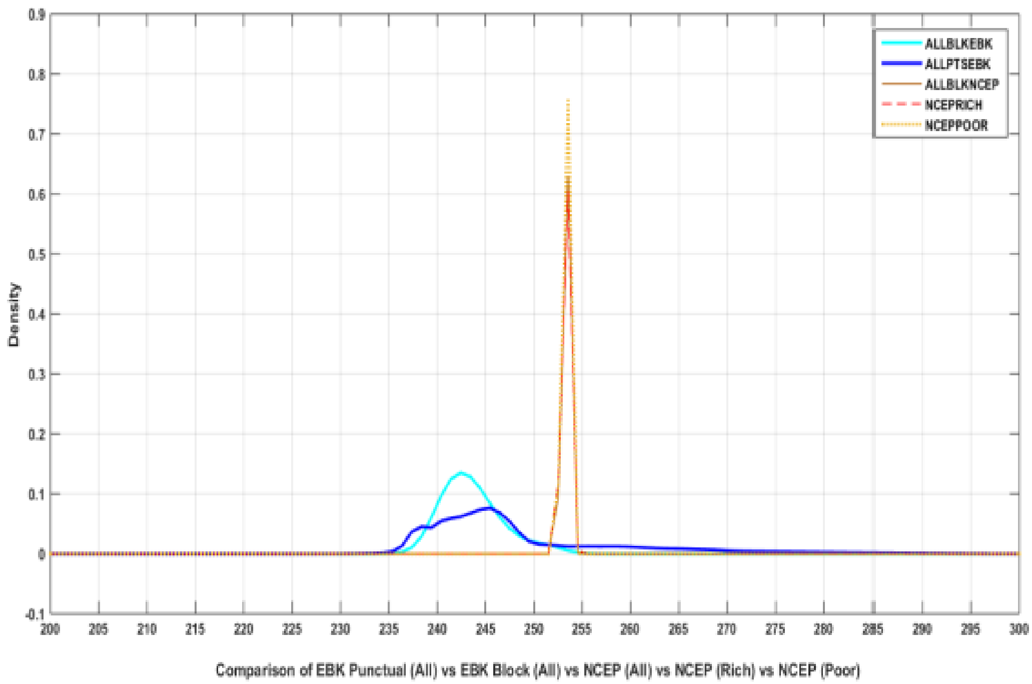


*Figure 86: Plot comparing Probability Density Graphs of EBK Point and Block estimates against NCEP estimates for Total MBR, Data Rich and Data Poor Regions*

| Temp Averages(K) | Block Poor | Block Rich | Block All | Point Poor | Point Rich | Point All |
|---|---|---|---|---|---|---|
| **NCEP** | 253 | 253 | 253 | - | - | - |
| **EBK** | 241 | 245 | 243 | 257 | 245 | 248 |

*Table 25: Comparison of EBK Point, Block Averages against NCEP in Total MBR, Data Rich & Poor Regions*

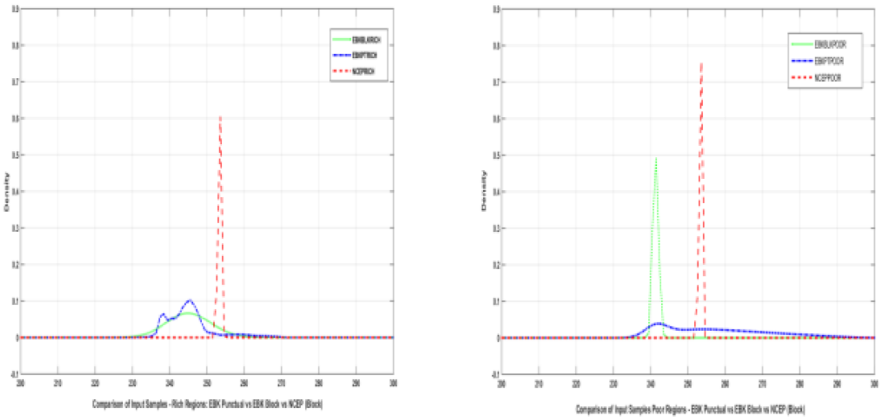

*Figure 87: Plots comparing EBK Estimates in Data Rich, Poor Regions against corresponding NCEP estimates*

From *Figure 86 and Figure 87* and *Table 25*, it is evident that, although both EBK Punctual & Block variants predict the same average values of around ~245K in data rich regions, the spread of small-scale variations differ widely in both methods. Also, from *Table 25* it is evident that, the difference in average values is higher between EBK Block estimates and NCEP only in data poor regions. So, with adequate sampling, EBK (Block) is a suitable method to augment NWP estimates.

# V. Application: Case Study – Aviation Weather Safety

The UK Met Office, in its article, titled, "How accurate are our public forecasts? - Met Office," n.d., has defined the following criteria to measure success of prediction of weather variables by models – "*For a three hour forecast of normal weather, the measure of success for prediction of temperatures is expected to be within ±2º C 92% of the time it is reported". The smallest size of the grid cell achieved for this study site with EBK was 4x2/2x4 units using Arc GIS software. The error range for this size of zone was found to be between 0K-2K. With Empirical Bayesian Kriging, the defined success rate was achieved for a spatial resolution as low as 2km x 4km. In the aerospace industry, this area roughly translates the detection of potential ash laden field, as early 20 seconds, ahead of time, by jet aircrafts in cruising altitude with high airspeeds and wind speed conditions. This methodology is therefore highly suited for a variety of other aerospace applications also, such as:

- To augment on-board severe weather alert systems, despite its probabilistic origins and simulation scope
- To help define guidelines for sample data collection using research aircrafts during future eruptions to assess the safety of an airspace
- To augment the outputs of NWP for developing Model Output Statistics (MOS) systems

Of the three potential applications, although MOS was envisaged in US in 1968 for airports in association with Meteorological Terminal Aviation Routine Weather Report (METAR), it is yet to be applied for mesoscale size regions due to limitations in accuracies of currently used methodologies. Model Output Statistics is largely a multiple linear regression technique in which predictands, near-surface weather variables such as, air temperature, wind direction, gusts, visibility are related statistically to one or more predictors. The predictors are typically forecasts from a NWP model, climatic data.

An example of MOS currently recommended by US FAA's NextGen Weather Concept of Operations for aviation is Localized Aviation MOS Program (LAMP). LAMP, discussed in Rudack and Ghirardelli, (2010) is based on international Global Forecasting System (GFS) model and is a statistical technique which provides both categorical and probabilistic forecast guidance for weather elements. LAMP produces forecasts from multiple linear regression equations that update the GFS MOS. LAMP updates GFS MOS on an hourly basis, to produce short range aviation forecast guidance and is disseminated from NCEP to 1600 stations as well as gridded stations on 2.5 km grid out to 25 hours.

Gridded LAMP provides gridded analyses of observations and operational LAMP forecasts for aviation forecasting. Verification of LAMP Forecast Guidance has shown improvements over the GFS MOS forecasts in accuracy and persistence.

Rudack and Ghirardelli, (2010) discuss how Nearest Neighbour (NN) and Bilinear Interpolation techniques are used in the context of comparing LAMP forecasts with Regional and Mesoscale Weather Models and Ensembles for various altitudes. Thus, in place of Multiple Linear Regression or Nearest Neighbour or Bilinear Interpolation techniques, Empirical Bayesian Kriging interpolation technique can be experimented for both continuous and discrete variables, for improving regridding method based NWP used in Volcanic Ash Dispersion advisories for better accuracy and persistence.

Thus, given a potential use case in the aviation industry, we generate Go/No-Go Zones using the point prediction map produced using EBK by comparing against NCEP values. The NCEP has a narrow temperature range of 251.4K-253.9K. *Figure 88* shows regions with same range of observations in EBK are highlighted in green color (~247K to ~254K). Areas with gradual variations in orange color, reveal EBK underestimations/overestimations against NCEP (±25K), while regions with red depict significant overestimations in comparison against NCEP (~+40K).

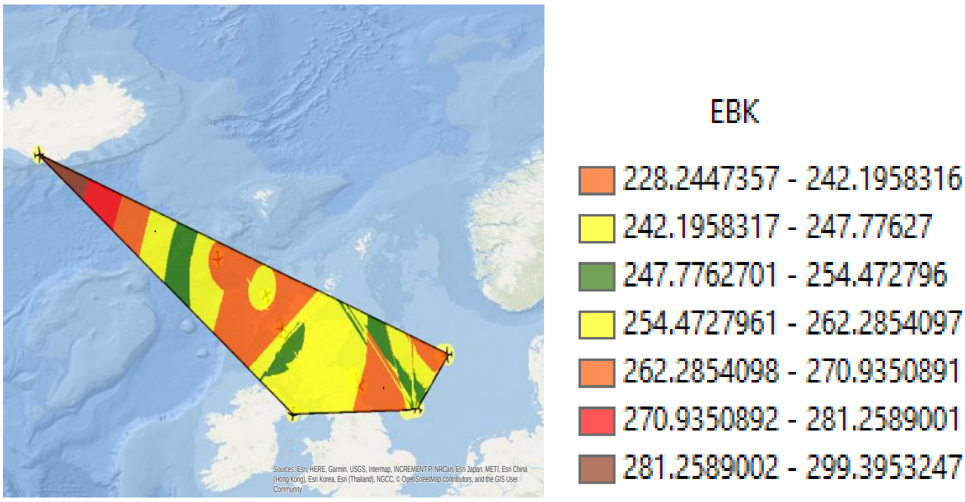


*Figure 88: Map Showing Risk Zones Categorized As Go/No-Go Regions*

Irrespective of the significant global variations in the input temperature across days, the EBK risk map reflects a balanced integration of unbiased global averages and small-scale variations, wherever adequate data is available.

## 1. Generation & Validation of Risk Map with Block Grade Go/No-Go Zones

Often in environmental monitoring projects, estimation of areal average values for large areas is required. Block kriging is a statistical method of computing areal averages that can be used with datasets that exhibit both regional trends and spatial persistence. This method generally provides average values for rectangular values and is appropriate for use with large datasets. A simple block analysis is performed to assess if there is a significant change in accuracy of values when compared against point kriging outputs. To compare the NCEP temperature averages (measured in Kelvin) with the prediction estimates of kriging, 1 degree x 1 degree grids were created using EBK estimates. EBK block averages shown in *Figure 89* reveal a narrow range of global temperature estimates ranging between, 241 K to 251 K. The global EBK block mean is around ~243K, which is ~10K lesser than NCEP average.

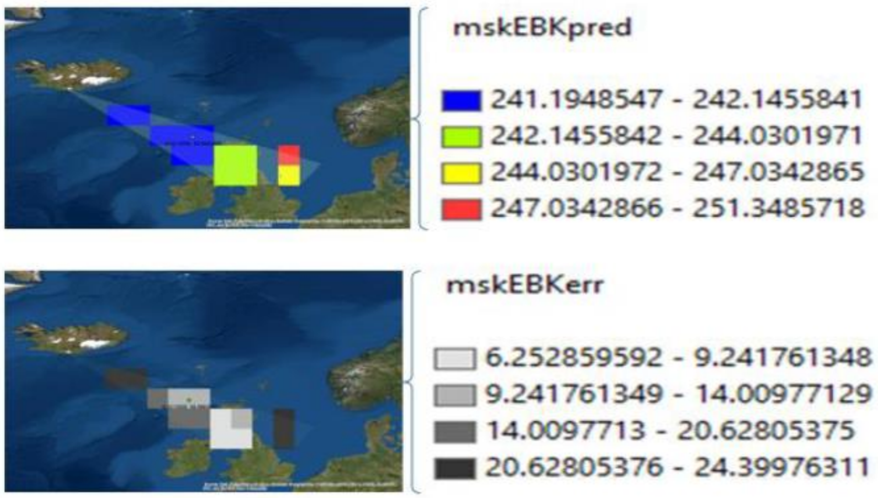


*Figure 89: Maps showing Block Grade EBK – Prediction Estimates (above) & Error Estimates (below)*

To generate the risk map with Go/No-Go Zones, shown in *Figure 90*, using only the EBK block grade estimates, the EBK map was merged with NCEP values using Fuzzy Overlay operation. While the Fuzzy AND overlay type operation returns the minimum value of the sets the cell location belongs, Fuzzy OR returns maximum values.

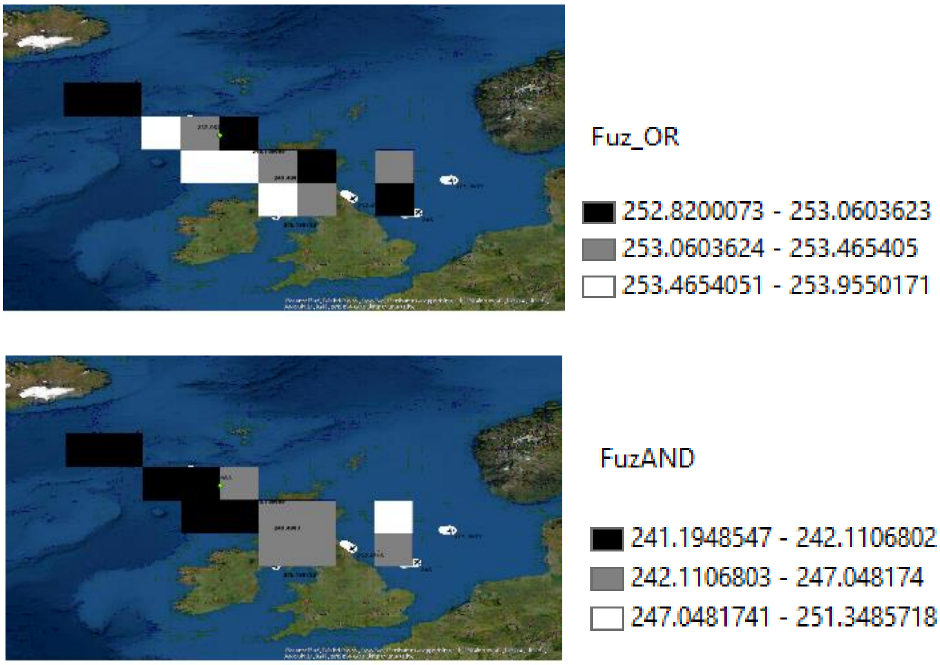


*Figure 90: Overlay maps generated using Fuzzy AND (above) and Fuzzy OR (below) Operations*

| **Overlay Operation** | **Min Temp (K)** | **Max Temp (K)** | **Mean Temp (K)** | **Std. Dev. (K)** |
|---|---|---|---|---|
| **Fuzzy AND** | 241.195 | 251.349 | 243.41 | 2.97592 |
| **Fuzzy OR** | 252.82 | 253.955 | 253.26 | 0.37248 |

*Table 26: Comparison of Fuzzy AND and Fuzzy OR minimum, maximum, mean and SD values*

As shown in *Table 26*, since each method outputs different ranges of values for the overlay maps generated, an alternative method is used to validate the accuracy of the merged outputs. To analyse the overlay values, a classical statistical method is used to merge two groups of same category that vary in their values using mean, sample size and standard deviation inputs as discussed in the article "Cochrane Handbook for Systematic Reviews of Interventions," n.d..

Using this approach, NCEP estimates were augmented using block grade EBK prediction estimates. (Sample Size: 46 in each category).

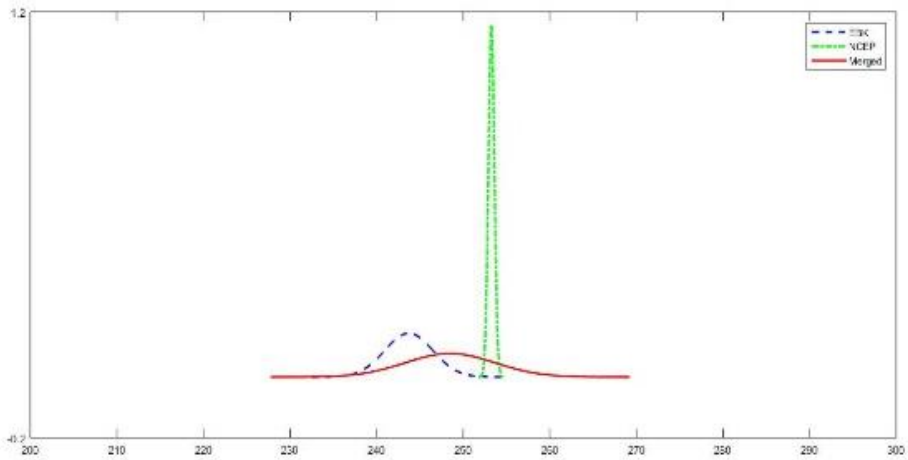

*Figure 91: Plot comparing the mean & SD values of EBK (Block), NCEP and Overlayed estimates*

From *Figure 91*, it is evident that, the acceptable Standard Deviation (SD) lies approximately at 4 sigma levels, which implies, 99.9% of the estimates are reliable in the merged output generated using EBK block grade prediction estimates and NCEP estimates.

| Temp (K) | EBK | NCEP | Merged |
|---|---|---|---|
| **Mean** | 243.7100 | 253.2500 | 248.4800 |
| **S.D.** | 2.7785 | 0.3448 | 5.1845 |

*Table 27: Comparison of temperature averages & SD amongst EBK, NCEP & Overlay estimates generated statistically*

Also from *Table 27*, it is observed that spatial Fuzzy AND operation produces values that are closer to statistically computed values to generate an overlayed risk map using NCEP and EBK estimates.

# VI. Conclusion

While volcanic ash dispersion modeling has been attempted using both spatial and non-spatial approaches, predicting and mapping the actual spatial distribution of airborne ash temperature using geostatistical methods such as kriging have not been researched till date. Geostatistical Kriging method was found to be more effective than traditional linear regression methods, such as, Multiple Linear Regression (MLR), used in this study, to represent stochastic spatial process locally as a stationary or non-stationary random field, where the parameters of the locally defined random field were found to vary across space. Empirical Bayesian Kriging (EBK), in particular, provided accurate predictions of data on a local scale developing a spatial model in which temperature concentrations were considered as the response variable; location variables, derived from flight data, were used as predictors. The methodology involved partitioning the whole dataset into small subsets to model each partition, and then by combining all outputs to predict at unknown locations using a distance metric in a Bayesian framework. A variety of verification and validation methods were used to assess the accuracy, consistency, profiles at various spatial scales for MLR, Simple Kriging (SK), EBK (without Transformation) and EBKT (EBK with data transformation) techniques against NCEP NWP estimations. A detailed analysis of errors was attempted to establish the best method out of all the explored techniques. It was observed that Empirical Bayesian Kriging (EBK) technique without data transformation yielded the best prediction and error estimates when compared against MLR, SK and EBKT techniques. Hence, a risk map was prepared for categorization of safe go zones and unsafe no-go zones using EBK method.

There are several merits of applying this geospatial approach to interpolation in aviation context. Empirical Bayesian Kriging is not affected by aerospace aspects such aircraft speed or engine type or the angle in which the flight path transects the ash cloud. It is also not directly dependent vulcanological explosion criteria such as VEI or volume of material erupted or eruption column height & angle. While the technique needs to be tested on temperature of resuspended ash datasets exclusively, modeling of past eruptions is feasible irrespective of the ash properties such as shape or size or refractive index or chemical composition. As a result, backward tracing of ash properties from weather parameters is also achievable even for volcanoes even in human inhabited regions and irrespective of age of the ash cloud.

The method also has no direct dependency on geological aspects such as terrain information or marine parameters. Even properties of volcanic gases such as sulphur dioxide, traditionally used as proxy for ash detection in other modeling methodologies are not required. As a result, the NWP data can be more tightly coupled with VAFDTM models.

Using EBK, each weather variable can be independently interpolated but co-kriging of weather variables is currently not explored using this technique. Nowcast weather simulation attempts are usually severely error prone in atmospheric models even for minor fluctuations to initial conditions. This modeling method eliminates such dependencies on assumptions on past data. The method is not vulnerable to false positives in estimates arising due to incorrect identification of dust or ice as ash and it can be applied without any modifications across seasons and diurnal variations. Sophisticated airborne remote sensing or in situ sensing instruments are not needed to source the sample values and can work with even small sample sizes. Data can be collected from drone, balloon platforms too with irregular sample distributions. Further this method works well with data from both transect and regionally distributed samples.

3D thematic maps and time lapse visualizations can be generated and overlayed for standardized GIS reporting across countries for regulatory authorities, aircraft OEMS, engine manufacturers and airliners to plan re-routing quickly. Although this technique is not based on the physics of the natural processes and uses the probabilistic approach, still the results were found to be consistent and reliable on validations. The method works irrespective of the absolute location of the phenomenon on any part of the earth and handles outliers effectively. Its usage is not limited to the immediate neighbourhood of volcanoes and can also output multi-layered grid cells as outputs. For generating prediction and error estimates for an area as large as a continental scale for a single weather variable, like temperature, the memory requirements are within the limits of a general-purpose computer and the process gets completed within few minutes for a sample size of ~1000 input points.

In summary, it is observed that EBK, not only produces estimates of block mean closer to NWP averages but also models the local, small scale spatial variances better than NWP models, even at coarser spatial resolutions. In addition, it is also evident that when EBK is applied as a punctual kriging method, it is observed to yield unbiased averages even for spatially clustered, heteroskedastic datasets.

Hence, even in nonstationary datasets with absence of significant spatial autocorrelation, EBK can be used to assess likelihood of the volcanic ash exceeding a defined threshold at a given place so that risk to operations can be determined. Thus, Kriging technique, which was initially conceived, designed, developed and implemented for Gaussian world with higher emphasis on Spatial Autocorrelation, this research validates the appropriateness of using EBK method to help model the simultaneous existence of spatial autocorrelation and spatial heterogeneity at different degrees that are observed in events that obey Pareto conditions, to generate accurate, synoptic scale profiles and distribution maps for airborne volcanic ash dispersion. By overlaying on prediction estimates on NWP outputs, risk maps categorizing the patterns in ash distribution can be visualized and risks to aviation operations can also be established.

# Glossary of Terms

AMDAR - is a program initiated by the World Meteorological Organization. AMDAR is used to collect meteorological data worldwide by using commercial aircraft.

ASHTAM - provides information on the status of activity of a volcano when a change in its activity is or is expected to be of operational significance. This information is provided using the volcano level of alert color code .

ATS - is a service which regulates and assists aircraft in real-time to ensure their safe operations by streamlining the flow, preventing collision of aircrafts and providing search and rescue services during accidents.

BADC - is the Natural Environment Research Council's (NERC) Designated Data Centre for the Atmospheric Sciences. The role of the BADC is to assist UK atmospheric researchers to locate, access and interpret atmospheric data and to ensure the long-term integrity of atmospheric data produced by NERC projects.

CAA - is a national or supranational statutory authority that oversees the regulation of civil aviation, including the maintenance of an aircraft register.

DLR – is a German Aerospace Center (DLR) operates the largest civilian fleet of research aircraft and helicopters in Europe. These highly modified aircraft are either themselves the subject of aeronautics research or are used to observe the Earth, the ocean surfaces and the atmosphere.

ECMWF – is an independent intergovernmental organization supported by most of the nations of Europe.

EnKF - is a recursive filter suitable for problems with a large number of variables, such as discretizations of partial differential equations in geophysical models. The EnKF originated as a version of the Kalman filter for large problems (essentially, the covariance matrix is replaced by the sample covariance), and it is now an important data assimilation component of ensemble forecasting.

ELR - is the rate of decrease of temperature with altitude in the stationary atmosphere at a given time and location.

EPS - are Numerical Weather Prediction (NWP) systems that allow one to estimate the uncertainty in a weather forecast as well as the most likely outcome.

ERA - is a global atmospheric reanalysis from 1979, continuously updated in real time. The data products include a variety of surface parameters, describing weather as well as ocean-wave and land-surface conditions.

ESP - are those parameters that describe the initiation condition for numerical (weather prediction) models. Different models require different input parameters, however a common feature of all numerical models is that the quality of model outputs is dependent on the quality of model inputs.

FAAM - is a research facility that operates a specially adapted research aircraft with the support of the UK atmospheric science community to measure most atmospheric parameters, and is capable of advanced remote sensing, cloud microphysics and measuring complex chemical species in the atmosphere.

FIR – is an airspace of defined dimensions within which flight information service and alerting service are provided

FL - in aviation and aviation meteorology, a flight level (FL) is an aircraft's altitude at standard air pressure, expressed in hundreds of feet. The air pressure is computed assuming an International Standard Atmosphere pressure of 1013.25 hPa (29.92 inHg) at sea level, and therefore is not necessarily the same as the aircraft's actual altitude, either above sea level or above ground level.

GEFS - is a weather forecast model made up of 21 separate forecasts, or ensemble members. The National Centers for Environmental Prediction (NCEP) started the GEFS to address the nature of uncertainty in weather observations, which are used to initialize weather forecast models.

GFS - is a weather forecast model produced by the National Centers for Environmental Prediction (NCEP). Dozens of atmospheric and land-soil variables are available through this dataset, from temperatures, winds, and precipitation to soil moisture and atmospheric ozone concentration.

HYSPLIT - is a computer model that is used to compute air parcel trajectories to determine how far and in what direction a parcel of air, and subsequently air pollutants, will travel. HYSPLIT is also capable of calculating air pollutant dispersion, chemical transformation, and deposition.

IAVW – is an International Civil Aviation Organization (ICAO) commission that defines international protocols for the monitoring and provision of warnings to aircrafts in presence of volcanic ash in the atmosphere.

IDW - is a type of deterministic method for multivariate interpolation with a known scattered set of points. The assigned values to unknown points are calculated with a weighted average of the values available at the known points.

IMD - is the principal agency responsible for meteorological observations, weather forecasting and seismology.

IFS - is a global numerical weather prediction system jointly developed and maintained by the European Centre for Medium-Range Weather Forecasts (ECMWF) based in Reading, England, and Météo-France based in Toulouse.

IN/CCN - Ice Nuclei / Cloud Condensation Nuclei

An ice nucleus, is a particle which acts as the nucleus for the formation of an ice crystal in the atmosphere.

Cloud condensation nuclei, also known as cloud seeds, are small particles typically 0.2 µm, or one hundredth the size of a cloud droplet.

LAMP - is a statistical system which provides forecast guidance for sensible weather elements. LAMP updates MOS on an hourly basis, is run on NOAA/NWS/NCEP Weather and Climate Operational Supercomputer Systems (WCOSS) computers and disseminated centrally from NCEP and provides guidance for over 1600 stations as well as gridded observation and forecast guidance on the NDFD CONUS 2.5-km grid out to 25 hours.

MBR - is a minimum bounding rectangle based on the combined spatial extent or envelope of one or more selected features.

MER - describes the eruption intensity of a volcano. The eruption rate is determined by the eruption column height and length of lava flows. In large eruptions it is possible for millions of tons of lava to be emitted every second. Mass eruption rates cover three orders of magnitude up to millions of tons per second.

MOGREPS-G – is a model from Met Office that recently introduced a short-range ensemble prediction system known as MOGREPS. This system consists of global and regional ensembles, with the global ensemble providing the boundary conditions and initial-condition perturbations for the regional ensemble.

MOS - is a multiple linear regression technique used in weather forecasting, in which predictands, often near-surface quantities (such as two-meter-above-ground-level air temperature, horizontal visibility, and wind direction, speed and gusts), are related statistically to one or more predictors. The predictors are typically forecasts from a numerical weather prediction (NWP) model, climatic data, and, if applicable, recent surface observations. Thus, output from NWP models can be transformed by the MOS technique into sensible weather parameters that are familiar to a layperson.

NAME - is a Lagrangian air pollution dispersion model for short range to global range scales. It employs 3-dimensional meteorological data provided by the Met Office's Unified National Weather Prediction Model. Random walk techniques using empirical turbulence profiles are utilized to represent turbulent mixing.

NATS - provides en-route air traffic control services to flights within the UK flight information regions and the Shanwick Oceanic Control Area. It also provides air traffic control services to 14 UK airports.

NCEP/NCAR - is an atmospheric reanalysis produced by the National Centers for Environmental Prediction (NCEP) and the National Center for Atmospheric Research (NCAR). It is a continually updated globally gridded data set that represents the state of the Earth's atmosphere, incorporating observations and numerical weather prediction (NWP) model output from 1948 to present.

NFZ - also known as a no-flight zone (NFZ), or air exclusion zone (AEZ), is a territory or area established by a military power over which certain aircraft are not permitted to fly.

NOTAM - is a notice filed with an aviation authority to alert aircraft pilots of potential hazards along a flight route or at a location that could affect the flight

NWP – is a system that uses mathematical models of the atmosphere and oceans to predict the weather based on current weather conditions.

OPC - is a sensor used for monitoring and diagnosing particle contamination within specific clean media, including air, water and chemicals.

PIREP - is a report of actual flight or ground conditions encountered by an aircraft. Reports commonly include information about atmospheric conditions (like temperature, icing, turbulence) or airport conditions (like runway condition codes or ground equipment failures).

SIGMET - is a severe weather advisory that contains meteorological information concerning the safety of all aircraft. Compared to AIRMETs, SIGMETs cover more severe weather.

VAA - analyses are made public in the form of volcanic ash advisories (VAAs), involving expertise analysis of satellite observations, ground and pilot observations and interpretation of ash dispersion models.

VAAC - is a group of experts responsible for coordinating and disseminating information on atmospheric volcanic ash clouds that may endanger aviation.

VAFTAD – is a model developed by the Air Resources Laboratory (ARL) of the National Oceanic and Atmospheric Administration (NOAA) for forecasting the visual transport of volcanic ash clouds.

VEI - is a relative measure of the explosiveness of volcanic eruptions.

VONA - issues reports for changes, both increases and decreases, in volcanic activities, providing a description on the nature of the unrest or eruption, potential or current hazards as well as likely outcomes.

WMO - is a specialized agency of the United Nations responsible for promoting international cooperation on atmospheric science, climatology, hydrology and geophysics.

WRF - is a system designed to serve both atmospheric research and operational forecasting needs.

VOL-CALPUFF - is a model designed to simulate the dispersion of buoyant, puff or continuous point and area pollution sources as well as the dispersion of buoyant, continuous line sources.

## List of Publications

Krishnan, M., & Rajan, K. S. (2021). Generating Spatial Distribution of Volcanic ASH Spread. 2021 IEEE International Geoscience and Remote Sensing Symposium IGARSS, 7271–7274. https://doi.org/10.1109/IGARSS47720.2021.9553353

Krishnan, M., & Krishnan Sundara, R. (2021). Generation of Spatial Profiles and Mapping of Volcanic Ash Distribution. GI_Forum, 1, 13–23. https://doi.org/10.1553/giscience2021_01_s13

## References


Beckett, F. M., Witham, C. S., Leadbetter, S. J., Crocker, R., Webster, H. N., Hort, M. C., Jones, A. R., Devenish, B. J., & Thomson, D. J. (2020). Atmospheric Dispersion Modelling at the London VAAC: A Review of Developments since the 2010 Eyjafjallajökull Volcano Ash Cloud. *Atmosphere*, *11*(4), Article 4. https://doi.org/10.3390/atmos11040352

Biondi, D., & Todini, E. (2018). Comparing Hydrological Postprocessors Including Ensemble Predictions Into Full Predictive Probability Distribution of Streamflow. *Water Resources Research*, *54*(12), 9860–9882. https://doi.org/10.1029/2017WR022432

Bonadonna, C., Folch, A., Loughlin, S., & Puempel, H. (2012). Future developments in modelling and monitoring of volcanic ash clouds: Outcomes from the first IAVCEI-WMO workshop on Ash Dispersal Forecast and Civil Aviation. *Bulletin of Volcanology*, *74*(1), 1–10. https://doi.org/10.1007/s00445-011-0508-6

Chilès, J.-P., & Desassis, N. (2018). Fifty Years of Kriging. In B. S. Daya Sagar, Q. Cheng, & F. Agterberg (Eds.), *Handbook of Mathematical Geosciences: Fifty Years of IAMG* (pp. 589–612). Springer International Publishing. https://doi.org/10.1007/978-3-319-78999-6_29

*Cochrane Handbook for Systematic Reviews of Interventions*. (n.d.). Retrieved April 20, 2023, from https://training.cochrane.org/handbook/current

Compo, G. P., Whitaker, J. S., Sardeshmukh, P. D., Matsui, N., Allan, R. J., Yin, X., Gleason, B. E., Vose, R. S., Rutledge, G., Bessemoulin, P., Brönnimann, S., Brunet, M., Crouthamel, R. I., Grant, A. N., Groisman, P. Y., Jones, P. D., Kruk, M. C., Kruger, A. C., Marshall, G. J., … Worley, S. J. (2011). The Twentieth Century Reanalysis Project. *Quarterly Journal of the Royal Meteorological Society*, *137*(654), 1–28. https://doi.org/10.1002/qj.776

*Dataset Collection Record: Eyjafjallajokull Volcanic Ash Cloud Measurements and Imagery*. (n.d.). Retrieved April 20, 2023, from https://catalogue.ceda.ac.uk/uuid/e6f5502c687f25a6c7009d4704b124b4

Denlinger, R. P., Pavolonis, M., & Sieglaff, J. (2012). A robust method to forecast volcanic ash clouds. *Journal of Geophysical Research: Atmospheres*, *117*(D13). https://doi.org/10.1029/2012JD017732

Gislason, S. R., Alfredsson, H. A., Eiriksdottir, E. S., Hassenkam, T., & Stipp, S. L. S. (2011). Volcanic ash from the 2010 Eyjafjallajökull eruption. *Applied Geochemistry*, *26*, S188–S190. https://doi.org/10.1016/j.apgeochem.2011.03.100

Gordeev, E. I., & Girina, O. A. (2014). Volcanoes and their hazard to aviation. *Herald of the Russian Academy of Sciences*, *84*(1), 1–8. https://doi.org/10.1134/S1019331614010079

Gribov, A., & Krivoruchko, K. (2020). Empirical Bayesian kriging implementation and usage. *Science of The Total Environment*, *722*, 137290. https://doi.org/10.1016/j.scitotenv.2020.137290

Hjaltadóttir, S., Vogfjörd, K. S., Hreinsdóttir, S., & Slunga, R. (2015). Reawakening of a volcano: Activity beneath Eyjafjallajökull volcano from 1991 to 2009. *Journal of Volcanology and Geothermal Research*, *304*, 194–205. https://doi.org/10.1016/j.jvolgeores.2015.08.001

*How accurate are our public forecasts? - Met Office*. (n.d.). Retrieved April 20, 2023, from https://www.metoffice.gov.uk/about-us/what/accuracy-and-trust/how-accurate-are-our-public-forecasts

Jones, A., Thomson, D., Hort, M., & Devenish, B. (2007). The U.K. Met Office's Next-Generation Atmospheric Dispersion Model, NAME III. In C. Borrego & A.-L. Norman (Eds.), *Air Pollution Modeling and Its Application XVII* (pp. 580–589). Springer US. https://doi.org/10.1007/978-0-387-68854-1_62

Krishnan, M., & Rajan, K. S. (2021). Generating Spatial Distribution of Volcanic ASH Spread. *2021 IEEE International Geoscience and Remote Sensing Symposium IGARSS*, 7271–7274. https://doi.org/10.1109/IGARSS47720.2021.9553353

Kristiansen, N. I., Stohl, A., Prata, A. J., Bukowiecki, N., Dacre, H., Eckhardt, S., Henne, S., Hort, M. C., Johnson, B. T., Marenco, F., Neininger, B., Reitebuch, O., Seibert, P., Thomson, D. J., Webster, H. N., & Weinzierl, B. (2012). Performance assessment of a volcanic ash transport model mini-ensemble used for inverse modeling of the 2010 Eyjafjallajökull eruption. *Journal of Geophysical Research: Atmospheres*, *117*(D20). https://doi.org/10.1029/2011JD016844

Krivoruchko, K., & Gribov, A. (2014). Pragmatic Bayesian Kriging for Non-Stationary and Moderately Non-Gaussian Data. *Lecture Notes in Earth System Sciences*. https://doi.org/10.1007/978-3-642-32408-6_15

Krivoruchko, K., & Gribov, A. (2019). Evaluation of empirical Bayesian kriging. *Spatial Statistics, 32*, 100368. https://doi.org/10.1016/j.spasta.2019.100368

Krivoruchko, K., & Mateu, J. (2020). *COVID-19 EPIDEMIC DATA MODELING IN SPACE-TIME USING INNOVATION DIFFUSION KRIGING*. https://www.semanticscholar.org/paper/COVID-19-EPIDEMIC-DATA-MODELING-IN-SPACE-TIME-USING-Krivoruchko-Mateu/e0a4f306c522942643666c90043030bf5eb622bc

Martucci, G., Ovadnevaite, J., Ceburnis, D., Berresheim, H., Varghese, S., Martin, D., Flanagan, R., & O'Dowd, C. D. (2012). Impact of volcanic ash plume aerosol on cloud microphysics. *Atmospheric Environment*, *48*, 205–218. https://doi.org/10.1016/j.atmosenv.2011.12.033

*METP WG MOG 8 VA SN 02_IAVW_Roadmap (attachment).pdf*. (n.d.). Retrieved April 20, 2023, from https://www.icao.int/airnavigation/METP/Eighth%20Meeting%20Documents/METP%20WG%20MOG%208%20VA%20SN%2002_IAVW_Roadmap%20(attachment).pdf

Miller, S. A. (2011). April 2010 UK Airspace closure: Experience and impact on the UK's air-travelling public and implications for future travel. *Journal of Air Transport Management*, *17*(5), 296–301. https://doi.org/10.1016/j.jairtraman.2011.03.008

New ash density limits agreed for flights in the UK. (2010, May 18). *BBC News*. https://www.bbc.com/news/newsbeat-10121554

Newman, S. M., Clarisse, L., Hurtmans, D., Marenco, F., Johnson, B., Turnbull, K., Havemann, S., Baran, A. J., O'Sullivan, D., & Haywood, J. (2012). A case study of observations of volcanic ash from the Eyjafjallajökull eruption: 2. Airborne and satellite radiative measurements. *Journal of Geophysical Research: Atmospheres*, *117*(D20). https://doi.org/10.1029/2011JD016780

O'Dowd, C., Ceburnis, D., Ovadnevaite, J., Martucci, G., Bialek, J., Monahan, C., Berresheim, H., Vaishya, A., Grigas, T., Jennings, S. G., McVeigh, P., Varghese, S., Flanagan, R., Martin, D., Moran, E., Lambkin, K., Semmler, T., Perrino, C., & McGrath, R. (2012). The Eyjafjallajökull ash plume – Part I: Physical, chemical and optical characteristics. *Atmospheric Environment*, *48*, 129–142. https://doi.org/10.1016/j.atmosenv.2011.07.004

Potts, R. (n.d.). *Development of an ensemble-based volcanic ash dispersion model for operations at Darwin VAAC*.

Rudack, D. E., & Ghirardelli, J. E. (2010). A Comparative Verification of Localized Aviation Model Output Statistics Program (LAMP) and Numerical Weather Prediction (NWP) Model Forecasts of Ceiling Height and Visibility. *Weather and Forecasting*, *25*(4), 1161–1178. https://doi.org/10.1175/2010WAF2222383.1

Saltykovskii, A. Ya. (2012). The eruption of Eyjafjallajökull (Iceland) in Spring 2010 and its possible consequences. *Izvestiya, Atmospheric and Oceanic Physics*, *48*(7), 683–695. https://doi.org/10.1134/S0001433812070067

Smolka, A., & Käser, M. (2015). *Volcanic Risks and Insurance* (pp. 301–314). https://doi.org/10.1016/B978-0-12-396453-3.00012-5

Stefanescu, E. R., Patra, A. K., Bursik, M. I., Madankan, R., Pouget, S., Jones, M., Singla, P., Singh, T., Pitman, E. B., Pavolonis, M., Morton, D., Webley, P., & Dehn, J. (2014). Temporal, probabilistic mapping of ash clouds using wind field stochastic variability and uncertain eruption source parameters: Example of the 14 April 2010 Eyjafjallajökull eruption. *Journal of Advances in Modeling Earth Systems*, *6*(4), 1173–1184. https://doi.org/10.1002/2014MS000332

Sturkell, E., Einarsson, P., Sigmundsson, F., Hooper, A., Ófeigsson, B. G., Geirsson, H., & Ólafsson, H. (2010). 2 Katla and Eyjafjallajökull Volcanoes. In A. Schomacker, J. Krüger, & K. H. Kjær (Eds.), *Developments in Quaternary Sciences* (Vol. 13, pp. 5–21). Elsevier. https://doi.org/10.1016/S1571-0866(09)01302-5

Thakur, M., Samanta, B., & Chakravarty, D. (2018). A non-stationary geostatistical approach to multigaussian kriging for local reserve estimation. *Stochastic Environmental Research and Risk Assessment*, *32*(8), 2381–2404. https://doi.org/10.1007/s00477-018-1533-1

Thordarson, T., & Larsen, G. (2007). Volcanism in Iceland in historical time: Volcano types, eruption styles and eruptive history. *Journal of Geodynamics*, *43*(1), 118–152. https://doi.org/10.1016/j.jog.2006.09.005

Turnbull, K., Johnson, B., Marenco, F., Haywood, J., Minikin, A., Weinzierl, B., Schlager, H., Schumann, U., Leadbetter, S., & Woolley, A. (2012). A case study of observations of volcanic ash from the Eyjafjallajökull eruption: 1. In situ airborne observations. *Journal of Geophysical Research: Atmospheres*, *117*(D20). https://doi.org/10.1029/2011JD016688

van Stein, B., Wang, H., Kowalczyk, W., Emmerich, M., & Bäck, T. (2020). Cluster-based Kriging approximation algorithms for complexity reduction. *Applied Intelligence*, *50*(3), 778–791. https://doi.org/10.1007/s10489-019-01549-7

Weinzierl, B., Sauer, D., Minikin, A., Reitebuch, O., Dahlkötter, F., Mayer, B., Emde, C., Tegen, I., Gasteiger, J., Petzold, A., Veira, A., Kueppers, U., & Schumann, U. (2012). On the visibility of airborne volcanic ash and mineral dust from the pilot's perspective in flight. *Physics and Chemistry of the Earth, Parts A/B/C*, *45–46*, 87–102. https://doi.org/10.1016/j.pce.2012.04.003

Wilkinson, S. M., Dunn, S., & Ma, S. (2012). The vulnerability of the European air traffic network to spatial hazards. *Natural Hazards*, *60*(3), 1027–1036. https://doi.org/10.1007/s11069-011-9885-6

Wilson, T. M., Stewart, C., Sword-Daniels, V., Leonard, G. S., Johnston, D. M., Cole, J. W., Wardman, J., Wilson, G., & Barnard, S. T. (2012). Volcanic ash impacts on critical infrastructure. *Physics and Chemistry of the Earth, Parts A/B/C*, *45–46*, 5–23. https://doi.org/10.1016/j.pce.2011.06.006

Zhu, R., Janowicz, K., & Mai, G. (2019). Making direction a first-class citizen of Tobler's first law of geography. *Transactions in GIS*, *23*(3), 398–416. https://doi.org/10.1111/tgis.12550

----*xxx*----